NON-SPECULAR RAM

by

Thomas B.A. Senior and Valdis V. Liepa
Radiation Laboratory
The University of Michigan
Ann Arbor, Michigan 48109

FINAL REPORT

April 1977

P. O. No. 1-83493 (F33615-76-C-1064)

5 April 1976 - 5 April 1977

Prepared for

Emerson and Cuming, Inc.
Microwave Products Division
Canton, Massachusetts 02021

14518-1-F = RL-2275

ABSTRACT

Techniques are developed for reducing the non-specular scattering displayed by ogival and wedge cylinders in an aspect range about edge-on. To achieve a cross section reduction over almost a 10:1 frequency band, it is necessary to decrease each type of contribution individually and also to minimize their interaction. The various contributors are discussed and analyses performed to specify the surface impedances necessary to adequately reduce them. With the restriction to a coating no more than 50 mils in thickness, materials have been assessed to determine their ability to realize the desired impedance. The best material found is capable of about 10 dB cross section reduction over most of the frequency range. Computer program RAMD has been used to optimize the application of this material and, in addition, to verify the results of experimental measurements.

TABLE OF CONTENTS

CHAPTER 1

INTRODUCTION

This is the final report on a sub-contract (P.O. 1-83493) from Emerson and Cuming, Inc. covering the period April 1976 - April 1977 and concerned with the theoretical design and evaluation of radar absorbing materials for a specific application.

The overall purpose of the prime Air Force Contract F33615-76-C-1064 was to study the availability of broadband absorbers for reducing non-specular scattering and to demonstrate their capability using two generic shapes: a 25^{o} included angle ogival cylinder and a 25^{o} wedge cylinder of length to width ratio 2.810, both of them with particular reference to H polarization in which the magnetic vector is parallel to the front edge, i.e. the electric vector perpendicular to the edge. At the lowest frequency of interest (2.0 GHz) the bodies are 0.800λ and 0.716λ long respectively where λ is the wavelength, but their surface lengths are almost identical (0.807λ and 0.803λ). This was one of the considerations that led to the choice of these specific shapes under the prior Contracts F33615-72-C-1439 and F33615-73-C-1174 held by the Radiation Laboratory.

The three main types of non-specular scatterers are edges (or other discontinuities in the slope and higher derivatives of the body profile), traveling waves and creeping waves and the bodies were selected to exemplify them. Thus, the ogival cylinder supports a traveling wave and, in addition, gives rise to edge scattering from both the leading and trailing edges. The wedge cylinder displays "edge" scattering from the join of the wedge and cylinder (where the curvature or second derivative of the profile is discontinuous) as well as from the leading edge, and in addition supports a traveling wave on the wedge, smoothly matched into a creeping wave on the shadowed portion of the cylindrical cap. All three types of scattering are geometry and polarization dependent and diminish with increasing frequency. Their magnitudes are generally small compared with any specular contribution that may exist, but at the aspects of most interest in this study ($\pm 30^{o}$ about edge-on), there is no specular contribution to the backscattering cross section. Non-specular scattering is therefore the only scattering that occurs.

Traveling and creeping waves are forms of surface waves whose propensity to cling to surfaces sets them apart from edge-diffracted contributions. The two types of waves are distinguished from one another mainly by the illumination of the surface on which they travel. Creeping waves are "born" at the shadow boundaries of bodies whose radii of curvature are electrically large. They propagate into the shadowed region following geodesic paths leaking off energy in the direction of the forward tangent to the path as they go. As a result of this leakage, the wave attenuates as it progresses and its electromagnetic properties at any point are almost exclusively determined by the local geometry of the surface. It is evident that such a wave can traverse the shadowed portion of, for example, the wedge cylinder, and on reaching the boundary of the shadowed/lit regions, the energy radiated will be in the backscattering direction and will contribute to the backscattering cross section. In theory and practice, creeping waves are only a significant source of scattering where the incident electric vector is perpendicular to the surface at the shadow boundary, i.e. for H polarization with the wedge cylinder. Once established, they are no longer dependent on the incident field. They are closely bound to the surface over which they travel, and this fact, coupled with their natural rate of decay even on a metallic surface, makes it possible to diminish their effect using lossy coatings.

Traveling waves are also significant only when the electric vector is perpendicular to the surface, i.e. for H polarization with either of the given bodies. They are supported by surfaces of large radius in the direction of propagation almost all of which is illuminated, and in contrast to creeping waves, they tend to build up as they travel, being fed by the incident wave. As regards backscattering, a traveling wave is harmless as long as it continues to travel forward, but when it reaches any discontinuity in the surface, a portion of it may be reflected and travel back to contribute to the backscattered field. The rear edge of the ogival cylinder provides such a discontinuity, and the resulting backscattered field has the fan-shaped pattern characteristic of a traveling wave antenna. Under the afore-mentioned prior contracts it was shown that traveling wave contributions could be significantly decreased by appropriately loading the surface. Not unexpectedly, the largest reductions were obtained when the entire surface was loaded, with the loading greatest near to the trailing edge where the reflection takes place.

The third source of non-specular scattering is edge diffraction and this is also strongly polarization dependent. With E polarization, for example, the leading edge is the primary source and methods for the reduction of this type of scattering were developed under Contract F33615-73-C-1174. For the present study, however, H polarization is of most concern. Although the rear edge of, for example, the ogival cylinder is now the dominant source, and its scattering can be suppressed by the same treatment used in regard to the traveling wave, the front edge does contribute a small amount. Its scattering is a function of the wedge angle as well as the incident field direction, and for a 25^{o} total angle wedge, the front edge contribution at an angle of 25^{o} from the symmetry axis is only 15 dB below that attributable to the rear edge. To reduce the complete scattering cross section by an amount greater than this therefore requires a front edge treatment as well.

In the aspect range about edge-on, two or more sources contribute to the backscattering cross section of each body, and to devise a cross section reduction scheme which has the potential for being broadband, it is essential to reduce all sources of scattering individually. Some progress was made under the prior contracts referred to above. It was found, for example, that a material presenting a given surface impedance could significantly reduce the traveling and creeping wave contributions and, provided the impedance was chosen appropriately, the front edge scattering as well. A computer program designated RAMD was developed to solve the integral equations for the currents induced on the surface of an arbitrary two-dimensional body subject to an impedance boundary condition and illuminated by either an E- or H-polarized plane wave incident in a plane perpendicular to the z-axis. The impedance may vary in any prescribed manner over the surface, and from a knowledge of the currents, the backscattering cross section is computed as a function of the angle of incidence. The program is described in Appendix B which also contains listings of two subroutines for computing the surface impedance of one and two layer metal-backed coatings.

Valuable as the concept of surface impedance is, it does have some shortcomings for an investigation such as this. A knowledge of the impedance does not

indicate the electromagnetic properties of a coating that will produce it, nor is there any assurance that a material can be found to yield an impedance which is independent of both the incident field and the surface geometry. For these reasons, our original intent was to rely heavily on a program called RAMVS which computes the scattering from a two-dimensional body in the presence of a number of resistive, conductive and/or combined (i.e. resistive and conductive) sheets. The program had been successfully applied to single and multiple (but well separated) sheets extending out from a body, and was a vital tool in our development of techniques for reducing the E-polarized backscattering from ogival and wedge cylinders under Contract F33615-73-C-1174 (Knott and Senior, 1974). By placing one or more sheets close to the surface of a perfectly conducting body, we hoped to simulate the effect of a coating whose properties could vary in depth as well as laterally and would be explicit in the formulation, in contrast to the situation when a surface impedance is used. Knowing the permittivities and permeabilities which different materials possess, we hoped then to arrive at the specification of a coating which would be effective in reducing the backscattering over the entire frequency range.

Unfortunately the program was not equal to the task. Because of the formulation adopted, numerical errors increase rapidly as the spacing between two sheets or between a sheet and the body becomes comparable to the sampling distance (or cell size) along either. Since the sheet must be located at the mid-point of the layer it is designed to simulate, a coating 50 mils thick would require a minimum sampling distance of no more than 25 mils, and significantly less if high accuracy is required. Even a body only one inch in length would now strain the core storage of the computers available for running the program, not to mention the financial resources on hand. A considerable amount of time was spent in attempting to overcome the spacing limitation, and some of the approaches tried are documented in Appendix A, which also contains a listing of program RAMVS in its most recent form. It was ultimately apparent that only a major restructuring of the program could suffice, and since the time and funds available would not allow this, we were forced to seek another tool to help in specifying an effective coating.

Meanwhile, the electromagnetic properties of some of the materials being proposed for a coating had been measured at the Avionics Laboratory of Wright Field, and in all cases the impedance of a layer 50 mils or less in thickness was virtually independent of the angle of incidence. This gave some confidence in returning to a surface impedance approach, and since the results obtained using program RAMD were also in good agreement with measured data for an ogival cylinder with material OG-C-1 used as a coating, we transferred our allegiance back to our old and well-trusted program.

Rapid progress was now made. Having delineated the scattering produced by the bare body at the four designated frequencies throughout the band (see Chapter 2), we exercised RAMD to determine the cross section reduction provided by impedances whose largest magnitudes were comparable to those of a 50 mil layer of the materials available, but which varied in some chosen manner over the length of the body. It was immediately apparent that to obtain any reduction at all at the lower frequencies, it was necessary to put as much material as possible on the body, i.e. to cover almost the entire surface with a coating 50 mils thick. The only departure from the uniform coverage was near to the front edge where the impedance and, hence, the layer thickness must be tapered to control the edge scattering. The procedures that were followed to arrive at a coating which is 'optimum' subject to the constraints provided by the materials available are described in Chapter 3. It should be noted that because of the difficulties posed by the lower frequencies (where the bodies are less than a wavelength long) and by the modest capabilities of the materials, there was little scope for a more subtle deployment of material. Indeed, the resulting prescriptions for both the ogival and wedge cylinders are identical in spite of the very different types of scattering exemplified. Finally, in Chapter 4, computed data are presented for some of the bare and coated bodies that have been considered experimentally by Emerson and Cuming.

CHAPTER 2

THEORETICAL CONSIDERATIONS

2.1 Geometries

The two bodies to be studied are shown in Figure 2-1. The first is a 25^{o} angle ogival cylinder whose relevant dimensions and the symbols used to denote them are as follows:

wedge half angle: $\Omega = 12.5^{o}$

surface radius: $R = 10.914$ inches

overall length: $\ell = 4.724$ inches $(= 2R\sin\Omega)$

surface length, top: $s_{max} = 4.762$ inches $(= \pi R\Omega/90)$

maximum width: $w = 0.5174$ inches $(= 4R\sin^{2}\Omega/2)$

The other is a wedge cylinder (the two dimensional analogue of a cone sphere) with the same wedge angle as the ogival cylinder:

wedge half angle: $\Omega = 12.5^{o}$

base radius: $a = 0.752$ inches

overall length: $\ell = 4.226$ inches $\left(= a\left[1 + \operatorname{cosec}\Omega\right]\right)$

surface length, top: $s_{max} = 4.737$ inches $\left(= a\left[(1 + \Omega/90)\pi/2 + \cot\Omega\right]\right)$

We observe that the surface lengths of the two bodies are almost the same, and would have been identical if, for example, the base radius of the wedge cylinder had been chosen as 0.756 inches.

The four designated frequencies throughout the band are 2.0, 3.75, 7.5 and 15.0 GHz, with wavelengths 5.901, 3.147, 1.574 and 0.787 inches respectively. Some corresponding electrical dimensions of the bodies are:

f(GHz)	ogival cylinder s_{max}/λ	wedge cylinder a/λ
= 2.0 ,	= 0.807 ,	= 0.127
= 3.75 ,	= 1.513 ,	= 0.239
= 7.5 ,	= 3.026 ,	= 0.478
= 15.0 ,	= 6.052 ,	= 0.956.

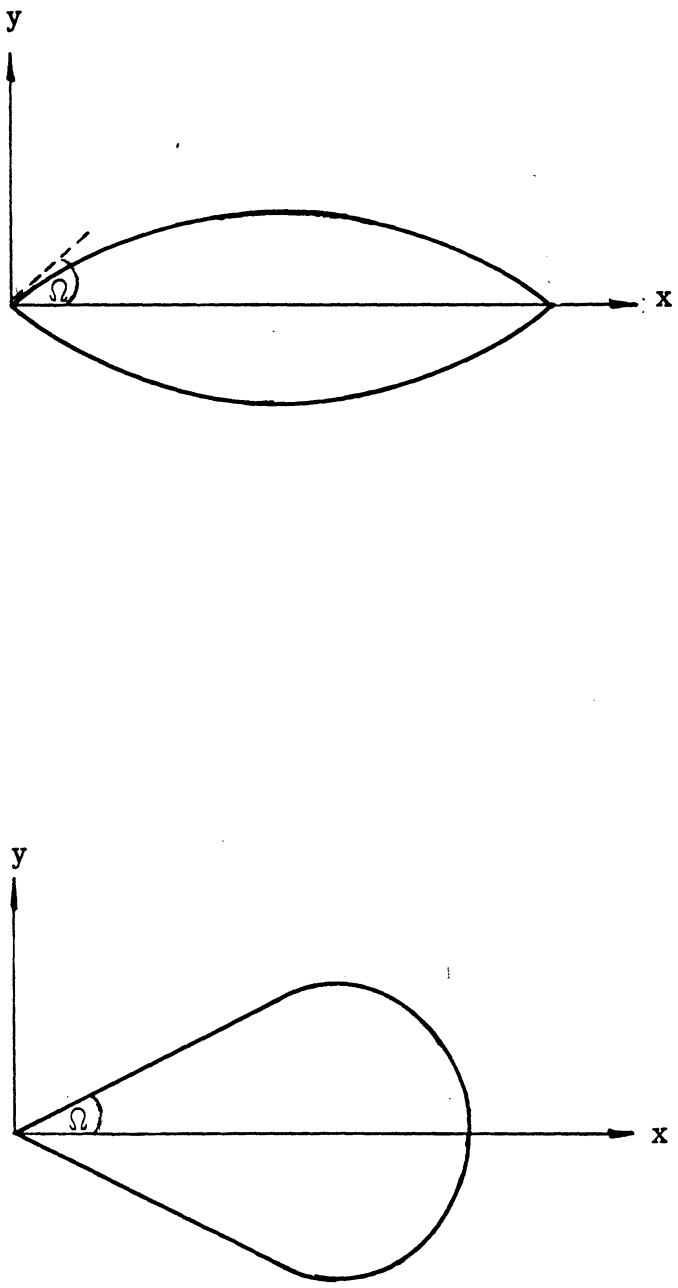

Figure 2-1: The bodies (not to scale).

At 7.436 GHz the surface length of the ogival cylinder is just 3λ, and the body is then electrically identical to that considered under Contracts F33615-72-C-1439 and F33615-73-C-1174.

In analyses and computations of the scattering we assume a plane wave incident at an angle ϕ_o to the symmetry axis of the body and with its phase zero at the center. The scattering angle ϕ will also be measured from the same axis so that $\phi = \phi_o$ represents backscattering with $\phi_o = \pi$ ($= 180^o$) for edge-on incidence. We shall treat only the case of H polarization in which the incident electric vector is parallel to the generators of the cylinders and to the front edge, i.e. in the z direction.

Since the bodies are two dimensional it is convenient to express the far zone scattered field in terms of the complex amplitude $P(\phi, \phi_o)$, i.e. the coefficient of $\left(\frac{2}{\pi k\rho}\right)^{1/2} e^{i(k\rho - \pi/4)}$ in the far field, where ρ is the distance from the origin of coordinates at the front edge (Bowman et al., 1969; p. 6) and a time factor $e^{-i\omega t}$ has been assumed and suppressed. The two dimensional scattering "cross section" is then

$$\sigma(\phi, \phi_o) = \frac{4}{k} \left|P(\phi, \phi_o)\right|^2$$

implying

$$\frac{\sigma}{\lambda} = \frac{2}{\pi} \left|P\right|^2 , \qquad (2.1)$$

which is independent of frequency if $\left|P\right|$ is. In presenting the results of our analyses and computations of backscattering, we will generally display σ/λ in dB, i.e. $10 \log \sigma/\lambda$. However, the experimental measurements performed by Emerson and Cuming, Inc. were carried out using cylinders of width L = 18 inches. Insofar as predictions based on two dimensional bodies are applicable, the connection between the measured (three dimensional) cross section σ_3 and the two dimensional cross section given above is

$$\sigma_3 = 2L^2 \frac{\sigma}{\lambda} \qquad (2.2)$$

(see Knott et al., 1973; Appendix C). Thus, σ_3 would also be independent of frequency if σ/λ were. For L = 18 inches (= 0.457 m), $2L^2$ = -3.79 dBsm, implying

$$\sigma_3 = 10 \log \frac{\sigma}{\lambda} - 3.79 \qquad \text{dBsm} , \tag{2.3}$$

and in all comparisons of theory and experiment we display σ_3 in dBsm as a function of $\theta = \pi - \phi_o$.

2.2 Bare Body Scattering

To fully appreciate the cross section reduction task confronting us, it is important to have some knowledge of the type and magnitudes of the contributions to the backscattering of the bare body, with particular reference to the aspect range $150^o \lesssim \phi_o \leq 180^o$. This will also indicate the most effective deployment of an absorber, but it should be emphasized that the idea of individual portions of a body scattering relatively independently is a high frequency concept. As the frequency decreases, interaction between the individual scatterers becomes more important and, in addition, each scattering contribution becomes less localized in origin, with the decomposition breaking down completely when the wavelength becomes greater than the relevant dimensions of the body. For the cylinders of interest in this study, the concept is quantitatively valid at the two highest frequencies at most, but even at the lower frequencies the concept can still provide some useful qualitative information.

The front edge is the same for both bodies, and its scattering can be estimated using the formula for diffraction by a wedge of included angle 2Ω:

$$P^f(\phi, \phi_o) = \frac{i}{2\nu} \sin\frac{\pi}{\nu} \left\{ \left(\cos\frac{\pi}{\nu} - 1 \right)^{-1} + \left(\cos\frac{\pi}{\nu} + \cos\frac{2}{\nu}(\pi - \phi_o) \right)^{-1} \right\} \tag{2.4}$$

where $\nu = 67/36$ (Bowman et al., 1969; p. 263). In particular, for edge-on incidence, $P^f = -i\,0.0633$ giving $\sigma/\lambda = -25.94$ dB.

The ogival cylinder has an identical rear edge and if it is fully visible the (direct) scattering which it contributes is

$$P^r(\phi_o, \phi_o) = P^f(\pi - \phi_o, \pi - \phi_o)\, e^{-2ik\ell\cos\phi_o} ,$$

where P^f is given by (2.4) and the phase factor has been introduced to maintain the phase reference at the origin. In addition, the rear edge reflects a wave which travels back along the surface of the cylinder to produce the scattering pattern characteristic of a traveling wave. The precise manner in which the rear edge diffraction merges into the traveling wave effect as $\phi_o \to \pi - \Omega$ is not well understood, but if, for the moment, we ignore the traveling wave contribution, the backscattering patterns of the ogival cylinder at the four frequencies computed using

$$\frac{\sigma}{\lambda} = \frac{2}{\pi}\left|P^f(\phi_o, \phi_o) + P^r(\phi_o, \phi_o)\right|^2 , \qquad (2.5)$$

i.e. on the basis of front and rear edge diffraction alone, are as shown in Figures 2-2 through 2-5. On each figure we have superimposed the cross sections attributable to the two edges individually, but it should be remembered that at least for $\phi_o \gtrsim 160^o$ the rear edge contributes primarily via the traveling wave which has not been included. We therefore expect the patterns to be meaningful only for $\phi_o \lesssim 160^o$ and at the higher frequencies.

The backscattering from the wedge cylinder is more complicated. In addition to diffraction by the front edge, there are contributions from the creeping wave supported by the smoothly-rounded base and from the discontinuities in curvature where the wedge and circular cylinder join. The front edge contribution is again given by (2.4). The upper join where a cylinder of radius a meets a cylinder of infinite radius (the wedge) yields

$$P^{j(u)}(\phi_o, \phi_o) = -\frac{1}{8ka}\sec(\phi_o - \Omega)\left\{1 + \sec^2(\phi_o - \Omega)\right\} e^{-2ika\cot\Omega\cos(\phi_o - \Omega)} \qquad (2.6)$$

(Senior, 1972) which decreases with increasing frequency, and similarly

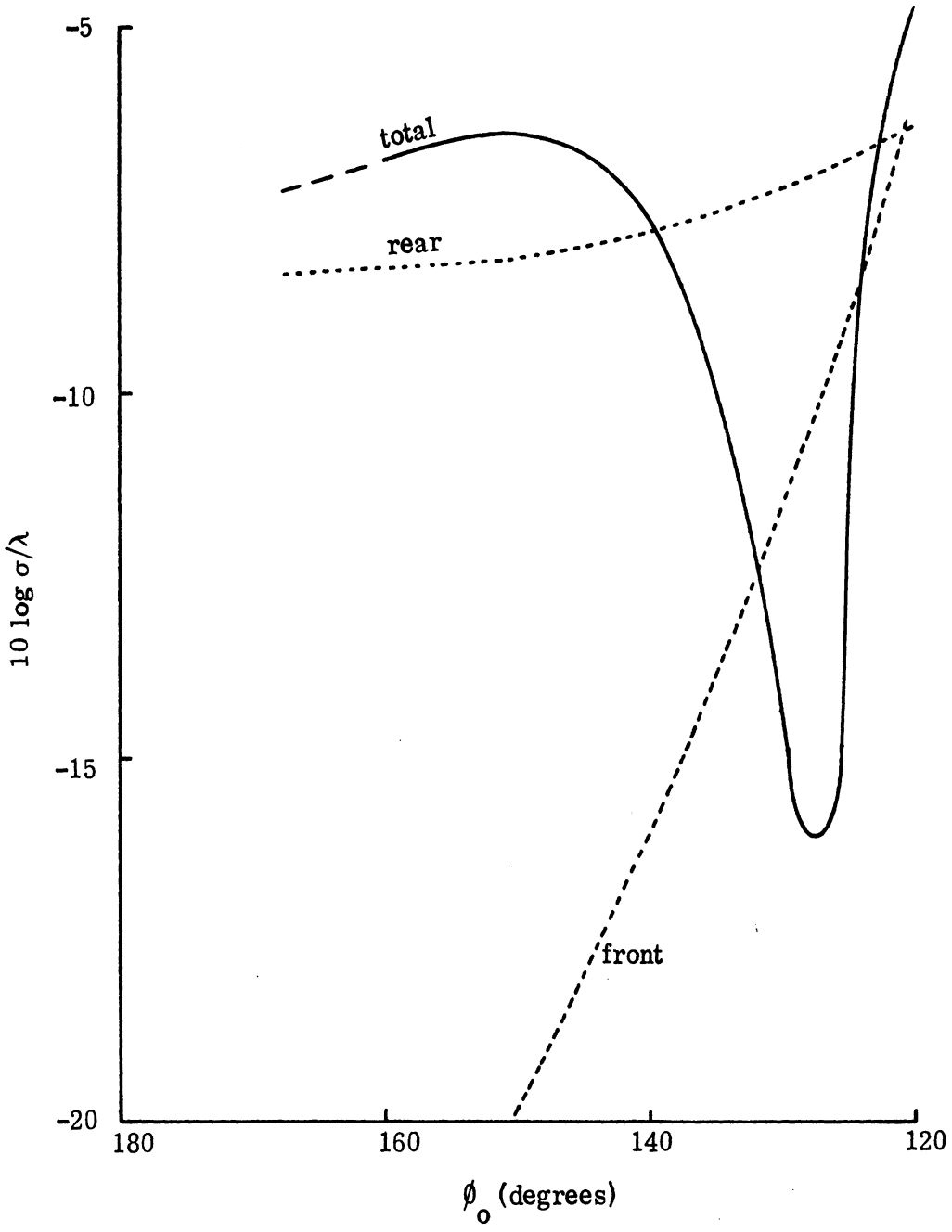

Figure 2-2: Ogival cylinder, 2 GHz: high frequency approx.

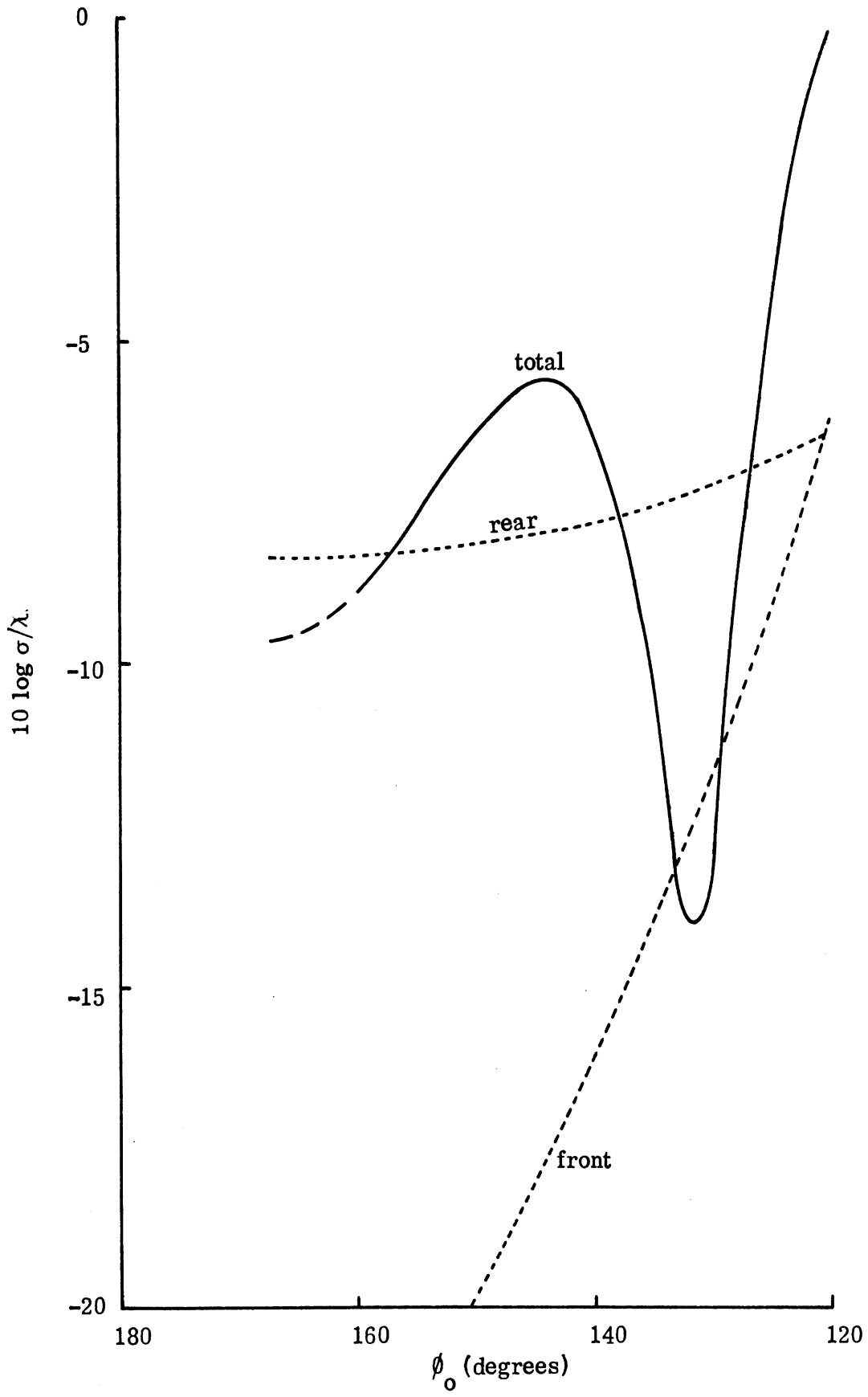

Figure 2-3: Ogival cylinder, 3.75 GHz: high frequency approx.

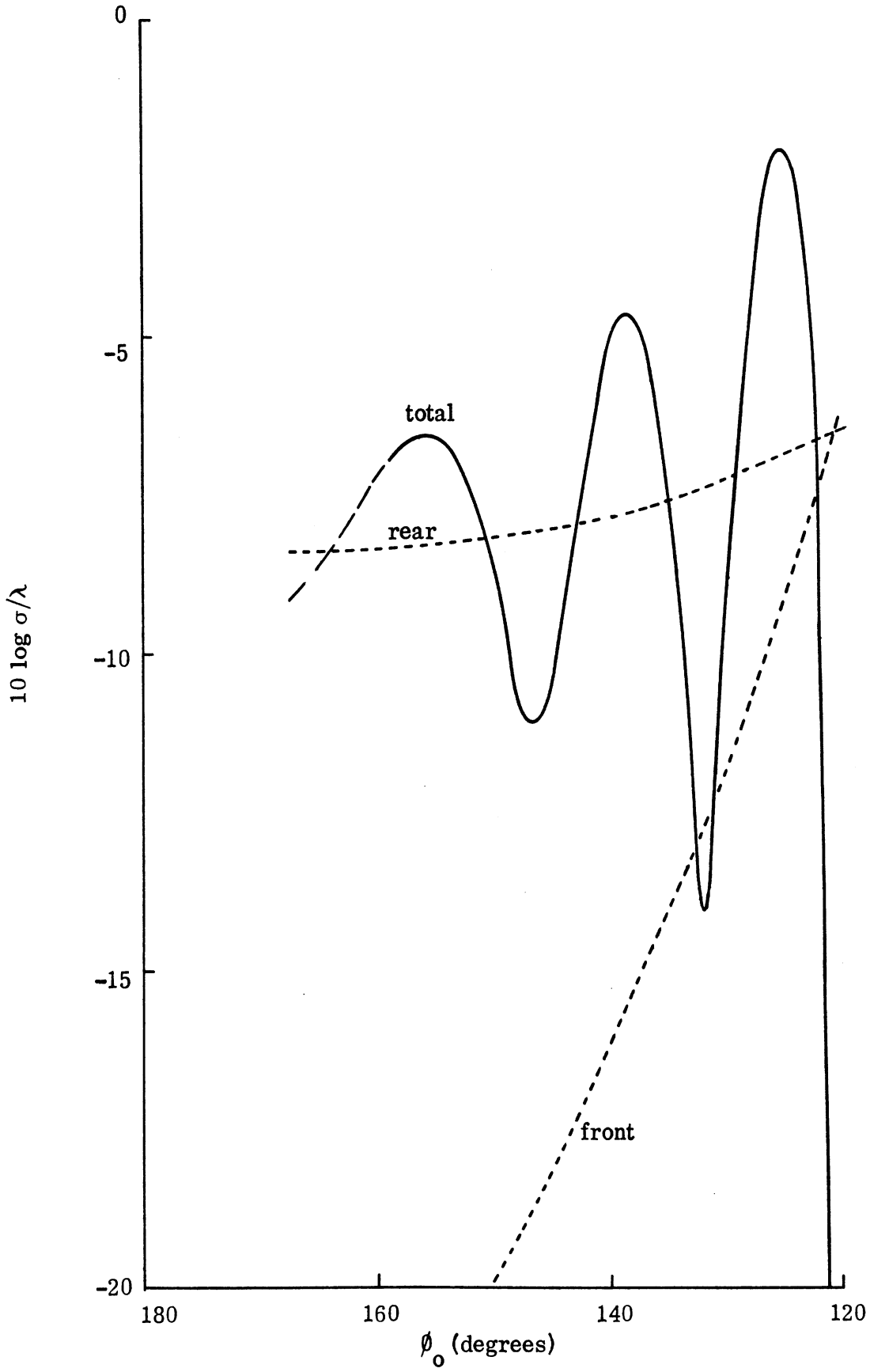

Figure 2-4: Ogival cylinder, 7.5 GHz: high frequency approx.

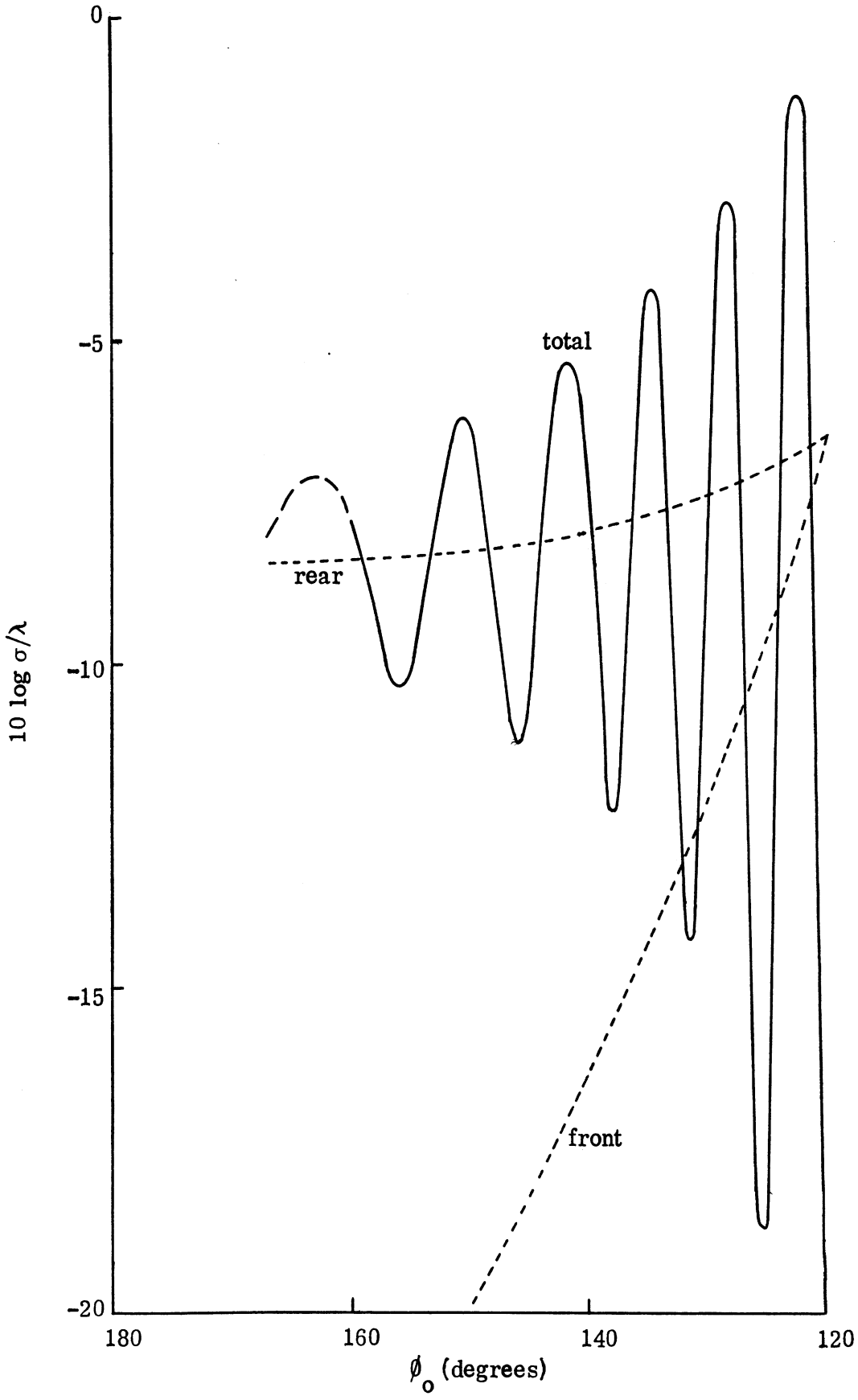

Figure 2-5: Ogival cylinder, 15 GHz: high frequency approx.

$$P^{j(\ell)}(\phi_o, \phi_o) = -\frac{1}{8ka}\sec(\phi_o + \Omega)\left\{1 + \sec^2(\phi_o + \Omega)\right\} e^{-2ika\cot\Omega\cos(\phi_o + \Omega)} \tag{2.7}$$

valid as long as the lower join is fully visible, i.e. $\phi_o > \pi - \Omega$. For this same aspect range the creeping wave contribution can be estimated using the known solution for a circular cylinder of radius a. Naturally, the result is independent of ϕ_o and from the formula in Bowman et al. (1969, pp. 110-111)

$$P^{cw} = \tau C\, e^{i\pi(\nu + 1/3)}\, e^{-2ika\,\mathrm{cosec}\Omega\cos\phi_o} \tag{2.8}$$

where $\tau = (ka/2)^{1/3}$, and $\nu = \bar{\nu}_1(\tau)$, $C = \bar{C}_1(\tau)$ have the asymptotic expansions given in this reference. If $ka >> 1$, P^{cw} decreased exponentially with increasing frequency, but for ka comparable to unity P^{cw} is relatively independent of frequency. For $\phi_o \lesssim \pi - \Omega$ the lower join and the creeping wave both contribute through an interaction with the front edge, but there is no simple method for estimating the scattering in this case.

The combination of the four contributions leads to a rather complicated backscattering behavior in the aspect range about edge-on, and instead of attempting to predict the net return at each of the four designated frequencies, we show only the individual cross sections σ/λ as functions of ϕ_0 at 7.5 GHz. The important conclusion to be drawn from Figure 2-6 is that all the contributions are similar in magnitude, implying that all must be reduced to obtain a significant and broadband reduction in the scattering.

Using the computer program RAMD (see Appendix B), we have computed the backscattering cross sections of the two bodies at each of the four frequencies. The results are tabulated in Chapter 4 and plotted for the aspect ranges $120^o \leq \phi_o \leq 180^o$ in Figures 2-7 through 2-10 for the ogival cylinder and Figures 2-11 through 2-14 for the wedge cylinder. We remark that the wedge cylinder always has a local maximum in the scattering pattern at edge-on incidence with a cross section in the range

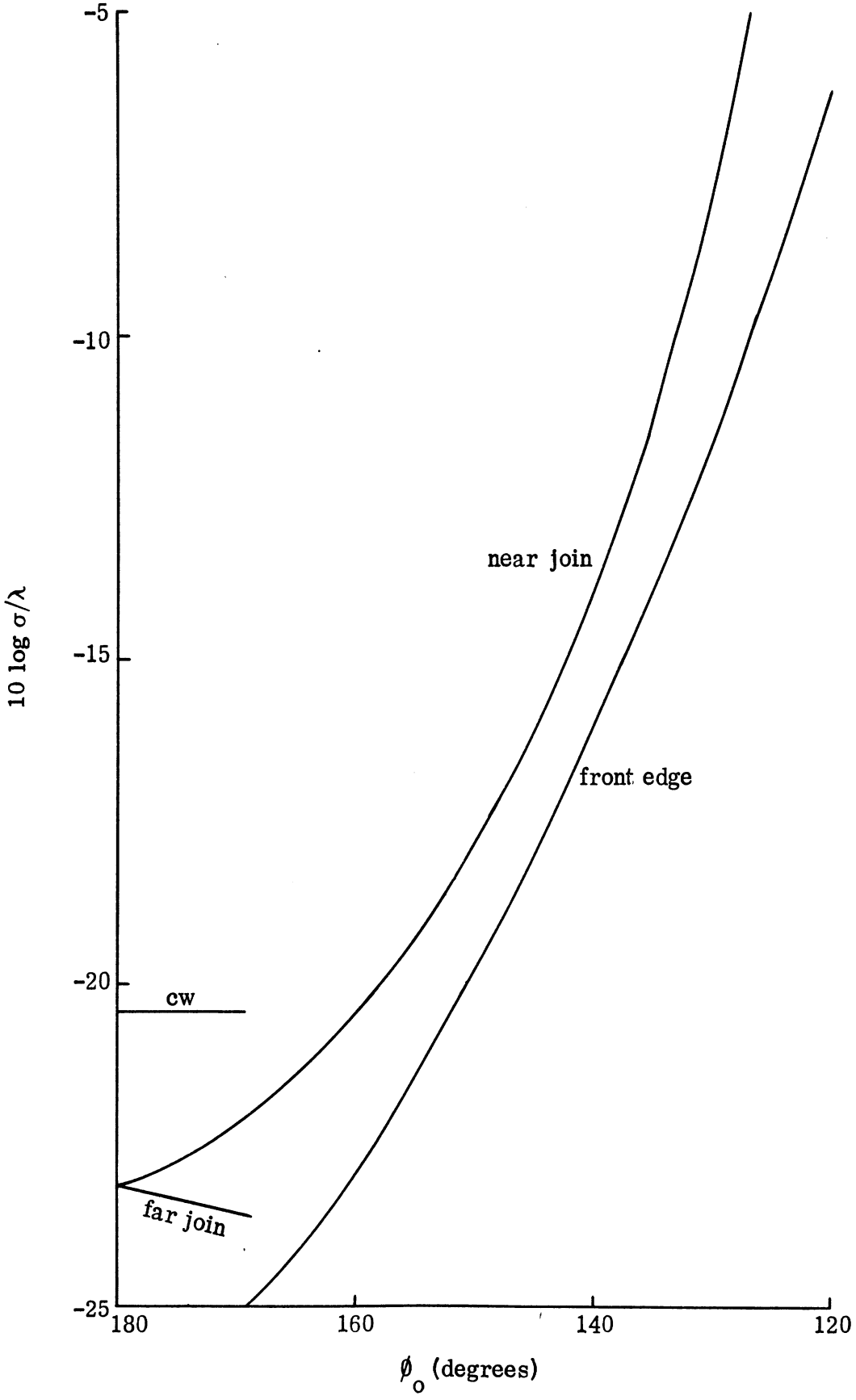

Figure 2-6: Estimated wedge cylinder contributors at 7.5 GHz.

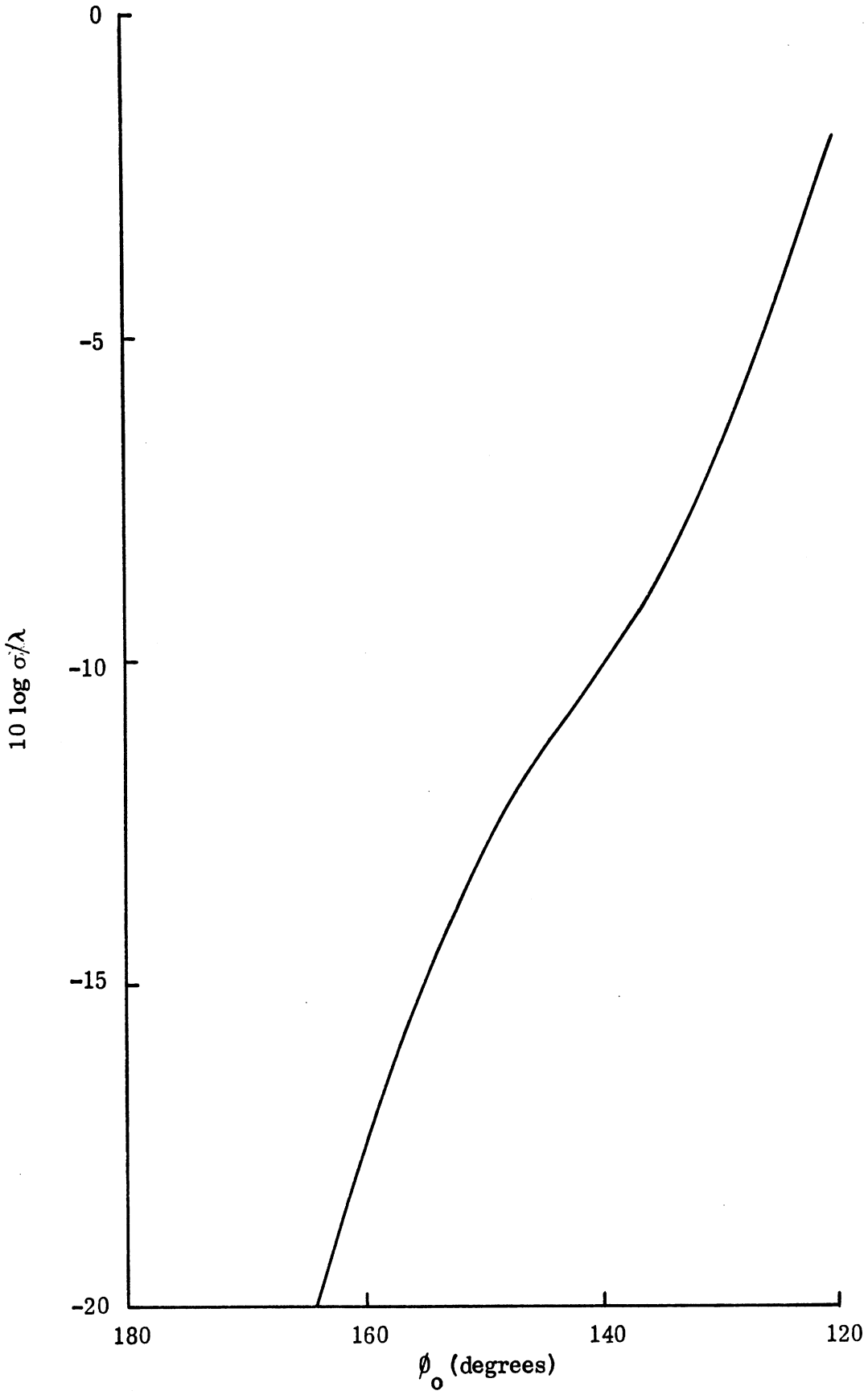

Figure 2-7: Bare ogival cylinder, 2 GHz: RAMD.

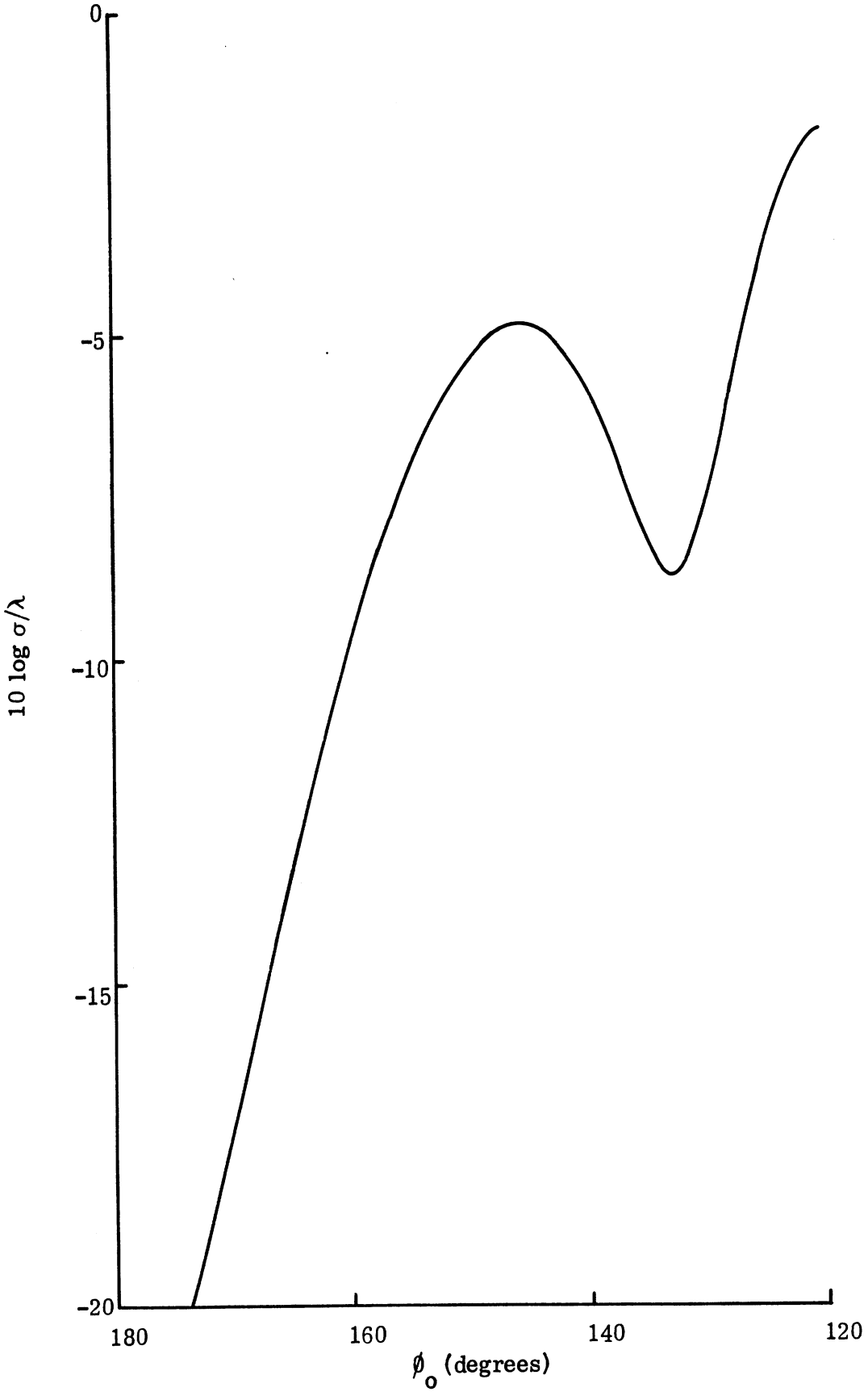

Figure 2-8: Bare ogival cylinder, 3.75 GHz: RAMD.

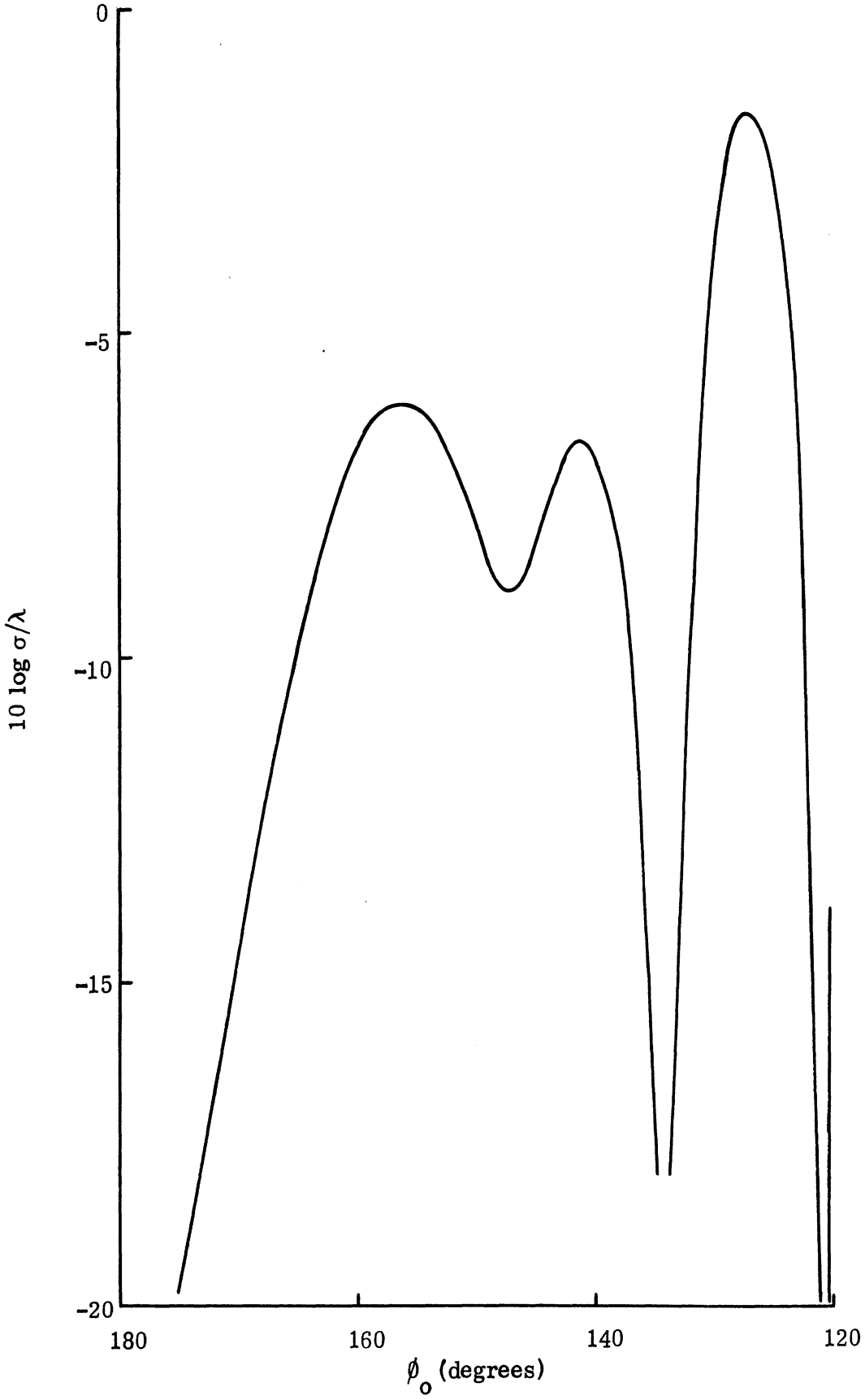

Figure 2-9: Bare ogival cylinder, 7.5 GHz: RAMD.

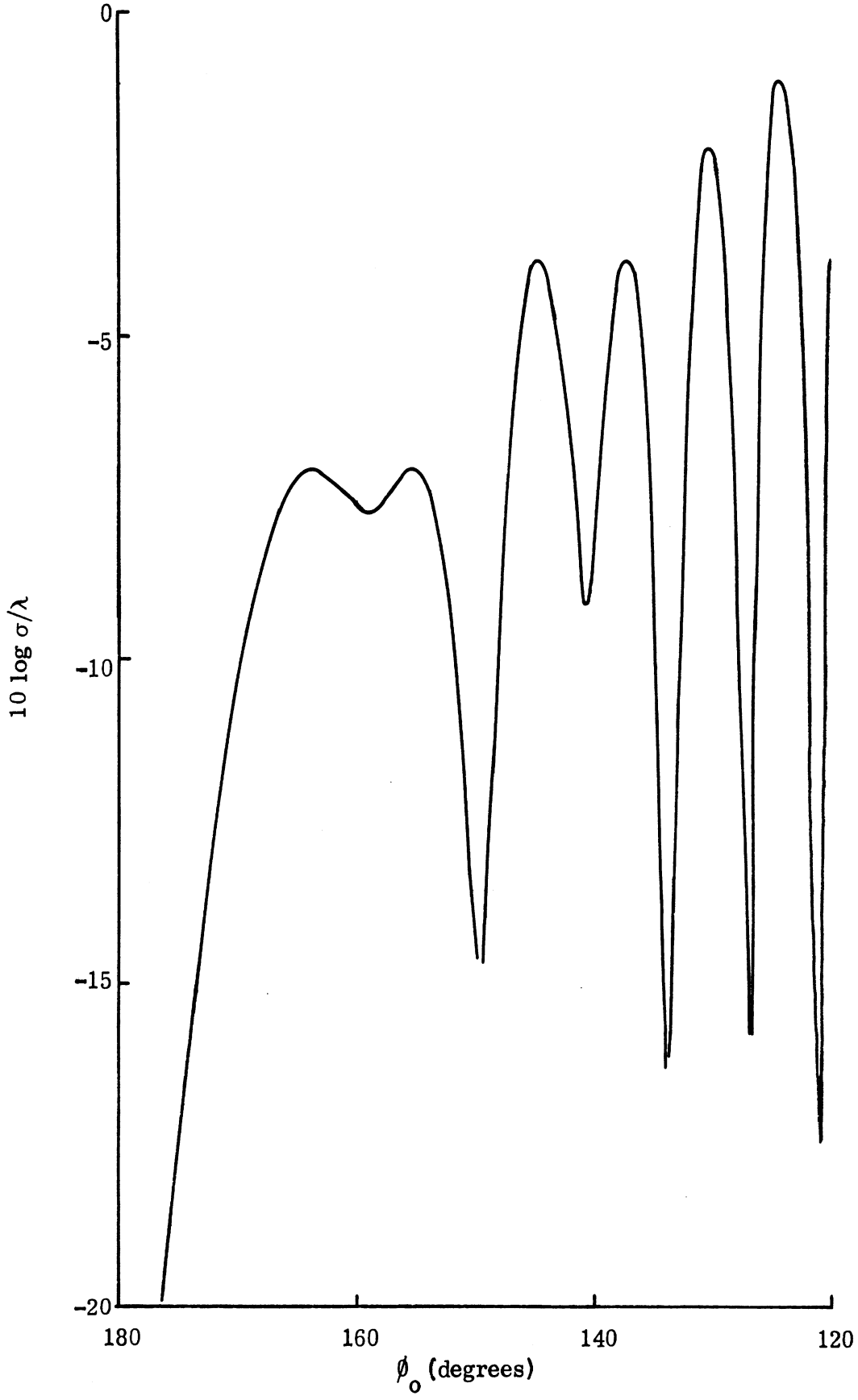

Figure 2-10: Bare ogival cylinder, 15 GHz: RAMD.

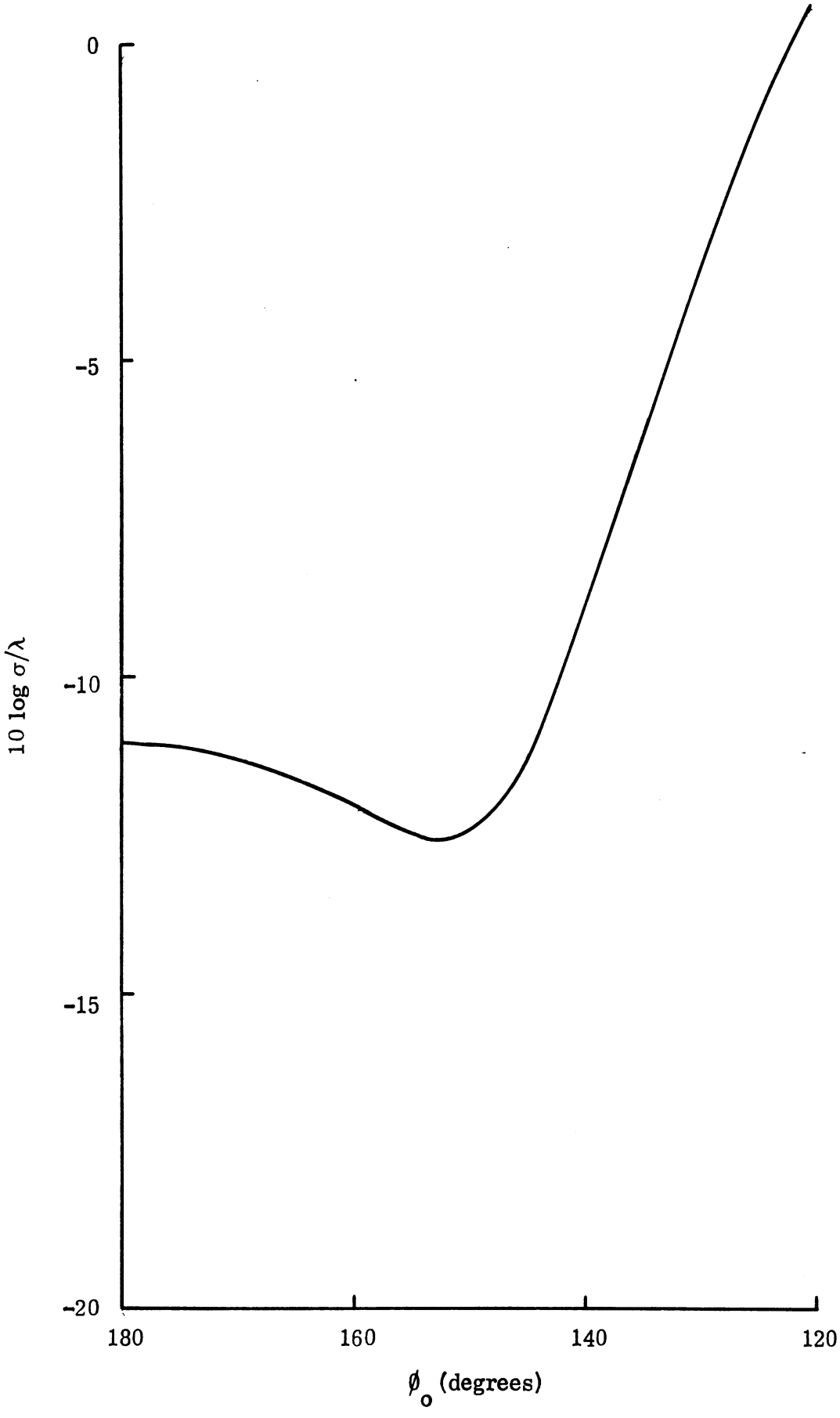

Figure 2-11: Bare wedge cylinder, 2 GHz; RAMD.

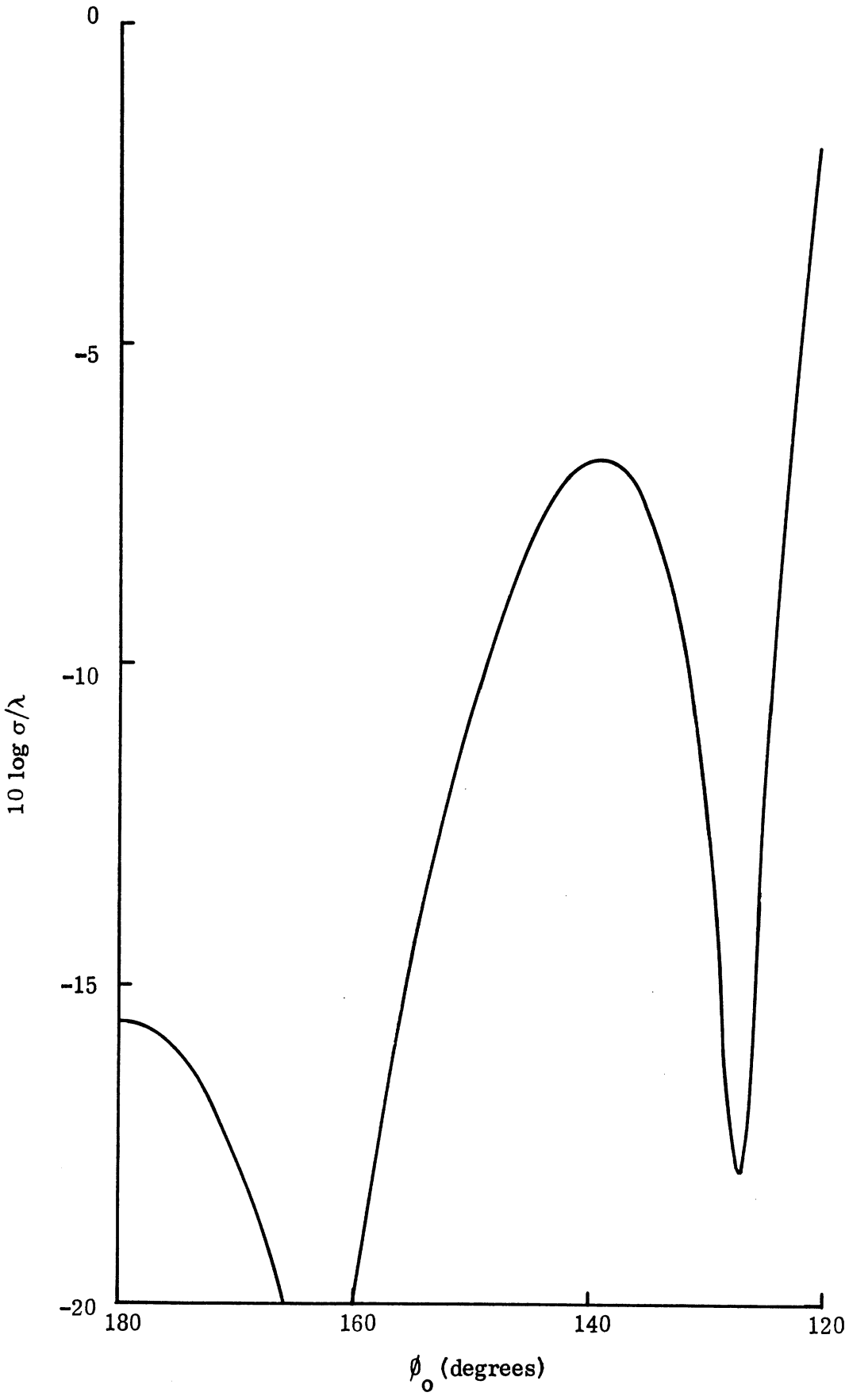

Figure 2-12: Bare wedge cylinder, 3.75 GHz: RAMD.

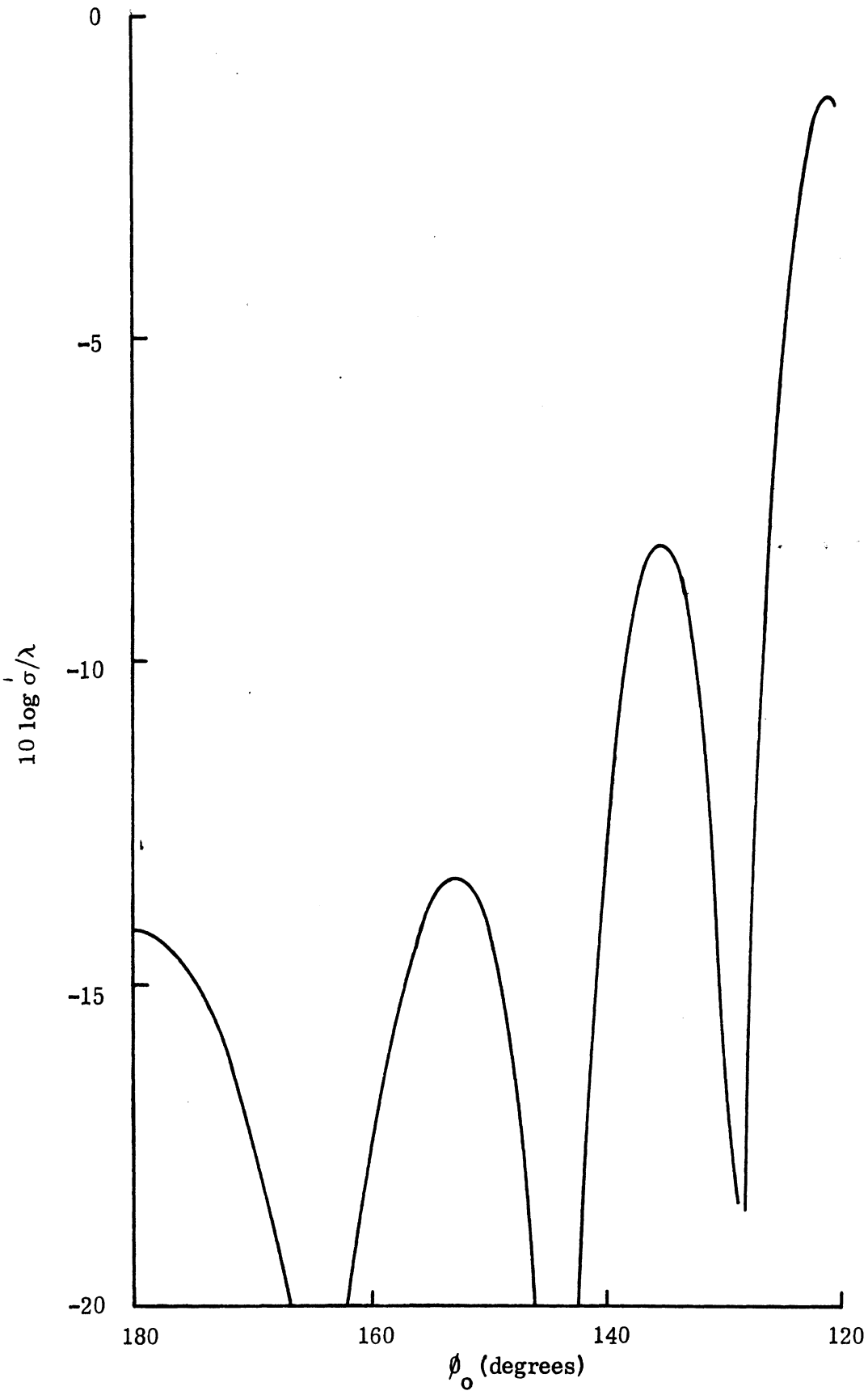

Figure 2-13: Bare wedge cylinder, 715 GHz: RAMD.

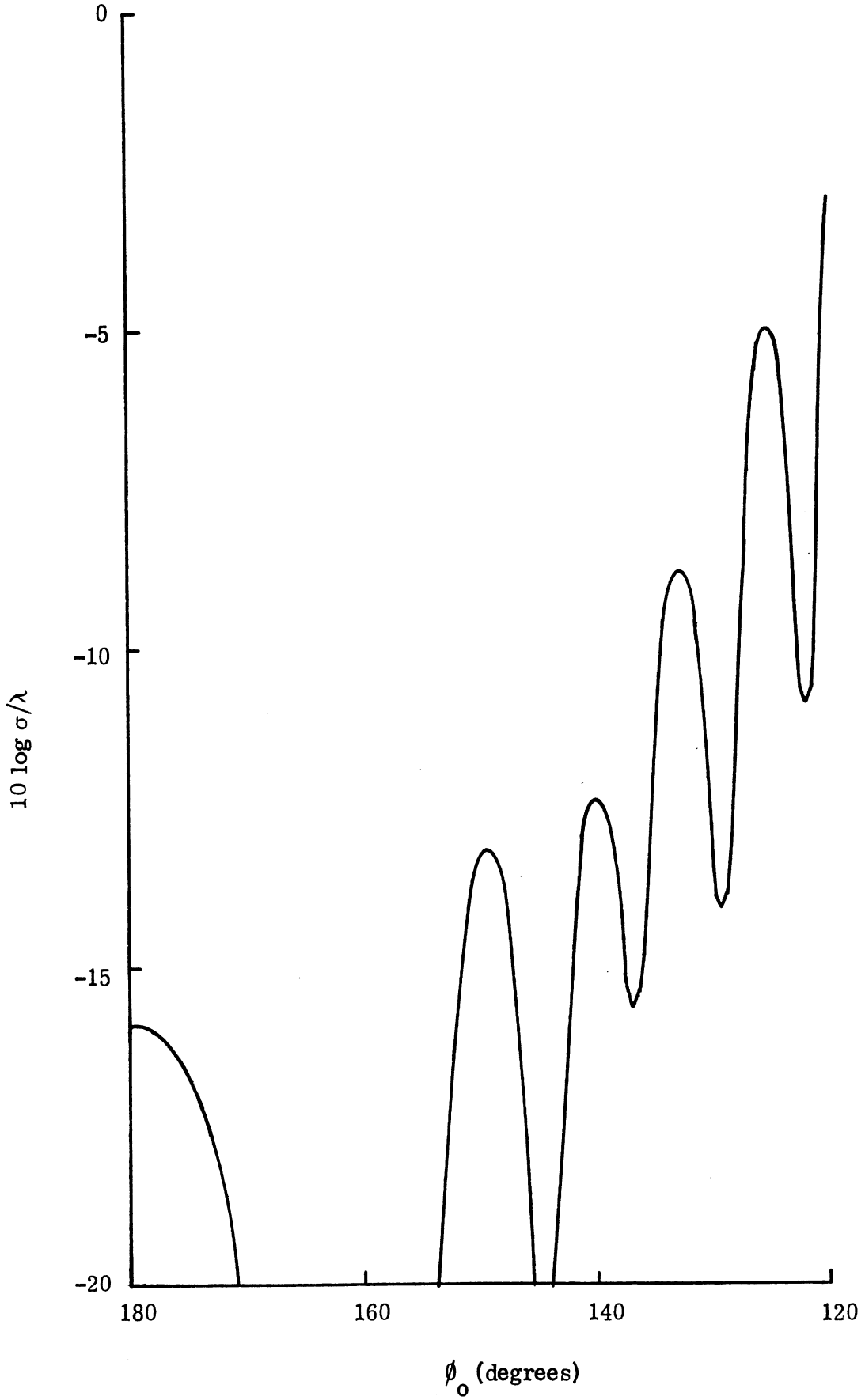

Figure 2-14: Bare wedge cylinder, 15 GHz: RAMD.

-10 to -20 dBλ. The ogival cylinder, on the other hand, has a minimum edge-on and here the cross section ranges from -20 to -40 dBλ. Comparison of the curves in Figures 2-7 through 2-10 with those in Figures 2-2 through 2-5 shows no agreement at the lowest frequency where the ogival cylinder is less than a wavelength long, but quite good agreement at the higher frequencies, particularly for scattering at aspects well away from edge-on where the traveling wave is no longer a significant contributor.

Of the two bodies, the ogival cylinder is the simpler, and it is convenient to concentrate on it. The only significant contributors to its backscattering cross section in an aspect range about edge-on are the front edge and a traveling wave. The latter appears by reflection of a forward traveling wave at the rear edge of the cylinder and gives rise to a lobed pattern with a minimum edge-on. Traveling wave theory has been fully developed only for a thin wire and its application to a two dimensional body having non-negligible thickness is difficult to justify. Nevertheless, the concept is a valuable working tool and proves surprisingly accurate even for a body like an ogival cylinder.

From an examination of measured data for the backscattering from a wire of length ℓ, Senior and Knott (1968, Appendix A) showed that if $\lambda << \ell$ the first traveling wave peak occurs at

$$\theta = \theta_1 = 49.9\sqrt{\frac{\lambda}{\ell}} \quad \text{degrees} \tag{2.9}$$

and the second at

$$\theta = \theta_2 = 98.1\sqrt{\frac{\lambda}{\ell}} \quad \text{degrees} \tag{2.10}$$

where $\theta = \pi - \phi_0$. For increasing $\lambda \gtrsim 0.6\,\ell$, (2.9) progressively underestimates the angular position θ of the first peak by an amount as much as 3^o for $\lambda \simeq \ell$; but since the magnitude of the peak decreases with increasing λ/ℓ, the peak is seldom evident for $\lambda \gtrsim \ell$. Unless $\lambda << \ell$, the second peak is not usually evident either,

being swamped by other scattering contributions. To see how these findings apply to the ogival cylinder, the angles at which the first maximum occurs in the computed data are compared with the predictions of (2.9) in Table 2.1. The agreement is reasonably good.

Table 2.1: Locations of first traveling wave peak for ogival cylinder.

Frequency (GHz)	θ_1^o (computed data)	θ_1^o (predicted)
2.0	?	55
3.75	37	40
7.5	26	28
15.0	18	20

Since there are two contributors to the backscattering at edge-on incidence, it does not follow that an absorber which reduces one of them will automatically reduce the cross section. Using program RAMD we have computed the backscattering patterns of the bare ogive at the frequencies f = 0.1 (0.1) 4.0 GHz, and the values of $\left\{\sigma(\pi, \pi)/\lambda\right\}^{1/2}$ are plotted in Figure 2-15. The dashed line is based on the empirical formula

$$\frac{1}{\lambda}\sigma(\pi, \pi) = \left| -i(0.0465 + i0.0345\, e^{2ik\ell}) \right|^2 \qquad (2.11)$$

obtained by curve fitting, where ℓ is the length of the cylinder. We remark that the first contributor, -i0.0465, is close to the high frequency prediction -i0.0505 for front edge diffraction, suggesting that the second term is the traveling wave contribution. We note that the two contributors are almost out of phase at 2.0 GHz and are precisely in phase at 3.75 GHz. If the above empirical formula were to hold at

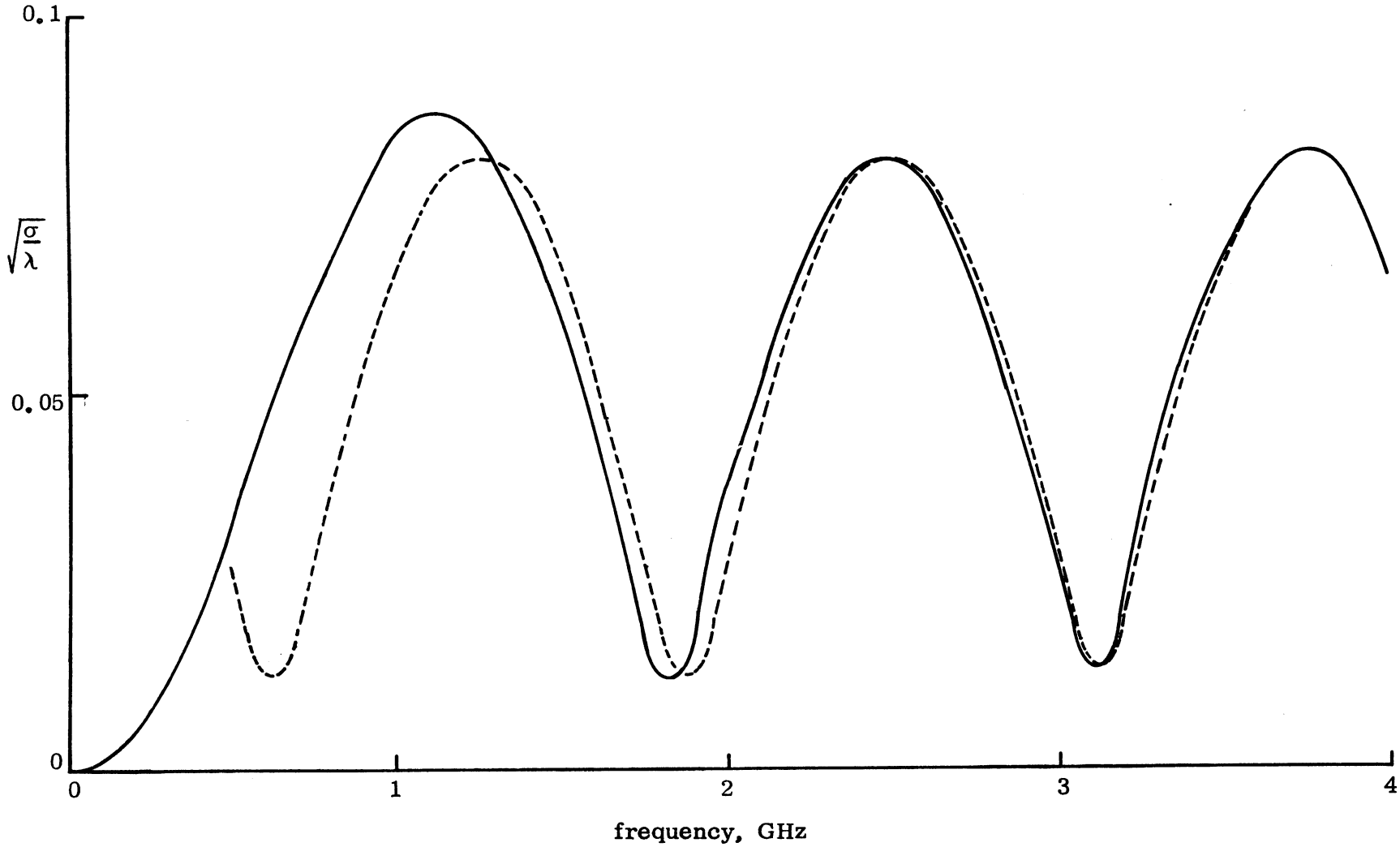

Figure 2-15: Edge-on backscattering from bare ogival cylinder: —— computed, ---- empirical (eq. 2.11).

all higher frequencies (and there is evidence to suggest that it does), the contributors would be almost in phase at 7.5 and 15.0 GHz as well. It therefore follows that an absorber which acts only on the traveling wave must increase the edge-on cross section at 2.0 GHz and can provide no more than 6 dB reduction at any frequency. As evident from the formula, both contributors must be decreased in magnitude to achieve a reduction in the edge-on cross section over a broad frequency range.

2.3 Surface Impedance Concept

Given a body whose geometry is fixed, the only feasible technique for cross section reduction is the judicious application of absorbers to suppress those forms of scattering which are responsible for the dominant return. According to the Contract specification we are limited to a coating no more than 50 mils in thickness applied to the bare (metal) body, and the task then is to choose the layer thickness and composition in such a way as to achieve the greatest cross section reduction over the entire frequency range. Unfortunately the problem as posed does not have a unique solution even within the bounds created by the properties of the available materials, but nevertheless progress can be made towards an 'engineering' solution.

As noted in the Introduction, our analyses and computations are based on the use of an impedance boundary condition to simulate the effect on the scattered field of a coating applied to the surface. It is assumed that the (normalized) surface impedance η is a function only of the local properties of the coating regardless of the field and the geometry of the surface to which the coating is applied, and this is an assumption which is incapable of prior validation. In particular, it is not evident that a coating will present the same impedance close to the edge of a body as it does when over a broad face, but in spite of this the results obtained using the impedance boundary condition have been found applicable under a wide range of circumstances, and the agreement between theory and experiment provides confidence in the validity of the procedure. Although this approach was not our first choice for meeting the objectives of the Contract, it does appear to be the only one

which is feasible at this time, and it enables us to predict the performance of a coating using a computer program which is reasonably efficient.

For a surface whose impedance η is specified at every point, the impedance (or Leontovich) boundary condition can be written as

$$\underline{E} - (\hat{n} \cdot \underline{E})\,\hat{n} = \eta Z\, \hat{n} \wedge \underline{H} \tag{2.12}$$

where $\hat{n}$ is the unit vector (outward) normal and Z is the intrinsic impedance of the free space medium above the surface. η may vary over the surface and is zero for perfect conductivity. The derivation of (2.12) has been discussed by Senior (1960) and we remark that in contrast to the analogous boundary condition involving the normal derivative of the fields, (2.12) does not contain any tangential derivatives of η. By trivial manipulation (2.12) can be expressed alternatively as

$$\underline{H} - (\hat{n} \cdot \underline{H})\,\hat{n} = -\frac{Y}{\eta}\,\hat{n} \wedge \underline{E} \tag{2.13}$$

(Senior, 1962) where $Y = 1/Z$, and this is the dual of (2.12) under the transformation $\underline{E} \longrightarrow \underline{H}$, $\underline{H} \longrightarrow -\underline{E}$, $Z \longleftrightarrow Y$, $\eta \longleftrightarrow 1/\eta$.

For a field incident on a surface at which the condition (2.12) is imposed, the resulting boundary value problem can be solved either analytically or numerically to yield the scattered field. In the case of a two dimensional surface of profile C illuminated by an H polarized plane wave, the scattered magnetic field is

$$H_z^s(\underline{\rho}) = \frac{ik}{4} \int_C \left\{ \hat{n}' \cdot \hat{r}\; H_1^{(1)}(kr) + i\eta(s')\, H_o^{(1)}(kr) \right\} K(s')\, ds' \tag{2.14}$$

where $K(s')$ is the current induced in the surface. $H_o^{(1)}$ and $H_1^{(1)}$ are the Hankel functions of the first kind of orders zero and one respectively, and $r = \underline{\rho} - \underline{\rho}'$ (Knott and Senior, 1974). The integral equation obtained from (2.14) is the basis of operation of computer program RAMD.

To determine the impedance presented by an absorber coating applied to the bare body, consider a plane wave incident on a homogeneous layer of infinite extent backed by a metallic sheet. If the plane wave is H polarized and incident at an angle θ to the normal,

$$\eta = -\frac{i}{\epsilon}\sqrt{\epsilon\mu - \sin^2\theta}\ \tan\left(kd\sqrt{\epsilon\mu - \sin^2\theta}\right) \tag{2.15}$$

where ϵ and μ are the complex relative permittivity and permeability of the material, d is the thickness of the layer and $k = 2\pi/\lambda$ is the free space wave number. Similarly, for a coating consisting of two homogeneous layers of thicknesses d_1 and d_2, we have

$$\eta = \frac{1}{\epsilon_1}\sqrt{\epsilon_1\mu_1 - \sin^2\theta}\ \frac{1 - A\exp\left(2ikd_1\sqrt{\epsilon_1\mu_1 - \sin^2\theta}\right)}{1 + A\exp\left(2ikd_1\sqrt{\epsilon_1\mu_1 - \sin^2\theta}\right)} \tag{2.16}$$

where

$$A = \frac{1+B}{1-B} \tag{2.17}$$

with

$$B = i\frac{\epsilon_1}{\epsilon_2}\sqrt{\frac{\epsilon_2\mu_2 - \sin^2\theta}{\epsilon_1\mu_1 - \sin^2\theta}}\ \tan\left(kd_2\sqrt{\epsilon_2\mu_2 - \sin^2\theta}\right) \tag{2.18}$$

(see Figure 2-16). Programs have been written to compute the surface impedances given in (2.15) and (2.16) for any material constants, layer thickness and θ. Versions appropriate to the particular case of grazing incidence ($\theta = 90^\circ$) have also been coupled into program RAMD to study the effect of a material having a specified thickness variation over the surface of the body.

The above impedances are functions of the angle θ and therefore violate our requirement that η be independent of the incident field direction, but if

$$|\epsilon\mu| >> 1\ , \tag{2.19}$$

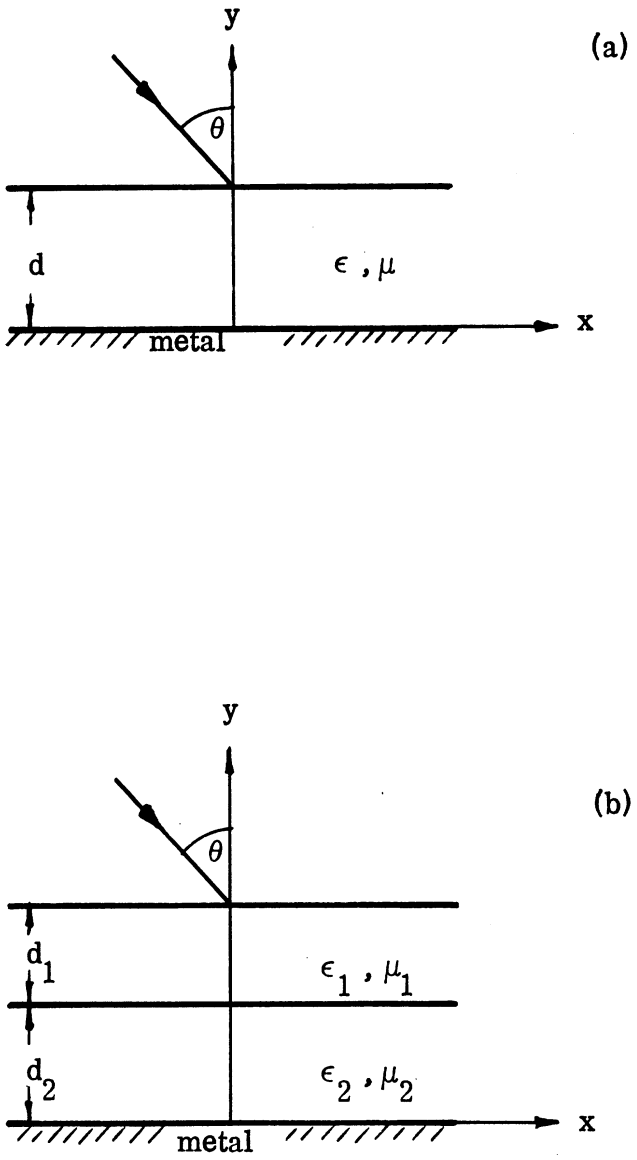

Figure 2-16: Geometries for (a) one layer and (b) two layer impedance calculations.

the angle dependence disappears to a first approximation. Equation (2.15) then becomes

$$\eta = -i\sqrt{\frac{\mu}{\epsilon}}\tan\left(kd\sqrt{\epsilon\mu}\right) , \tag{2.20}$$

and for a two layer coating,

$$\eta = \sqrt{\frac{\mu_1}{\epsilon_1}}\,\frac{1 - A\exp\left(2ikd_1\sqrt{\epsilon_1\mu_1}\right)}{1 + A\exp\left(2ikd_1\sqrt{\epsilon_1\mu_1}\right)} \tag{2.21}$$

where A is again given by (2.17) and

$$B = i\sqrt{\frac{\epsilon_1\mu_2}{\epsilon_2\mu_1}}\tan\left(kd_2\sqrt{\epsilon_2\mu_2}\right) . \tag{2.22}$$

The condition (2.19) is satisfied to an adequate degree by all of the materials considered. This is illustrated by the results in Tables 2-2 through 2-5 for the surface impedance of a layer of thickness d = 0(0.005) 0.050 inches of material OG-C-1 at each of the four designated frequencies. This material figured prominently in our investigation and the measured values of its permittivity and permeability are as follows:

f (GHz) = 2.0 :	ϵ = 22.46 + i 0.17 ,	= 5.29 + i 2.99
3.75 :	23.38 + i 1.87 ,	3.57 + i 3.15
7.5 :	20.53 + i 1.80 ,	1.72 + i 2.66
15.0 :	22.08 + i 0.39 ,	1 + i 1.68 .

The left hand columns in each of the Tables 2-2 through 2-5 are for normal incidence ($\theta = 0$) and those on the right are for grazing incidence ($\theta = 90^{\circ}$). We observe that the impedance η differs by no more than about one percent between these extreme values of θ.

2.4 Theoretical Approach to Cross Section Reduction

In seeking to choose impedances and, hence, material coatings that are effective in reducing the scattering from the bodies at aspects close to edge-on,

```
&data ang=0.,d=0.,f=2.,mu=(5.29,2.99),eps=(22.46,0.17) &end
 ANGLE      D          F          MU                EPS                ETA
 0.0      0.0        2.000    5.290  2.990     22.460  0.170     0.0     0.0

&data d=0.005 &end
 ANGLE      D          F          MU                EPS                ETA
 0.0      0.005      2.000    5.290  2.990     22.460  0.170     0.016 -0.028

&data d=0.010 &end
 ANGLE      D          F          MU                EPS                ETA
 0.0      0.010      2.000    5.290  2.990     22.460  0.170     0.032 -0.056

&data d=0.015 &end
 ANGLE      D          F          MU                EPS                ETA
 0.0      0.015      2.000    5.290  2.990     22.460  0.170     0.049 -0.085

&data d=0.02 &end
 ANGLE      D          F          MU                EPS                ETA
 0.0      0.020      2.000    5.290  2.990     22.460  0.170     0.066 -0.114

&data d=0.025 &end
 ANGLE      D          F          MU                EPS                ETA
 0.0      0.025      2.000    5.290  2.990     22.460  0.170     0.084 -0.143

&data d=0.03 &end
 ANGLE      D          F          MU                EPS                ETA
 0.0      0.030      2.000    5.290  2.990     22.460  0.170     0.104 -0.173

&data d=0.035 &end
 ANGLE      D          F          MU                EPS                ETA
 0.0      0.035      2.000    5.290  2.990     22.460  0.170     0.125 -0.204

&data d=0.04 &end
 ANGLE      D          F          MU                EPS                ETA
 0.0      0.040      2.000    5.290  2.990     22.460  0.170     0.148 -0.236

&data d=0.045 &end
 ANGLE      D          F          MU                EPS                ETA
 0.0      0.045      2.000    5.290  2.990     22.460  0.170     0.174 -0.268

&data d=0.05 &end
 ANGLE      D          F          MU                EPS                ETA
 0.0      0.050      2.000    5.290  2.990     22.460  0.170     0.202 -0.302
```

```
&data d=0.0, ang=90. &end
 ANGLE      D          F          MU                EPS                ETA
 90.00    0.0        2.000    5.290  2.990     22.460  0.170     0.0     0.0

&data d=0.005 &end
 ANGLE      D          F          MU                EPS                ETA
 90.00    0.005      2.000    5.290  2.990     22.460  0.170     0.016 -0.028

&data d=0.01 &end
 ANGLE      D          F          MU                EPS                ETA
 90.00    0.010      2.000    5.290  2.990     22.460  0.170     0.032 -0.056

&data d=0.015 &end
 ANGLE      D          F          MU                EPS                ETA
 90.00    0.015      2.000    5.290  2.990     22.460  0.170     0.049 -0.084

&data d=0.02&&end
 ANGLE      D          F          MU                EPS                ETA
 90.00    0.020      2.000    5.290  2.990     22.460  0.170     0.066 -0.113

&data d=0.025 &end
 ANGLE      D          F          MU                EPS                ETA
 90.00    0.025      2.000    5.290  2.990     22.460  0.170     0.084 -0.142

&data d=0.03 &end
 ANGLE      D          F          MU                EPS                ETA
 90.00    0.030      2.000    5.290  2.990     22.460  0.170     0.104 -0.172

&data d=0.035 &data
 ANGLE      D          F          MU                EPS                ETA
 90.00    0.035      2.000    5.290  2.990     22.460  0.170     0.125 -0.202

&data d=0.04 &end
 ANGLE      D          F          MU                EPS                ETA
 90.00    0.040      2.000    5.290  2.990     22.460  0.170     0.148 -0.234

&data d=0.045 &end
 ANGLE      D          F          MU                EPS                ETA
 90.00    0.045      2.000    5.290  2.990     22.460  0.170     0.173 -0.266

&data d=0.05 &end
 ANGLE      D          F          MU                EPS                ETA
 90.00    0.050      2.000    5.290  2.990     22.460  0.170     0.202 -0.299
```

Table 2-2: Surface impedance η for material OG-C-1 at 2.0 GHz.

```
&data ang=0.,d=0.,f=3.75,mu=(3.57,3.15),eps=(23.38,1.87) &end
 ANGLE      D          F          MU                EPS               ETA
 0.0      0.0        3.750    3.570  3.150      23.380  1.870     0.0     0.0

&data d=0.005 &end
 ANGLE      D          F          MU                EPS               ETA
 0.0      0.005      3.750    3.570  3.150      23.380  1.870     0.032 -0.036

&data d=0.010 &end
 ANGLE      D          F          MU                EPS               ETA
 0.0      0.010      3.750    3.570  3.150      23.380  1.870     0.064 -0.071

&data d=0.015 &end
 ANGLE      D          F          MU                EPS               ETA
 0.0      0.015      3.750    3.570  3.150      23.380  1.870     0.099 -0.107

&data d=0.020 &end
 ANGLE      D          F          MU                EPS               ETA
 0.0      0.020      3.750    3.570  3.150      23.380  1.870     0.138 -0.142

&data d=0.025 &end
 ANGLE      D          F          MU                EPS               ETA
 0.0      0.025      3.750    3.570  3.150      23.380  1.870     0.181 -0.177

&data d=0.030 &end
 ANGLE      D          F          MU                EPS               ETA
 0.0      0.030      3.750    3.570  3.150      23.380  1.870     0.231 -0.210

&data d=0.035 &end
 ANGLE      D          F          MU                EPS               ETA
 0.0      0.035      3.750    3.570  3.150      23.380  1.870     0.289 -0.240

&data d=0.040 &end
 ANGLE      D          F          MU                EPS               ETA
 0.0      0.040      3.750    3.570  3.150      23.380  1.870     0.358 -0.263

&data d=0.045 &end
 ANGLE      D          F          MU                EPS               ETA
 0.0      0.045      3.750    3.570  3.150      23.380  1.870     0.438 -0.274

 ANGLE      D          F          MU                EPS               ETA
 0.0      0.050      3.750    3.570  3.150      23.380  1.870     0.527 -0.268
```

```
&data d=0.,ang=90. &end
 ANGLE      D          F          MU                EPS               ETA
 90.00    0.0        3.750    3.570  3.150      23.380  1.870     0.0     0.0

&data d=0.005 &end
 ANGLE      D          F          MU                EPS               ETA
 90.00    0.005      3.750    3.570  3.150      23.380  1.870     0.032 -0.035

&data d=0.010 &end
 ANGLE      D          F          MU                EPS               ETA
 90.00    0.010      3.750    3.570  3.150      23.380  1.870     0.064 -0.070

&data d=0.015 &end
 ANGLE      D          F          MU                EPS               ETA
 90.00    0.015      3.750    3.570  3.150      23.380  1.870     0.099 -0.106

&data d=0.020 &end
 ANGLE      D          F          MU                EPS               ETA
 90.00    0.020      3.750    3.570  3.150      23.380  1.870     0.137 -0.140

&data d=0.025 &end
 ANGLE      D          F          MU                EPS               ETA
 90.00    0.025      3.750    3.570  3.150      23.380  1.870     0.181 -0.175

&data d=0.030 &end
 ANGLE      D          F          MU                EPS               ETA
 90.00    0.030      3.750    3.570  3.150      23.380  1.870     0.230 -0.207

&data d=0.035 &end
 ANGLE      D          F          MU                EPS               ETA
 90.00    0.035      3.750    3.570  3.150      23.380  1.870     0.288 -0.236

&data d=0.040 &end
 ANGLE      D          F          MU                EPS               ETA
 90.00    0.040      3.750    3.570  3.150      23.380  1.870     0.356 -0.258

&data d=0.045 &end
 ANGLE      D          F          MU                EPS               ETA
 90.00    0.045      3.750    3.570  3.150      23.380  1.870     0.435 -0.270

&data d=0.050 &end
 ANGLE      D          F          MU                EPS               ETA
 90.00    0.050      3.750    3.570  3.150      23.380  1.870     0.523 -0.263
```

Table 2-3: Surface impedance η for material OG-C-1 at 3.75 GHz.

```
&data ang=0.,d=0.,f=7.50,mu=(1.72,2.66),eps=(20.53,1.80) &end
 ANGLE      D          F          MU                EPS               ETA
 0.0      0.0        7.500    1.720  2.660     20.530  1.800     0.0     0.0

&data d=0.005 &end
 ANGLE      D          F          MU                EPS               ETA
 0.0      0.005      7.500    1.720  2.660     20.530  1.800     0.054 -0.034

&data d=0.010 &end
 ANGLE      D          F          MU                EPS               ETA
 0.0      0.010      7.500    1.720  2.660     20.530  1.800     0.110 -0.066

&data d=0.015 &end
 ANGLE      D          F          MU                EPS               ETA
 0.0      0.015      7.500    1.720  2.660     20.530  1.800     0.172 -0.094

&data d=0.020 &end
 ANGLE      D          F          MU                EPS               ETA
 0.0      0.020      7.500    1.720  2.660     20.530  1.800     0.242 -0.114

&data d=0.025 &end
 ANGLE      D          F          MU                EPS               ETA
 0.0      0.025      7.500    1.720  2.660     20.530  1.800     0.320 -0.119

&data d=0.030 &end
 ANGLE      D          F          MU                EPS               ETA
 0.0      0.030      7.500    1.720  2.660     20.530  1.800     0.402 -0.103

&data d=0.035 &end
 ANGLE      D          F          MU                EPS               ETA
 0.0      0.035      7.500    1.720  2.660     20.530  1.800     0.478 -0.057

&data d=0.040 &end
 ANGLE      D          F          MU                EPS               ETA
 0.0      0.040      7.500    1.720  2.660     20.530  1.800     0.531  0.014

&data d=0.045 &end
 ANGLE      D          F          MU                EPS               ETA
 0.0      0.045      7.500    1.720  2.660     20.530  1.800     0.549  0.097

&data d=0.050 &end
 ANGLE      D          F          MU                EPS               ETA
 0.0      0.050      7.500    1.720  2.660     20.530  1.800     0.532  0.170
```

```
&data ang=90.,d=0. &end
 ANGLE      D          F          MU                EPS               ETA
90.00     0.0        7.500    1.720  2.660     20.530  1.800     0.0     0.0

&data d=0.005 &end
 ANGLE      D          F          MU                EPS               ETA
90.00     0.005      7.500    1.720  2.660     20.530  1.800     0.054 -0.033

&data d=0.010 &end
 ANGLE      D          F          MU                EPS               ETA
90.00     0.010      7.500    1.720  2.660     20.530  1.800     0.110 -0.064

&data d=0.015 &end
 ANGLE      D          F          MU                EPS               ETA
90.00     0.015      7.500    1.720  2.660     20.530  1.800     0.172 -0.091

&data d=0.020 &end
 ANGLE      D          F          MU                EPS               ETA
90.00     0.020      7.500    1.720  2.660     20.530  1.800     0.241 -0.110

&data d=0.025 &end
 ANGLE      D          F          MU                EPS               ETA
90.00     0.025      7.500    1.720  2.660     20.530  1.800     0.318 -0.114

&data d=0.030 &end
 ANGLE      D          F          MU                EPS               ETA
90.00     0.030      7.500    1.720  2.660     20.530  1.800     0.398 -0.097

&data d=0.035 &end
 ANGLE      D          F          MU                EPS               ETA
90.00     0.035      7.500    1.720  2.660     20.530  1.800     0.472 -0.052

&data d=0.040 &end
 ANGLE      D          F          MU                EPS               ETA
90.00     0.040      7.500    1.720  2.660     20.530  1.800     0.523  0.017

&data d=0.045 &end
 ANGLE      D          F          MU                EPS               ETA
90.00     0.045      7.500    1.720  2.660     20.530  1.800     0.541  0.098

&data d=0.050 &end
 ANGLE      D          F          MU                EPS               ETA
90.00     0.050      7.500    1.720  2.660     20.530  1.800     0.526  0.169
```

Table 2-4: Surface impedance η for material OG-C-1 at 7.5 GHz.

```
 &data d=0.,ang=0.,f=15.0,mu=(1.0,1.68),eps=(22.08,0.39) &end
ANGLE       D          F        ---MU---          ---EPS---          ---ETA---
  0.0       0.0      15.000    1.000  1.680      22.080  0.390      0.0     0.0

 &data d=0.005 &end
ANGLE       D          F        ---MU---          ---EPS---          ---ETA---
  0.0       0.005    15.000    1.000  1.680      22.080  0.390      0.069 -0.039

 &data d=0.010 &end
ANGLE       D          F        ---MU---          ---EPS---          ---ETA---
  0.0       0.010    15.000    1.000  1.680      22.080  0.390      0.146 -0.071

 &data d=0.015&&end
ANGLE       D          F        ---MU---          ---EPS---          ---ETA---
  0.0       0.015    15.000    1.000  1.680      22.080  0.390      0.240 -0.083

 &data d=0.020 &end
ANGLE       D          F        ---MU---          ---EPS---          ---ETA---
  0.0       0.020    15.000    1.000  1.680      22.080  0.390      0.342 -0.051

 &data d=0.025 &end
ANGLE       D          F        ---MU---          ---EPS---          ---ETA---
  0.0       0.025    15.000    1.000  1.680      22.080  0.390      0.413  0.038

 &data d=0.030 &end
ANGLE       D          F        ---MU---          ---EPS---          ---ETA---
  0.0       0.030    15.000    1.000  1.680      22.080  0.390      0.410  0.142

 &data d=0.035 &end
ANGLE       D          F        ---MU---          ---EPS---          ---ETA---
  0.0       0.035    15.000    1.000  1.680      22.080  0.390      0.356  0.203

 &data d=0.040 &end
ANGLE       D          F        ---MU---          ---EPS---          ---ETA---
  0.0       0.040    15.000    1.000  1.680      22.080  0.390      0.300  0.215

 &data d=0.045 &end
ANGLE       D          F        ---MU---          ---EPS---          ---ETA---
  0.0       0.045    15.000    1.000  1.680      22.080  0.390      0.262  0.203

 &data d=0.050 &end
ANGLE       D          F        ---MU---          ---EPS---          ---ETA---
  0.0       0.050    15.000    1.000  1.680      22.080  0.390      0.243  0.185
```

```
 &data d=0.,ang=90. &end
ANGLE       D          F        ---MU---          ---EPS---          ---ETA---
 90.00      0.0      15.000    1.000  1.680      22.080  0.390      0.0     0.0

 &data d=0.005 &end
ANGLE       D          F        ---MU---          ---EPS---          ---ETA---
 90.00      0.005    15.000    1.000  1.680      22.080  0.390      0.069 -0.037

 &data d=0.010 &end
ANGLE       D          F        ---MU---          ---EPS---          ---ETA---
 90.00      0.010    15.000    1.000  1.680      22.080  0.390      0.146 -0.067

 &data d=0.015 &end
ANGLE       D          F        ---MU---          ---EPS---          ---ETA---
 90.00      0.015    15.000    1.000  1.680      22.080  0.390      0.238 -0.077

 &data d=0.020 &end
ANGLE       D          F        ---MU---          ---EPS---          ---ETA---
 90.00      0.020    15.000    1.000  1.680      22.080  0.390      0.336 -0.045

 &data d=0.025 &end
ANGLE       D          F        ---MU---          ---EPS---          ---ETA---
 90.00      0.025    15.000    1.000  1.680      22.080  0.390      0.404  0.040

 &data d=0.030 &end
ANGLE       D          F        ---MU---          ---EPS---          ---ETA---
 90.00      0.030    15.000    1.000  1.680      22.080  0.390      0.402  0.141

 &data d=0.035 &end
ANGLE       D          F        ---MU---          ---EPS---          ---ETA---
 90.00      0.035    15.000    1.000  1.680      22.080  0.390      0.352  0.200

 &data d=0.040 &end
ANGLE       D          F        ---MU---          ---EPS---          ---ETA---
 90.00      0.040    15.000    1.000  1.680      22.080  0.390      0.298  0.214

 &data d=0.045 &end
ANGLE       D          F        ---MU---          ---EPS---          ---ETA---
 90.00      0.045    15.000    1.000  1.680      22.080  0.390      0.262  0.203

 &data d=0.050 &end
ANGLE       D          F        ---MU---          ---EPS---          ---ETA---
 90.00      0.050    15.000    1.000  1.680      22.080  0.390      0.242  0.186
```

Table 2-5: Surface impedance η for material OG-C-1 at 15.0 GHz.

some insignt can be gained by looking at the integral expression (2.14) for the scattered field. At large distances from the body, i.e. in the far zone

$$H_1^{(1)}(kr) \sim -iH_o^{(1)}(kr) \sim -i\sqrt{\frac{2}{\pi k\rho}}\, e^{i(k\rho - \pi/4)}\, e^{-ik\hat{\rho}\cdot\underline{\rho}'}$$

and since $\hat{r} \sim \hat{\rho}$, we then have

$$H_z^s(\underline{\rho}) \sim \sqrt{\frac{2}{\pi k\rho}}\, e^{i(k\rho - \pi/4)}\, P$$

where the far field amplitude is

$$P = \frac{k}{4}\int_C \left\{\hat{n}'\cdot\hat{\rho} - \eta(s')\right\} K(s')\, e^{-ik\hat{\rho}\cdot\underline{\rho}'}\, ds' \,. \tag{2.23}$$

The form of this expression suggests three possible procedures for reducing the scattering in some chosen direction $\hat{\rho}$, and these could be employed singly or in combination:

(i) reduce the amplitude of the surface current $K(s')$ over the entire surface of the body,

(ii) adjust the phase of the current to ensure that there is no stationary phase point in the range of integration, and

(iii) choose the surface impedance so that $\hat{n}'\cdot\hat{\rho} - \eta(s')$ is small over the surface.

The first two are the bases for the more conventional approaches to cross section reduction. An absorber does serve to reduce $|K|$, but not always by a sufficient amount to rely on this technique alone. Shaping of the body is directed at the second method, and the elimination of all specular reflections is, in fact, equivalent to the elimination of the stationary phase points associated with the incident field phase. Unfortunately, such shaping may also accentuate surface wave effects. In the case of the ogival cylinder, there is a stationary phase point created by the (backward) traveling wave, and it is then necessary to reduce this portion of the surface field as much as possible.

The third method is more novel. If

$$\eta(s') = \hat{n}' \cdot \hat{\rho} \tag{2.24}$$

at every point of the surface, the scattering will be zero in the direction of $\hat{\rho}$ and (presumably) small in some range of aspects about this direction. The required impedance depends neither on the frequency nor the angle of incidence and is always real, but there is a difficulty: for any closed surface the specification demands a negative real impedance over a portion of the surface. Thus, to suppress the edge-on backscattering from the ogival cylinder, η must vary from 0.21644 (= cos 77.5°) at the front, through zero at the middle, to -0.21644 at the rear. We have verified the validity of the scheme by using program RAMD to compute the bistatic scattering from the ogival cylinder for edge-on incidence ($\phi_o = 180^o$) at a frequency of 2 GHz. The results are shown in Figure 2-17 along with the corresponding curve for the bare body. We observe that the optimum impedance has reduced the scattering at angles within 18° of edge-on, but has increased it by as much as 4 dB at wider angles. We also show the curves for the modulus of the optimum impedance and for a treatment in which the cylinder is left bare where the optimum impedance is negative. Neither impedance is effective and the scattering is even larger than that of the bare body.

Although the optimum surface impedance is non-physical for any finite body of non-zero thickness, one geometry for which it is both realizable and simple is the infinite wedge, and for edge-on incidence in particular, the requirement is that

$$\eta = \sin\Omega$$

where 2Ω is the included angle of the wedge. As we have already noted, the scattering from the front edge of the ogival and wedge cylinders can be analyzed using the infinite wedge as a model, and it is therefore of interest to examine the edge diffraction coefficient for a wedge with arbitrary but constant surface impedances the same on both faces.

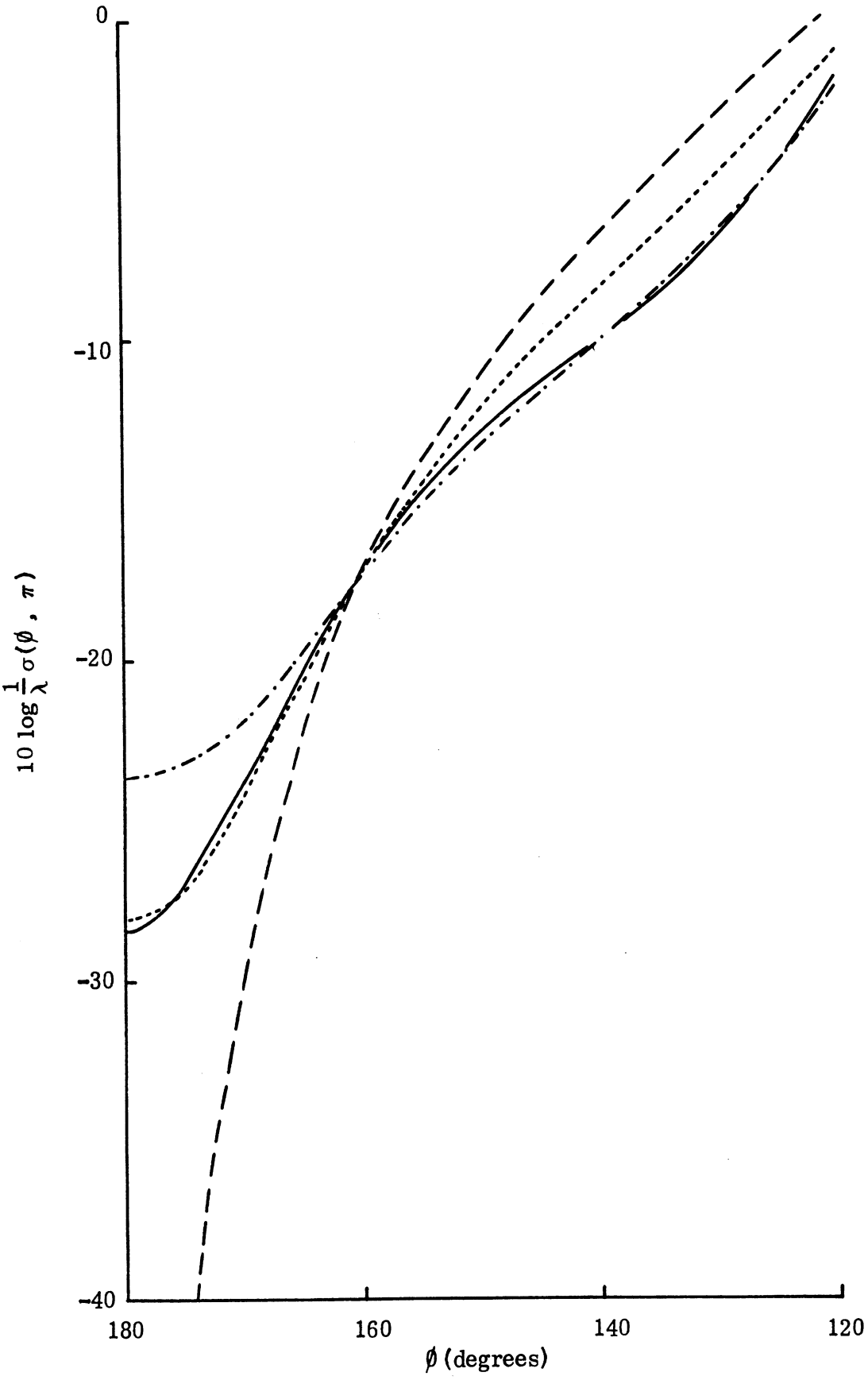

Figure 2-17: Bistatic scattering from the ogival cylinder for $\phi = 180^{\circ}$ at 2 GHz: (——) $\eta = 0$, (– – –) $\eta = \hat{n}' \cdot \hat{\rho}$, (– · – · –) $\eta = |\hat{n}' \cdot \hat{\rho}|$, and (- - - -) $\eta = \max(\hat{n}' \cdot \hat{\rho}, 0)$.

Using the method of Maliuzhinets (1959) it can be shown that for backscattering

$$P(\phi,\phi,\eta) = -\frac{i}{2}\,\frac{\cos^2\frac{1}{\nu}(\pi-\phi)\cos\frac{\pi}{2\nu}}{\nu\sin\frac{\pi}{2\nu}\cos\frac{1}{\nu}(\frac{\pi}{2}-\phi)\cos\frac{1}{\nu}(\frac{3\pi}{2}-\phi)}\left\{\cos\frac{1}{\nu}(\frac{\pi}{2}-\phi)\cos\frac{1}{\nu}(\frac{3\pi}{2}-\phi)-\sin^2\frac{\chi}{\nu}\right\}$$

$$\cdot\, F(\phi,\chi) \qquad (2.25)$$

(Senior, 1977) where

$$\nu = 2(1-\Omega/\pi) \qquad (2.26)$$

$$\eta = \cos\chi$$

and $F(\phi,\chi)$ is expressible in terms of functions defined by Maliuzhinets. In the special case $\eta = 0$ of a perfectly conducting wedge

$$P(\phi,\phi,0) = -\frac{i}{2}\,\frac{\cos\frac{\pi}{2\nu}}{\nu\sin\frac{\pi}{2\nu}\cos\frac{1}{\nu}(\frac{\pi}{2}-\phi)\cos\frac{1}{\nu}(\frac{3\pi}{2}-\phi)}\left\{\cos\frac{1}{\nu}(\frac{\pi}{2}-\phi)\cos\frac{1}{\nu}(\frac{3\pi}{2}-\phi)-\sin^2\frac{\pi}{2\nu}\right\} \qquad (2.27)$$

and hence

$$P\left|\phi,\phi,\eta\right| = \cos^2\frac{1}{\nu}(\pi-\phi)\,\frac{\cos\frac{1}{\nu}(\frac{\pi}{2}-\phi)\cos\frac{1}{\nu}(\frac{3\pi}{2}-\phi)-\sin^2\frac{\chi}{\nu}}{\cos\frac{1}{\nu}(\frac{\pi}{2}-\phi)\cos\frac{1}{\nu}(\frac{3\pi}{2}-\phi)-\sin^2\frac{\pi}{2\nu}}\,F(\phi,\chi)\,P(\phi,\phi,0) \qquad (2.28)$$

Apart from the infinity of $P(\phi,\phi,0)$ in the specular direction $\phi = \frac{\pi}{2}-\Omega$, the expression for $P(\phi,\phi,\eta)$ is finite for all ϕ, $\Omega \le \phi \le \pi$, and is zero if

$$\sin\frac{\chi}{\nu} = \left\{\cos\frac{1}{\nu}(\frac{\pi}{2}-\phi)\cos\frac{1}{\nu}(\frac{3\pi}{2}-\phi)\right\}^{1/2}. \qquad (2.29)$$

This can be solved to find χ and hence η for any given value of ϕ, and for a wedge of half angle 12.5° ($\nu = 67/36$) the impedance necessary to null out the edge-diffracted backscattered field is listed as a function of ϕ in Table 2-6. Over a range of 30° about edge on, the optimum impedance varies from 0.216 to 0.357 and is, of course, real.

ϕ (deg.)	η	ϕ (deg.)	η	ϕ (deg.)	η
180	0.21644	120	0.72613	65	1.57259
175	0.22046	115	0.80194	60	1.63633
170	0.23247	110	0.88005	55	1.69527
165	0.25234	105	0.95976	50	1.74895
160	0.27986	102.5	1	45	1.79690
155	0.31472	100	1.04038	40	1.83876
150	0.35655	95	1.12120	35	1.87417
145	0.40493	90	1.20154	30	1.90284
140	0.45936	85	1.28070	25	1.92456
135	0.51929	80	1.35446	20	1.93913
130	0.58415	75	1.43286	15	1.94645
125	0.65331	70	1.50458	12.5	1.94737

Table 2-6: Impedance for zero backscatter at angle θ.

To compute the width of the null and/or the effect of an impedance which is not real, it is necessary to know the function $F(\phi, \chi)$. Although this can be determined for a wedge of any angle, its expression is tractable only if ν is the quotient of two integers whose numerator is odd. An example is a wedge of half angle $\Omega = 15^{\circ}$ for which $\nu = \frac{11}{6}$, and since this is similar to the wedge appropriate to our cylinders, it is worthwhile to examine it in detail. As shown by Senior (1977), we then have

$$F(\phi, \chi) = \left\{ \frac{f(\frac{17}{12}\pi)\, f(\frac{17}{12}\pi)\, f(\frac{5}{12}\pi)\, f(\frac{5}{12}\pi)}{f(\chi - \phi + \frac{23}{12}\pi)\, f(\chi + \phi - \frac{23}{12}\pi)\, f(\chi - \phi + \frac{\pi}{12})\, f(\chi + \phi - \frac{\pi}{12})} \right\}^2 \tag{2.30}$$

where

$$f(\alpha) = \sec\frac{\alpha}{22}\;\frac{\prod_{p=1}^{3}\left\{\cos\frac{\alpha}{11}+\cos\frac{2p-1}{11}\pi\right\}\prod_{p=1}^{6}\left\{\cos\frac{\alpha}{11}+\cos\frac{6p-10}{33}\pi\right\}}{\prod_{p=1}^{2}\left\{\cos\frac{\alpha}{11}+\cos\frac{2p}{11}\pi\right\}\prod_{p=1}^{5}\left\{\cos\frac{\alpha}{11}+\cos\frac{6p-7}{33}\pi\right\}}\,. \qquad (2.31)$$

The impedance necessary to null out the backscattering in the direction ϕ is

$$\eta = \cos\left(\frac{11}{6}\sin^{-1}\left\{\cos\frac{6}{11}\left(\frac{\pi}{2}-\phi\right)\cos\frac{6}{11}\left(\frac{3\pi}{2}-\phi\right)\right\}^{1/2}\right) \qquad (2.32)$$

and the values for $\phi = 180^{\circ}\ (-5^{\circ})\ 150^{\circ}$ are as follows:

ϕ (deg.)	η	ϕ (deg.)	η
180	0.25882	160	0.32267
175	0.26287	155	0.35771
170	0.27497	150	0.39973 .
165	0.29498		

Over this range of ϕ the average backscattering is a minimum if the null is located at $\phi = 165^{\circ}$. The corresponding impedance is 0.29498 and the edge diffraction coefficient is plotted as a function of ϕ in Figure 2-18. For $180^{\circ} \geq \phi \geq 150^{\circ}$ the cross section reduction averages 16.8 dB, but much of this effect is lost if the impedance is complex. This is evident from the curves for $\eta = 0.29498 \exp(\pm i\gamma)$ with $\gamma = \pi/6$, $\pi/3$ and $\pi/2$ which are included in Figure 2-18. If $\gamma = \pi/6$ the average cross section reduction over the same range of aspects is only 9.8 dB and if $\gamma = \pi/2$ (reactive impedance) the scattering actually exceeds that of the bare body.

In contrast to edge diffraction, reduction of a traveling wave contribution is not so critical in its specification of the required impedance. Indeed, there is no optimum impedance per se and it matters little whether the impedance is real or not. Since the wave travels over the surface of the body before and after reflection at the rear edge, any coating that will adequately attenuate the wave will suffice. For ogival cylinders with a uniform surface impedance η, computations have shown that the backscattering cross section in the direction of the first traveling wave lobe

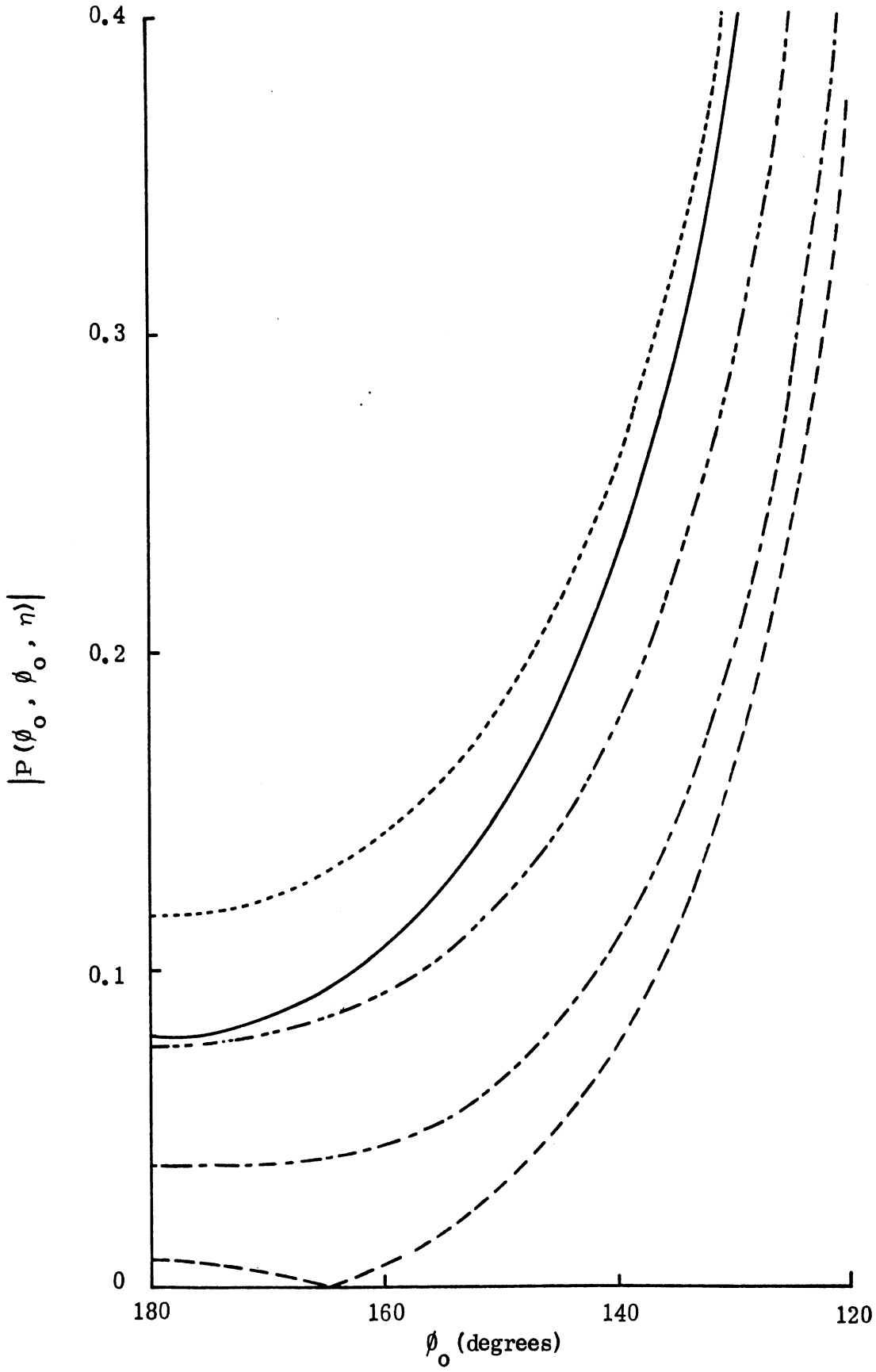

Figure 2-18: Edge diffraction coefficient for backscattering from a wedge having $\Omega = 15^o$: (——) bare wedge, (– – –) $\gamma = 0$, (— – —) $\gamma = \pi/6$, (— – – —) $\gamma = \pi/3$, (– – – –) $\gamma = \pi/2$, where $\eta = 0.29498 \exp(\pm i\gamma)$.

is roughly proportional to

$$\exp\left(-0.7\, ks_{max}\, \mathrm{Re} \cdot \eta\right)$$

and to achieve a 20 dB reduction requires only that

$$\mathrm{Re} \cdot \eta \gtrsim \lambda / s_{max} . \tag{2.33}$$

The imaginary part of η appears to have little effect apart from a slight change in the electrical length of the body with a resulting change in the phase of the traveling wave contribution.

If the condition (2.33) can be satisfied at all frequencies of interest, it may then be possible to coat only a portion of the body. Coatings applied to the rear half of an ogival cylinder were examined by Knott and Senior (1973). They showed the importance of extreme care in fairing in the leading edge of the absorber and arrived at an 'optimum' impedance specification of the form $\eta \propto (s - \frac{1}{2} s_{max})^2$ where s is the surface distance measured from the front of the cylinder. It will be observed that this places the maximum impedance at the rear edge where the traveling wave reflection occurs. To reduce the front edge contribution as well requires an impedance of about 0.3 in the vicinity of this edge, and an impedance which would be effective in reducing both types of scattering is one which starts at 0.3, increases slowly over the front half of the body, and then more rapidly over the rear. Indeed, for a body of adequate electrical length for which the two main contributors to the scattering are (or can be made) substantially independent of one another, it is possible to pose a true optimization problem in which the task is to determine the impedance variation for a maximum average cross section reduction over some range of aspects subject to a limitation on the maximum value of the impedance available.

Unfortunately, such considerations are irrelevant as regards the present problem. At the lowest frequency of interest, the ogival cylinder is only 0.807λ in length, and to satisfy the condition (2.33) now requires that $\mathrm{Re} \cdot \eta \gtrsim 1.2$. Even for a coating of the maximum allowed thickness, none of the materials available provide

an impedance greater than about 0.2 at 2 GHz, and complete coverage of the body would now reduce the traveling wave return by only 3 dB. The constraints provided by the lower frequencies effectively prohibit anything other than a coating of maximum thickness over almost the entire surface of the body, the only departure being in the immediate vicinity of the front edge. Even for the front edge contribution precise control is no longer possible because of its secondary excitation by the residual traveling wave. The combination of the direct and secondary excitations now produces a front edge return which is frequency resistive for all of the impedance values available to us, and provided the edge impedance does not exceed about 0.3, there is no evidence that one value is better than another.

CHAPTER 3

SPECIFICATION OF A COATING

To describe the procedures that were followed to arrive at effective coatings for the bodies, it is convenient to follow a chronological approach.

At the outset of the program we had no precise knowledge of the impedances presented by the materials available, and our first task was to explore the performance of various impedance specifications to determine that which would be most effective. Then, as the properties of the available materials were measured, it became apparent what impedance magnitudes could be realized, and our objective changed from a specification of impedance to the specification of a layer of the most promising material. The entire study was numerical and based on an ogival cylinder whose length was extended to simulate the increase in size resulting from the application of a coating of about 50 mils thickness. The dimensions of the extended body are as follows:

wedge half angle :	$\Omega = 13.065^{o}$
surface radius :	$R = 10.942$ inches
overall length :	$\ell = 4.947$ inches
surface length, top :	$s_{max} = 4.991$ inches .

3.1 Impedance Specification

Four types of surface impedance variation were initially considered, all of them at a frequency of 3.75 GHz. They were

$$\eta = \eta_{max} \left(\frac{s}{s_{max}} \right)^{m}$$

for $m = 0$ (uniform coating), $m = 1/2$, $m = 1$ (linear variation) and $m = 2$ (quadratic variation), and for $\eta_{max} = 0.2(0.2)1.0$, where s is the surface distance along the ogive measured from the front. Backscattering patterns were computed in each case, and the values of $10 \log \sigma/\lambda$ in the broadside specular ($\phi = 90^{o}$), peak traveling wave ($\phi = 144^{o}$) and edge-on ($\phi = 180^{o}$) directions are plotted as functions of η_{max} in

Figures 3-1 through 3-3 respectively. We observe that in the broadside and traveling wave directions the uniform coating which "puts most material on the body" is by far the best. At edge-on, the uniform coating is best only for $\eta_{max} < 0.33$ (we did not explore the behavior for $\eta < 0.2$). With increasing $\eta_{max} > 0.33$ it becomes inferior to all the other coatings (and actually raises the edge-on return if $\eta_{max} > 0.57$), and the $s^{1/2}$ variation is then the best.

These are quite different from the findings of Knott and Senior (197) at a frequency equivalent to 7.5 GHz, but it must be recalled that the coatings were then applied only to the rear half of the ogival cylinder. To avoid the potentially large scattering from the leading edge of the absorber, it was found necessary to have the first and second derivatives of $\eta(s)$ zero there, forcing us to the s^2 variation of the impedance. By covering the entire ogive we are able to circumvent this difficulty.

Since all of the coatings used are reasonably effective in reducing the traveling wave contribution, particularly for the larger values of η_{max}, attention was now directed at the front edge or 'tip' contribution. From an analysis of a uniform impedance wedge (see Section 2.4), the optimum impedance for edge-on incidence is $\eta = \sin\Omega$, implying $\eta = 0.21644$ for $\Omega = 12.5^{o}$. To see if there is any improvement in performance by starting all of our tapered coatings with this non-zero value of η at the edge, we considered

$$\eta = \eta_{tip} + \left(\eta_{max} - \eta_{tip}\right)\left(\frac{s}{s_{max}}\right)^{m}$$

for m = 1/2, 1 and 2 with $\eta_{max} = 0.4(0.2)1.0$ and $\eta_{tip} = 0.216$. The results are shown as broken curves in Figures 3-1 through 3-3, and are not particularly surprising. The greater amount of material on the body reduces the broadside and traveling wave returns compares with the values previously attained for the corresponding η_{max}; and at edge-on the scattering is now almost independent of η_{max}, suggesting that the tip is the dominant contributor. However, in the important traveling wave direction the uniform coating is still superior.

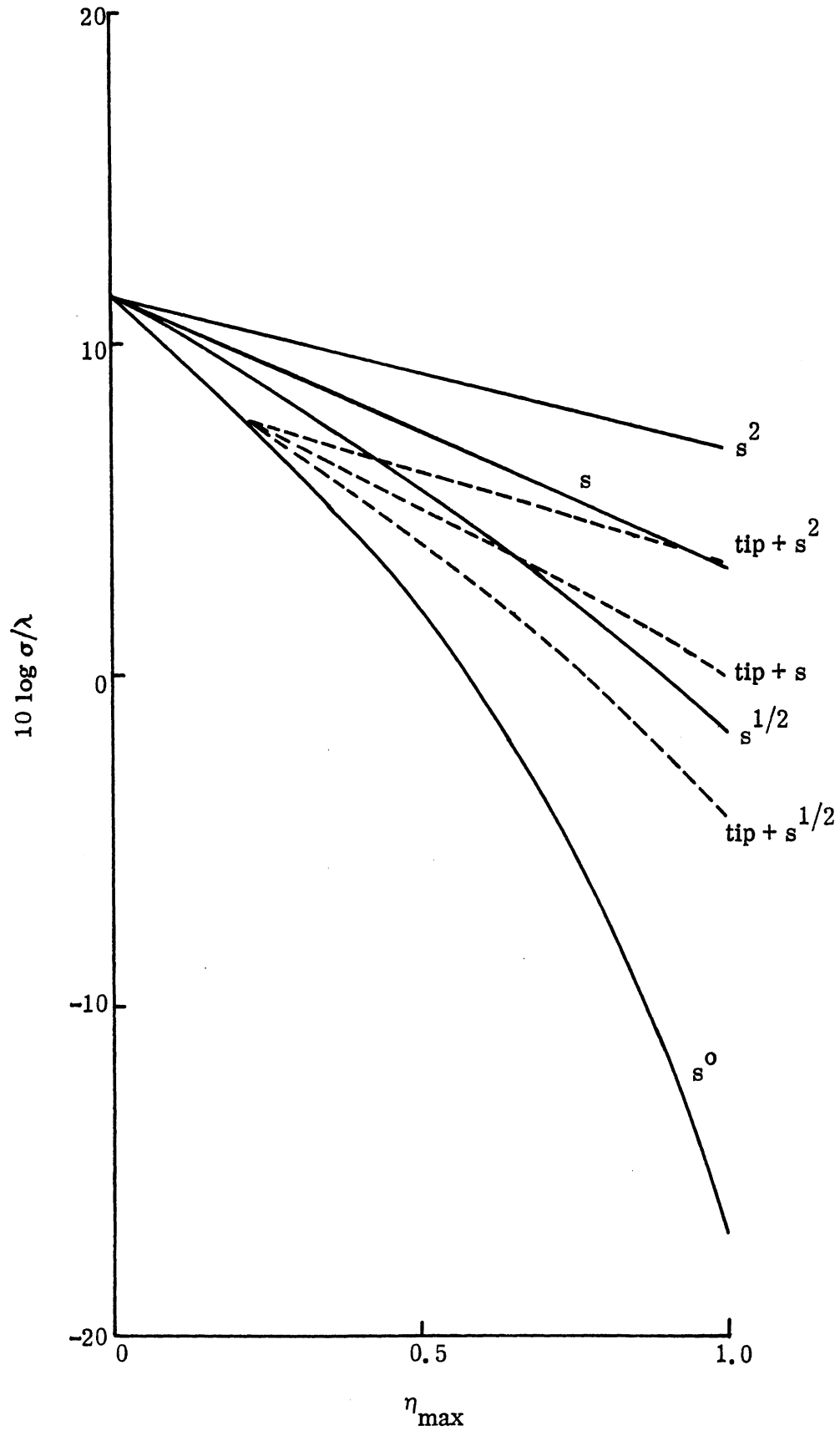

Figure 3-1: Broadside backscattering for different coatings.

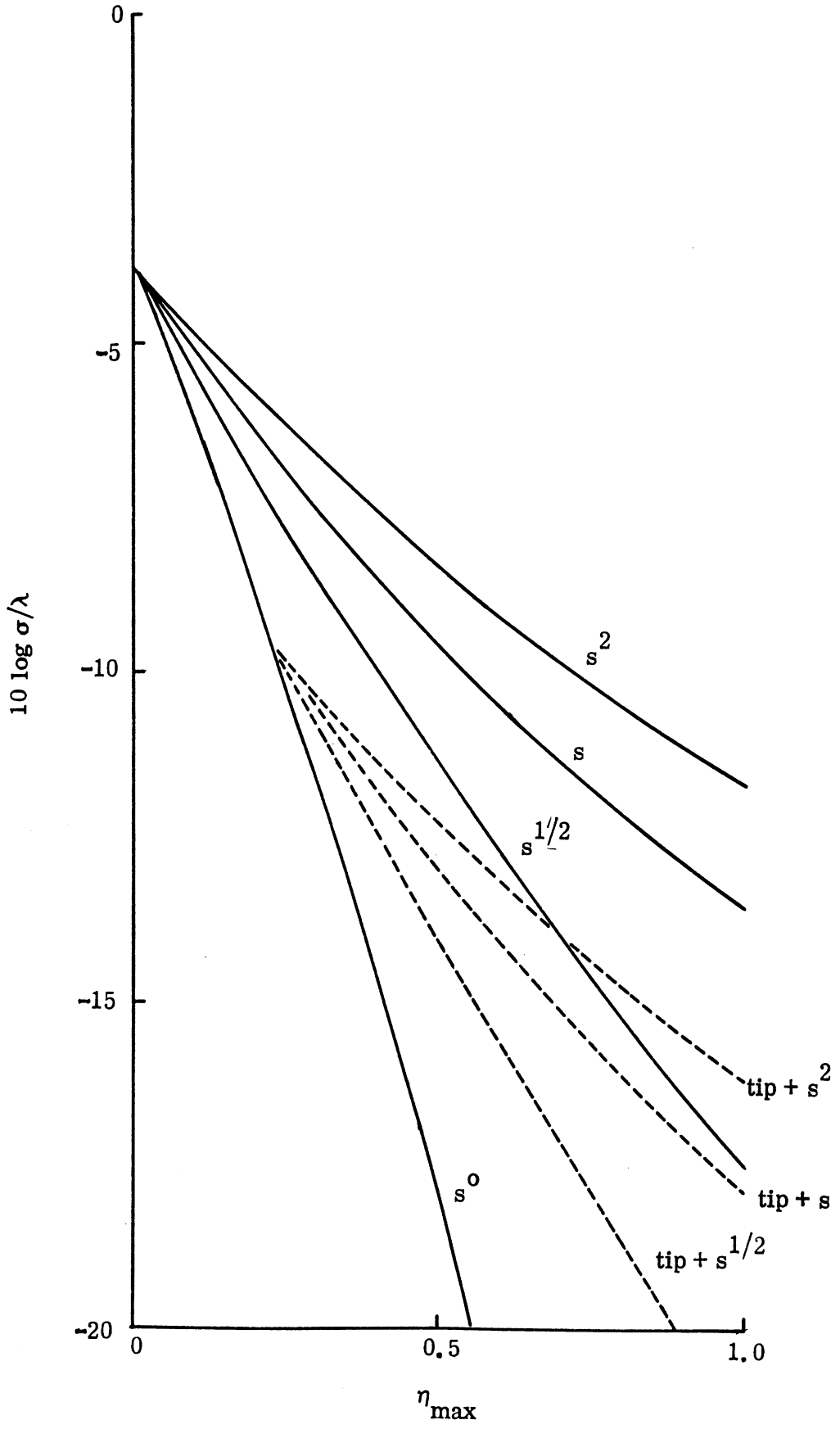

Figure 3-2: Traveling wave peak returns for different coatings.

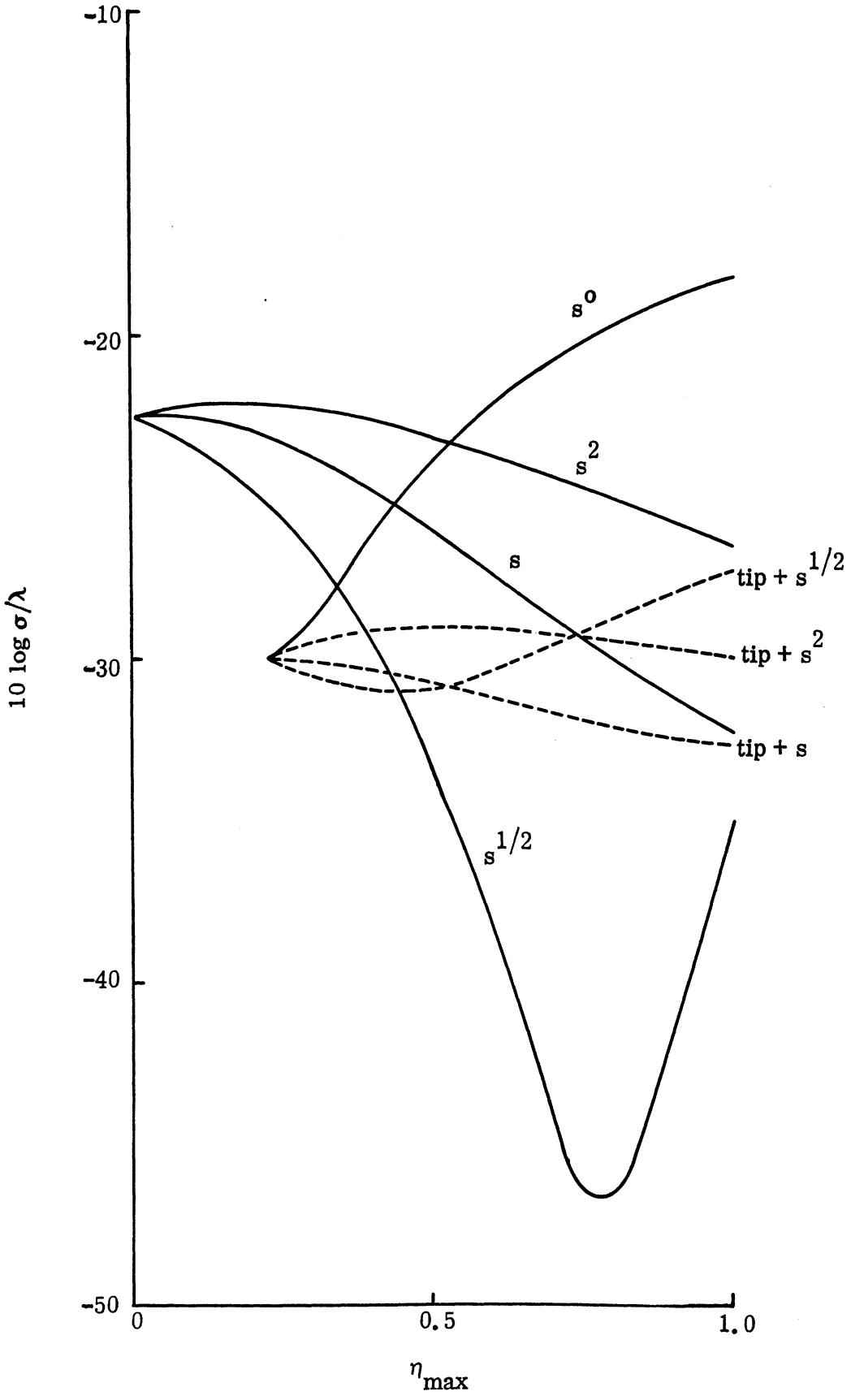

Figure 3-3: Edge-on backscattering for different coatings.

It seemed likely that we could improve the edge-on capability of a uniform coating whilst retaining its performance in other directions by tapering the impedance down to a pre-assigned level at the tip. To pursue this idea, we selected the case $\eta_{max} = 0.4$ and replaced the impedance over the first inch of the surface by a sinusoidal taper. The actual impedance variation used was

$$\eta = \eta_{tip} + \left(\eta_{max} - \eta_{tip}\right) \sin\left(\frac{\pi s}{2s_1}\right) , \qquad 0 \leq s \leq s_1$$

$$= \eta_{max} , \qquad s_1 \leq s \leq s_{max}$$

with s = 1 inch and $\eta_{max} = 0.4$. We first tried $\eta_{tip} = 0.214$ and then progressively reduced η_{tip} in steps of 0.01 until the edge-on cross section had bottomed out. The reduction in η_{tip} produced a very slight (0.09 dB) increase in the broadside cross section, a somewhat larger (0.73 dB) increase in the traveling wave peak, but a substantial (8.95 dB) reduction in the edge-on return. The edge-on and traveling wave cross sections are plotted as functions of η_{tip}, $0.094 \leq \eta_{tip} \leq 0.214$, in Figure 3-4, with the values for $\eta_{tip} = 0$ and 0.4 (uniform coating) included for comparison.

The backscattering pattern for the optimum tip ($\eta_{tip} = 0.104$) is plotted in Figure 3-5 as a function of angle, $130^o \leq \phi \leq 180^o$ along with the corresponding curves for the bare body and the uniform ($\eta = 0.4$) coating. The 'optimum' tip would certainly seem to have had a desirable effect and the average cross section reduction (straight dB averaging every 5^o over a 30^o range) is 14.6 dB compared with the 7.2 dB provided by the uniform coating. However, these figures are a little misleading since most of the energy is in the traveling wave lobe. If, instead, we compute the total scattered power over the 30^o range by converting the dB to actual powers and then sampling every 4^o, we find that the optimum tip provides a reduction of 10.8 dB in the bare body return, while the uniform coating gives 9.4 dB. On this criterion, the optimally-tapered tip provided only a small improvement, most of which could also have been obtained by tapering the impedance to zero. The 0-tip pattern is included in Figure 3-5, and though the cross sections in the edge-on

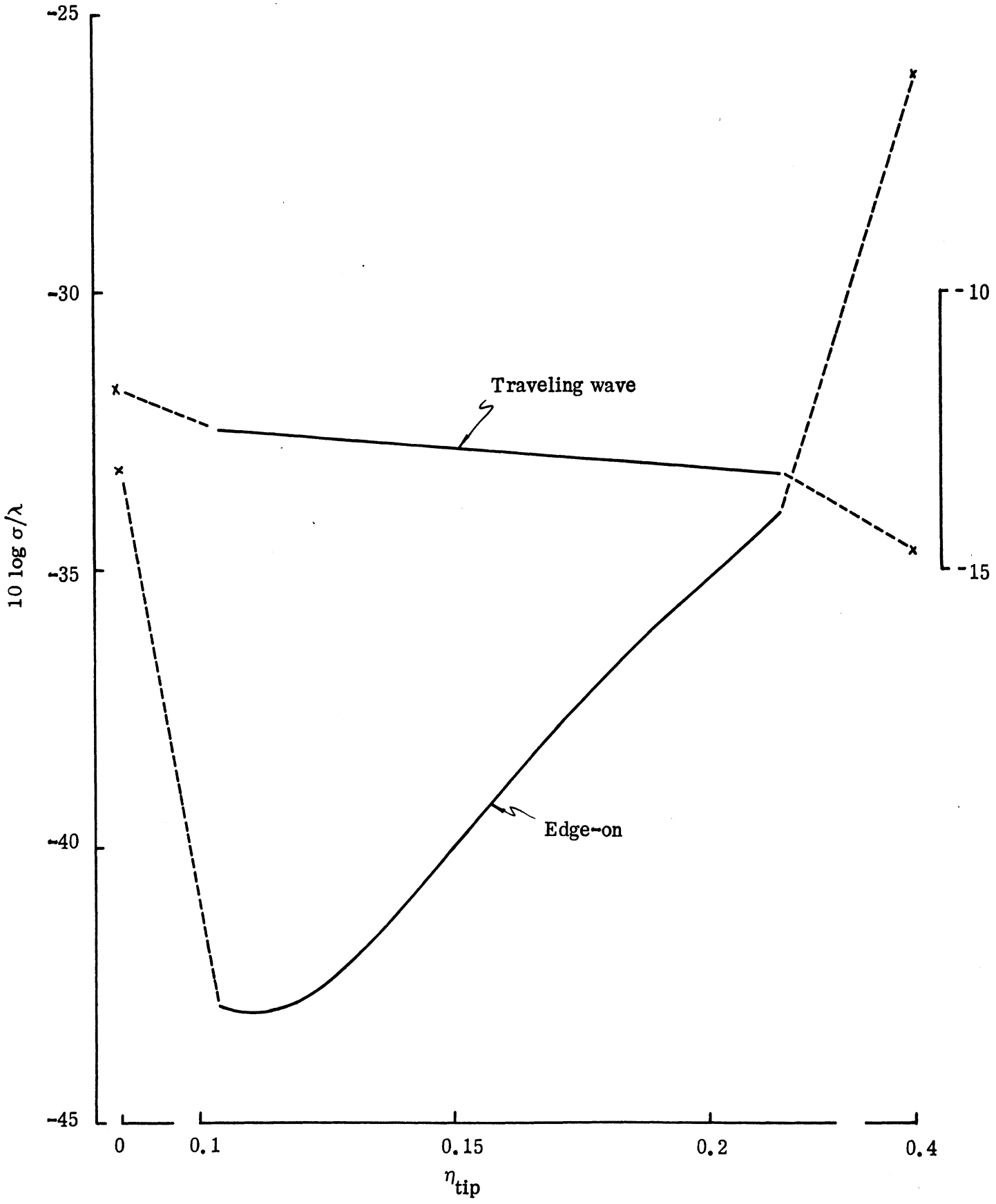

Figure 3-4: Effect of tip taper on uniform coatings ($\eta = 0.4$).

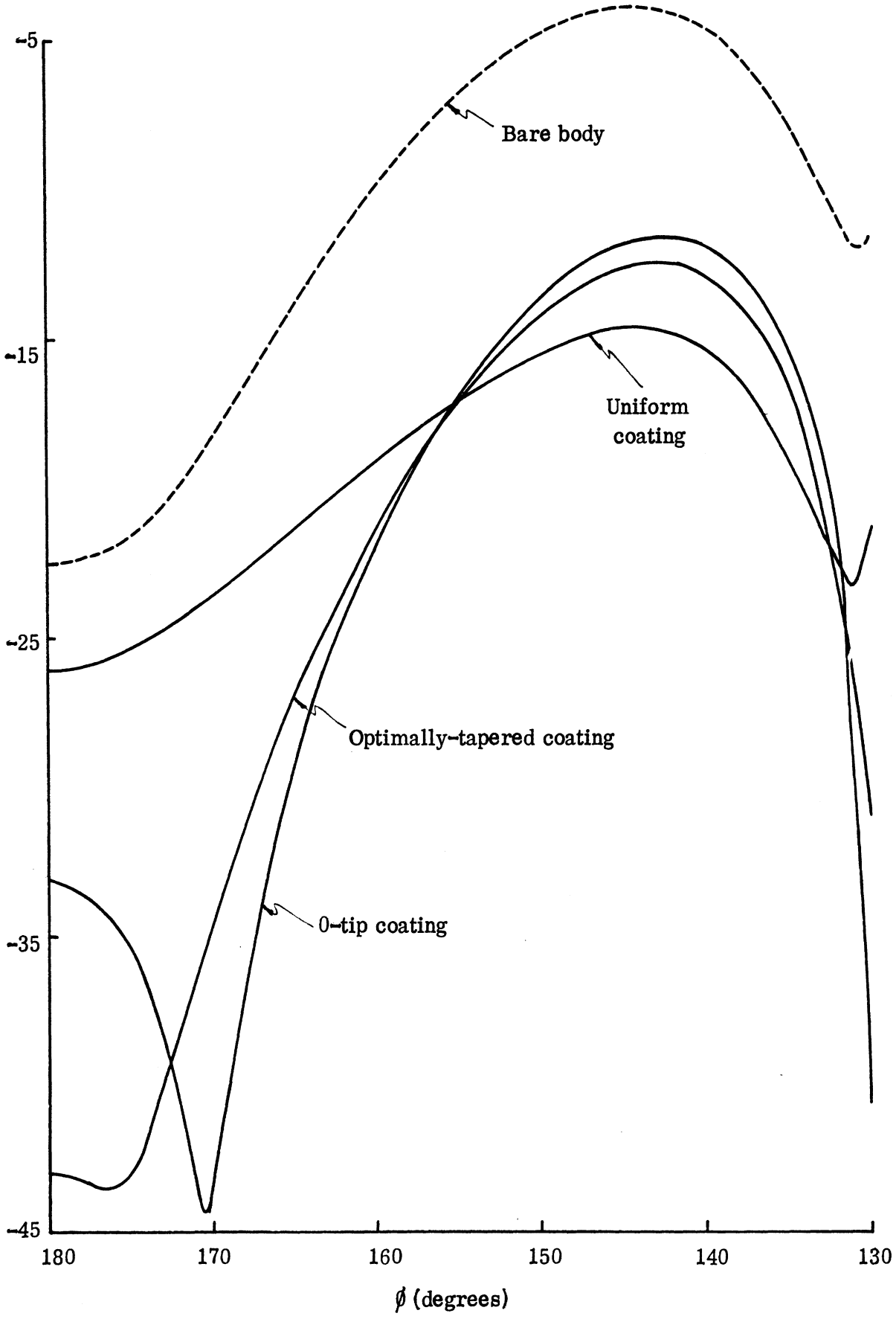

Figure 3-5: Scattering cross sections for $\eta_{max} = 0.4$.

and traveling wave directions both exceed the values provided by the optimally-tapered coating, the total power reduction of the bare body scattering is only 0.3 dB less.

Apart from the difficulty of fabricating an optimally-tapered coating, it was apparent that the optimum tip value is highly frequency sensitive because of the phasing between the direct tip scattering and that which is traveling wave induced. This conclusion was reached from a consideration of the near edge-on scattering behavior and was reinforced by the results of computations for complex surface impedances. For these tests we chose a complex impedance suggested by the values for material OG-C-1 whose properties had just become available. By scaling the impedance in Table 2-2 for a coating 50 mils thick at grazing incidence so as to obtain an impedance whose real part is 0.4, we have

$$\eta = 0.4 - i0.201 = 0.4(1 - i\alpha)$$

with $\alpha = 0.5025$. When the previous tapering experiments were repeated with this impedance, we were unable to locate a value of Re. η_{tip} at which the edge-on cross section 'bottomed out'. Indeed, the minimum for Re. $\eta_{tip} \geq 0$ was obtained with $\eta_{tip} = 0$. In Table 3-1 we list the cross sections for edge-on, traveling wave peak and broadside directions for a series of Re. η_{tip}, along with the total scattered power reductions computed as before.

Re. η_{tip}	Edge-on	Tr. wave	Broadside	Total power
0	-33.51	-12.83	4.70	-10.2
0.05	-31.47	-12.96	4.63	-9.6
0.10	-29.25	-13.09	4.57	-8.9
0.15	-27.31	-13.20	4.51	-8.3
0.4	-21.11	-13.68	4.21	-5.6
bare	-22.44	-3.88	11.67	---

Table 3-1: Effect of tapering the impedance $\eta = 0.4(1 - i\alpha), \alpha = 0.5025$.

The 0-tip coating is now markedly superior to the uniform coating. It is, in effect, the optimum coating for this material, and yields a total power reduction which is almost the same as the best that was achieved with η real. The scattering patterns for the uniform and 0-tip coatings of this material are shown in Figure 3-6.

3.2 Coating Specification

From the expression (2.20) for the impedance of a single layer, it is easy to discern the properties desired in a coating material. If $\left|kd\sqrt{\epsilon\mu}\right| << 1$,

$$\eta \simeq -ikd\mu$$

and to get Re. η large the material must have high magnetic loss. This is particularly important at the lowest frequencies of interest, and to have Re. $\eta > 0.5$ at 2 GHz with a layer only 50 mils thick requires Im. $\mu > 9.4$. To maintain the same cross section reduction capability at all frequencies (as regards, for example, the front edge contribution), η should be constant over the band and this would be true if ϵ and μ were each inversely proportional to frequency. In practice, however, we could accept some reduction in Re. η with increasing frequency because of the increasing electrical size of the body, and this suggests the possibility of seeking a material which resonates at the lowest frequency.

Unfortunately these properties are hard to achieve, and of the materials that were measured, none had values of Re. η in excess of 0.6, with even 0.2 being difficult to attain at 2 GHz. All that we could now do was to select the best of the materials that were available and attempt to optimize its application to the cylinders. Because of its magnetic loss the material chosen was OG-C-1 whose relative permittivity and permeability at each of the four designated frequencies are listed on p. 32. Henceforth our optimization procedures were aimed at specifying the thickness d of a coating of this material and we started by paralleling our previous investigation of real impedances at 3.75 GHz.

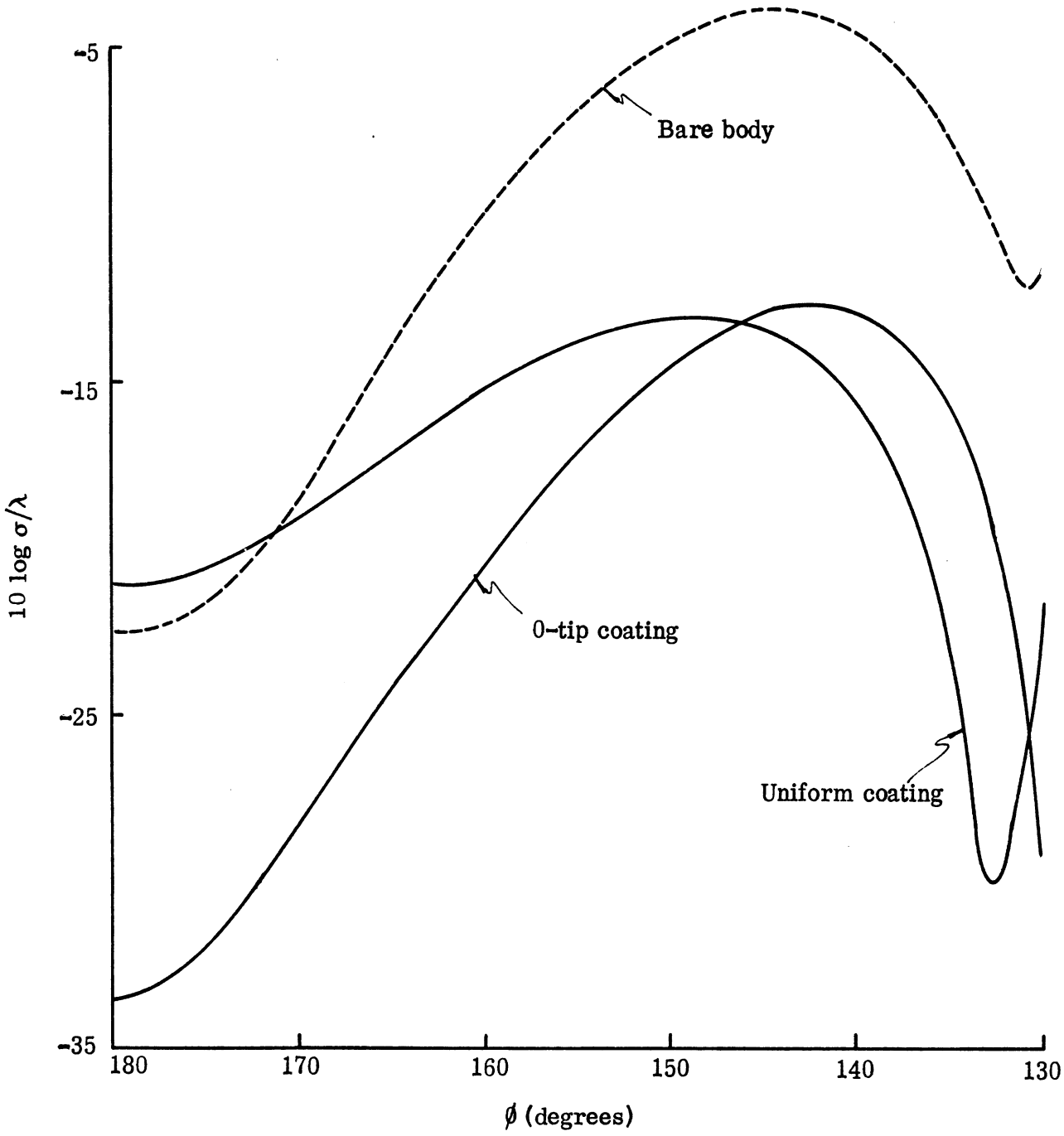

Figure 3-6: Scattering cross sections for $\eta_{max} = 0.4 - i0.201$.

Program RAMD was run for coatings of the OG-C-1 material having the following thicknesses:

$$d = d_{max} \left(\frac{s}{s_{max}} \right)^2 ,$$

$$d = d_{max} ,$$

$$d = \begin{cases} d_{max} \sin \dfrac{\pi s}{2 s_1} & 0 \leq s \leq s_1 \\ \text{for} & \\ d_{max} & s_1 \leq s \leq s_{max} \end{cases}$$

where $d_{max} = 0.050$ inches

and $s_1 = 1.0$ inches .

The three coatings will be referred to as the s^2 , uniform and 0-tip coatings respectively. The thickness variation was specified as an input to the program, and the corresponding values of the surface impedance were determined using the single layer subroutine described in Appendix B. The resulting scattering patterns are plotted in Figure 3-7 along with the pattern for the bare body. The cross section reductions achieved are summarized in Table 3-2 and we note the superiority of the 0-tip coating.

Coating	Edge-on	Tr. wave	Broadside	Total power
s^2	1.90	-2.20	-2.19	-2.2
Uniform	2.66	-11.11	-9.87	-6.2
0-tip	-12.74	-10.90	-8.92	-13.1

Table 3-2: Performance of material OG-C-1 at 3.75 GHz.

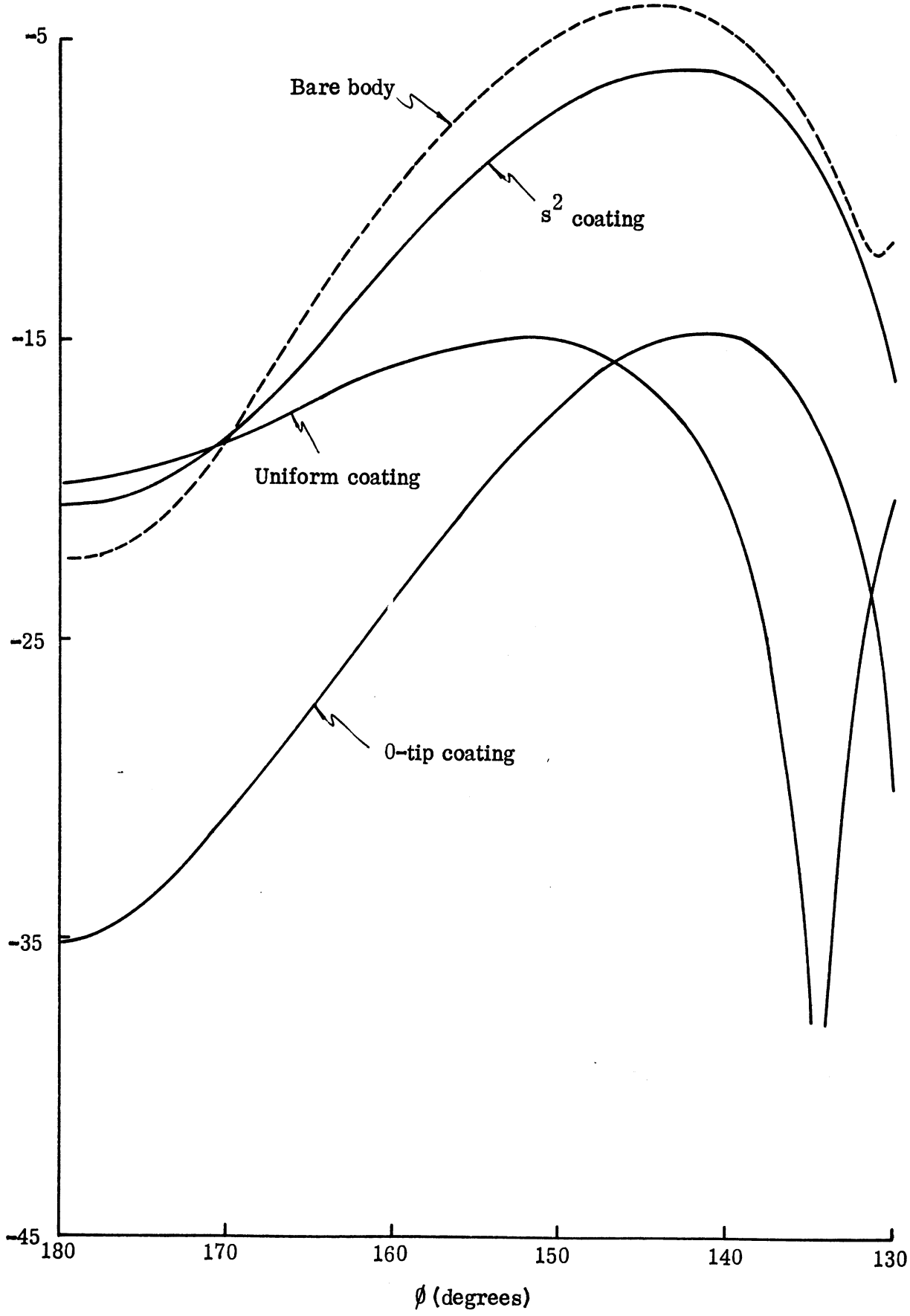

Figure 3-7: Scattering cross sections for material OG-C-1 at 3.75 GHz.

To explore the effect of a change in the length s_1 of the tapering distance, we also ran the program for $s_1 = 0(0.25)1.5$ inches. The case $s_1 = 0$ is, of course, the uniform coating. The cross sectional changes relative to the bare body are plotted in Figure 3-8. The traveling wave peak for the bare body occurs at $\phi = 144^o$, but since the presence of the coating displaces the peak (from 152^o for $s_1 = 0$ to 142^o for $s_1 = 1.5$), we have simply compared the peak return wherever it occurs with the bare body peak in computing the cross section change. The calculation for the total power was carried out as previously described. We conclude from Figure 3-8 that a taper length of about one inch is optimum at this frequency and provides between 11 and 13 dB reduction in those features which are significant in the aspect region about edge-on (see Figure 3-9).

To see whether this choice is also the best at other frequencies we now repeated the experiment starting with the frequency 2.5 GHz at which the edge and traveling wave contributions to the bare body scattering are in phase for edge-on incidence. The relative permittivity ϵ and permeability μ used were

$$\epsilon = 22.46 + i\,0.31\,, \qquad \mu = 4.80 + i\,3.24$$

in accordance with the data measured by the Avionics Laboratory. For the bare body the traveling wave peak occurs at approximately 136^o and Figure 3-10 shows the change in the cross sections at edge-on incidence ($\phi = 180^o$), in the direction of the traveling wave peak ($\phi = 136^o$), at broadside ($\phi = 90^o$) and based on the total power, as a function of the taper length s_1 in inches. The traveling wave peak is a minimum for $s_1 \simeq 0.75$, but the minimum of the edge-on return does not occur until $s_1 \simeq 1.30$. Since we have computed the total power only over a range of 30^o from edge-on, the total power is more affected by the edge-on return, and its minimum occurs at $s_1 \simeq 1.55$. However, this is probably due as much to phase cancellation as to the actual reduction of the two contributors involved, and there is no more than about 1 dB improvement resulting from the use of any taper lengths other than one inch. From $s_1 = 1$ inch, the total power and traveling wave reductions obtainable are between 4 and 5 dB, and the scattering pattern for this coating is compared with that of the bare body in Figure 3-11.

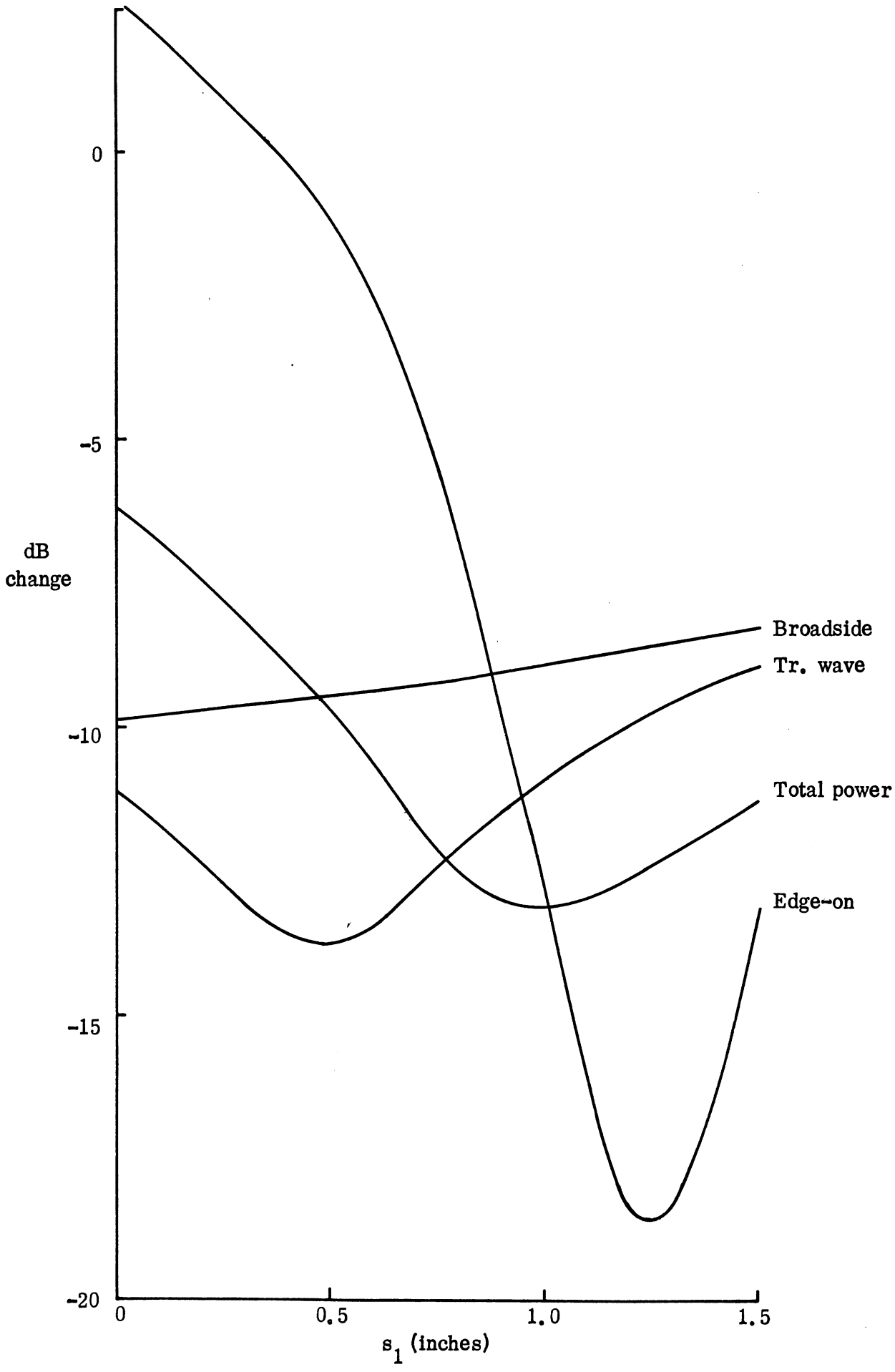

Figure 3-8: Effect of taper length for material OG-C-1 at 3.75 GHz.

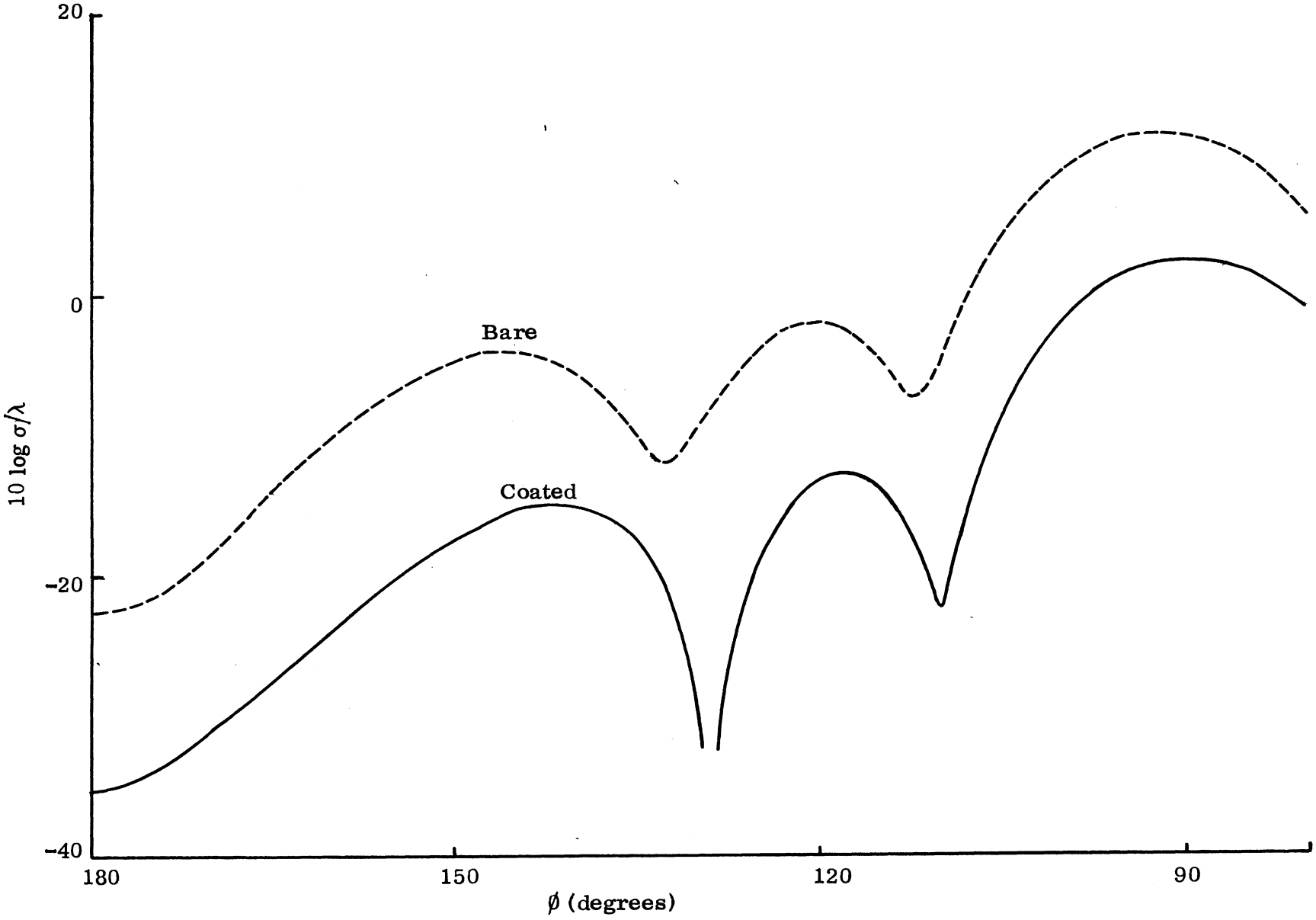

Figure 3-9: Effect of OG-C-1 coating with $s_1 = 1$ inch at 3.75 GHz.

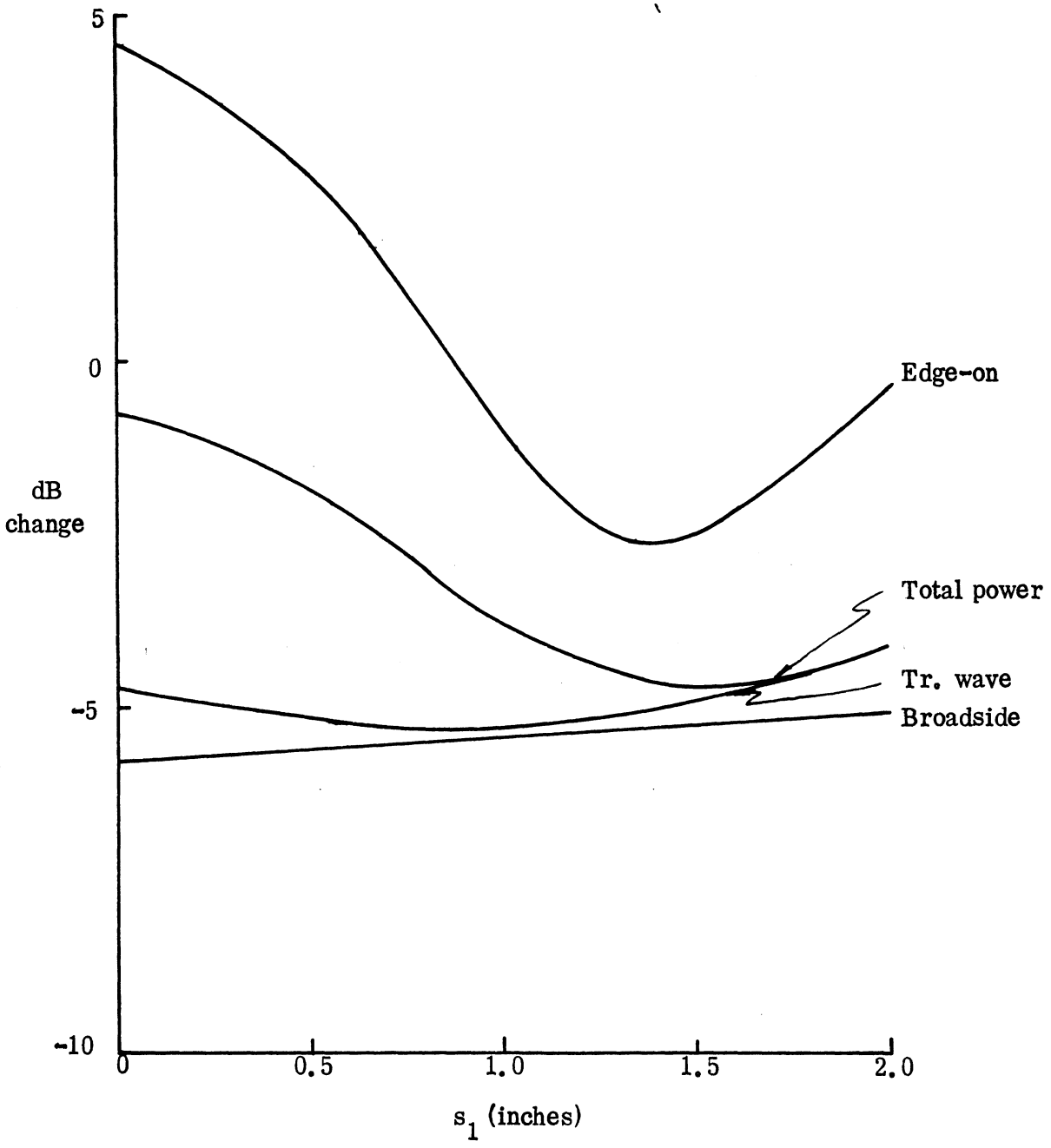

Figure 3-10: Effect of taper length for material OG-C-1 at 2.5 GHz.

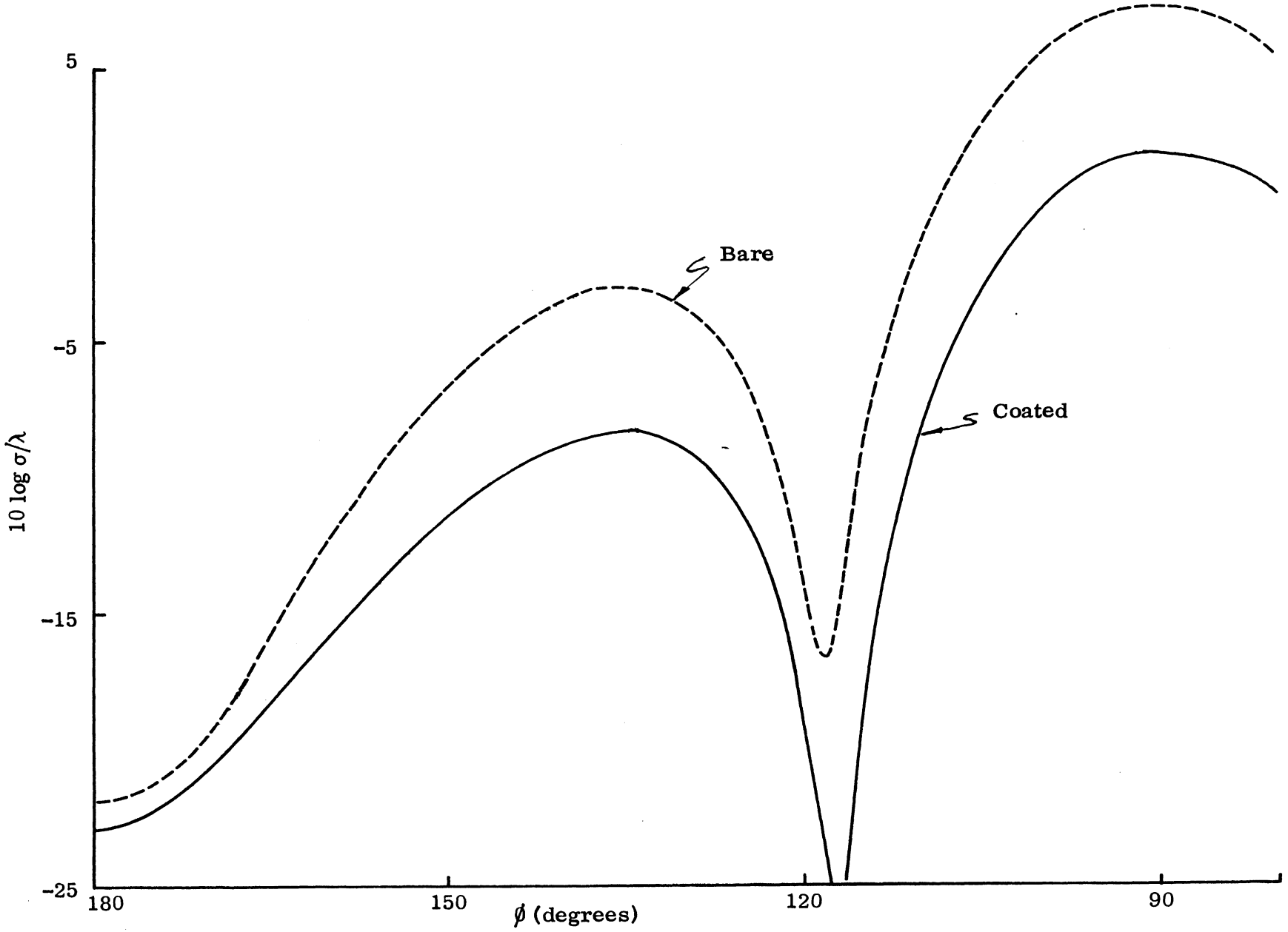

Figure 3-11: Effect of OG-C-1 coating with s_1 = 1 inch at 2.5 GHz.

At 2 GHz, on the other hand, the same coating is almost completely ineffective (see Figure 3-12). Because the two bare body contributors are nearly out of phase at edge-on incidence, the coating actually raises the edge-on cross section by 3 dB and the total power reduction over the 0 to 30^{o} aspect range is only 0.4 dB.

Similar computations were also performed at 7.5 GHz for which the edge and traveling wave contributions are again in phase for edge-on incidence on the bare body and the cross sectional changes for $s_1 = 0(0.25)1.0$ inches are shown in Figure 3-13. The traveling wave peak now occurs at $\phi = 154^{o}$. The decrease in the broadside return with increasing s_1 is due to the fact that the specular and edge contributions to the bare (extended) body scattering for $\phi = 90^{o}$ are almost out of phase at this frequency (see Knott and Senior, 1974): the precise out of phase situation occurs at 7.820 GHz, and it is therefore not surprising that the increase in the specular contributor resulting from the increase in s_1 (less material on the surface) can actually produce a decrease in the scattering at $\phi = 90^{o}$.

The improvement in behavior produced by the taper is somewhat less than at 3.75 GHz. The various curves have minima that occur at smaller values of s_1 and for the traveling wave the minimum is actually at $s_1 = 0$ (uniform coating). The best overall performance is obtained with $s_1 \simeq 0.5$ inches, but it is not significantly better than that achieved with $s_1 = 1.0$ inches. Although the edge-on reduction for $s_1 = 1.0$ inches is only 5 dB, we remark that the edge-on return for the bare body is itself low, and this choice of taper length is sufficient to produce 14 to 16 dB reduction in those features of the scattering which are of most concern. The patterns of the bare and coated bodies are shown in Figure 3-14.

As evident from Figure 3-14, there is still a significant traveling wave contribution, but to see whether the entire lobe centered on $\phi = 154^{o}$ is due to the traveling wave alone, we have examined the surface fields for the above series of coatings. By looking at the magnitudes of the currents for $\phi_o = 154^{o}$ over that portion of the upper surface where the rearmost oscillation occurs, the forward traveling wave amplitude can be deduced from the levels of the maximum and minimum in the

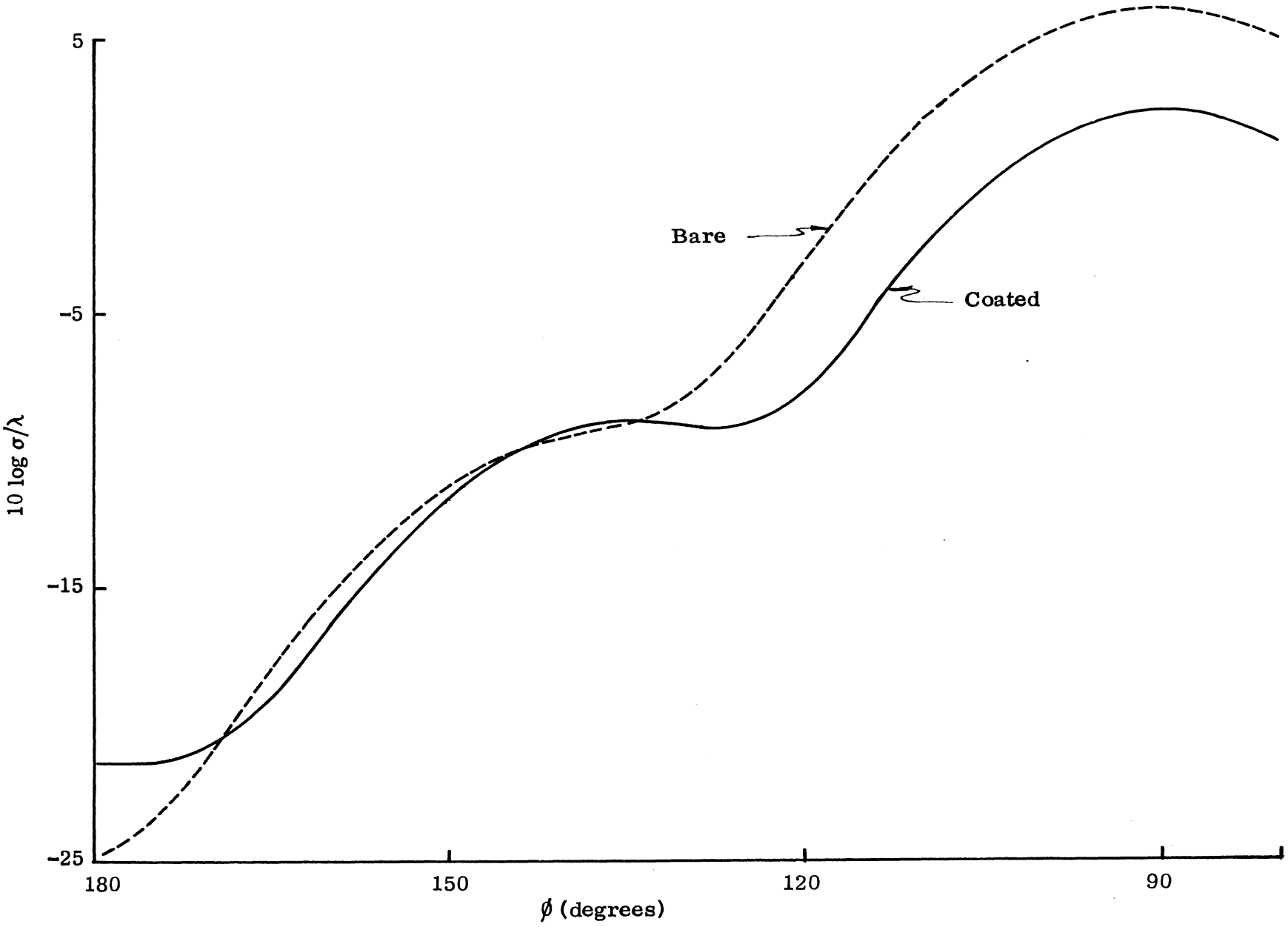

Figure 3-12: Effect of OG-C-1 coating with s_1 = 1 inch at 2 GHz.

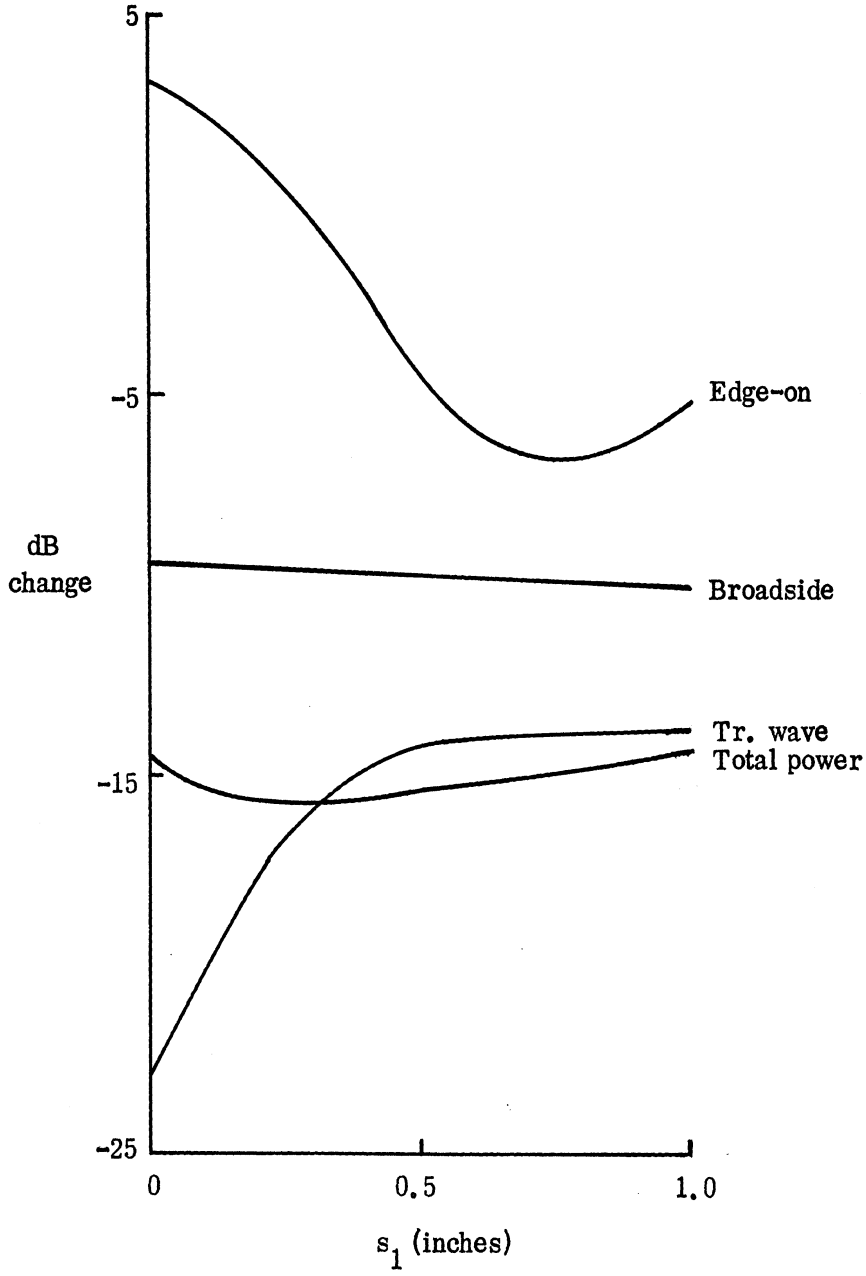

Figure 3-13: Effect of taper length for material OG-C-1 at 7.5 GHz.

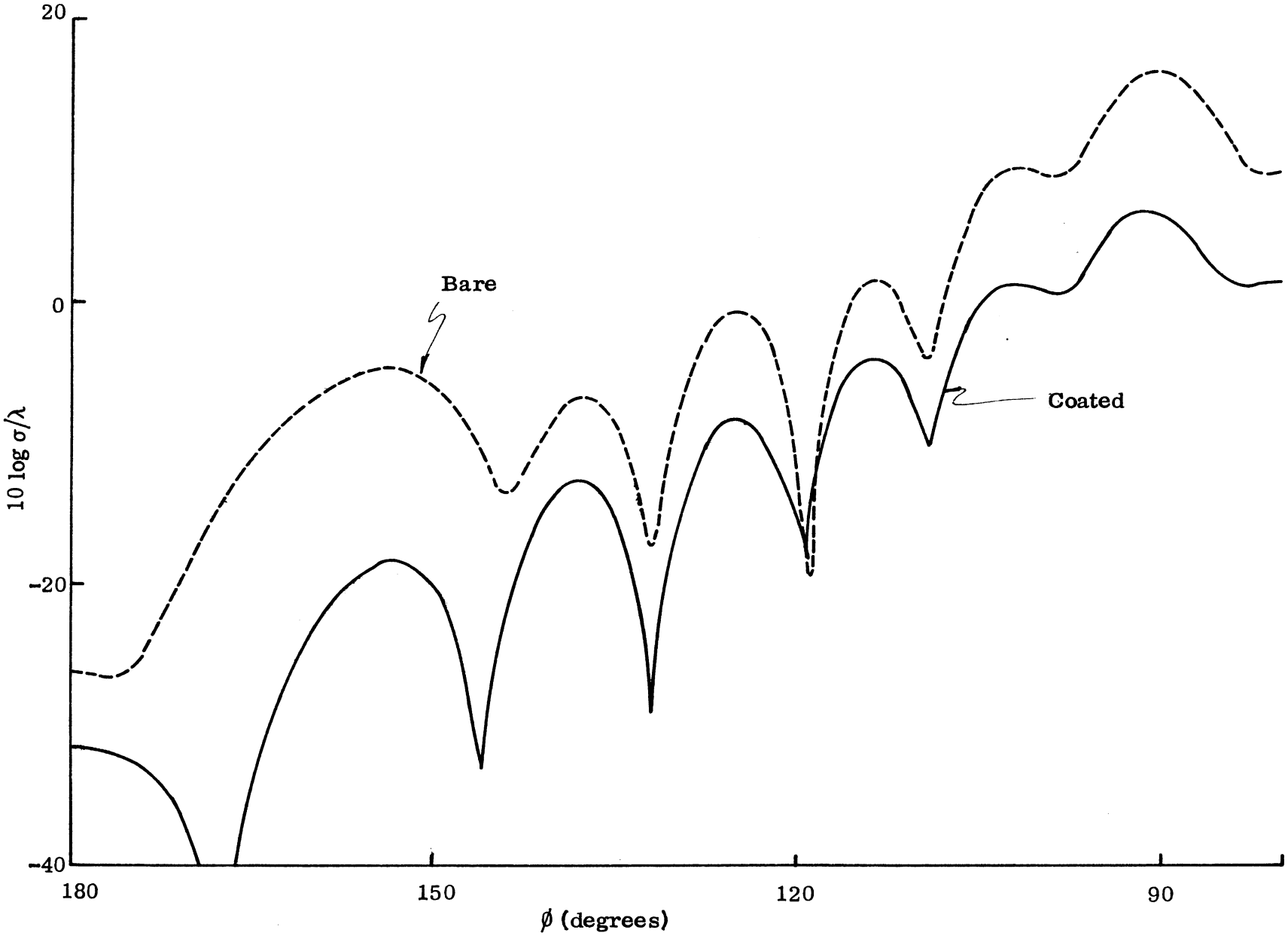

Figure 3-14: Effect of OG-C-1 coating with s_1 = 1 inch at 7.5 GHz.

oscillation. Since the traveling wave contribution is proportional to the square of this amplitude, comparison with the corresponding value for the bare body enables us to determine the reduction which has actually been achieved. The reductions are listed in Table 3-3 along with those deduced from the backscattering, either on the basis of the scattering at 154^{o} or by selecting always the peak return in the vicinity of this direction (we remark that for the uniform coating the peak actually occurs at 148^{o}, with the peak moving progressively back to its bare body position of 154^{o} as s_1 increases to 1 inch). Three conclusions that can be reached are (i) the traveling wave reduction deduced from the surface field data is independent of s_1, as expected; (ii) consideration of the cross section at 154^{o} as done in Figure 3-13 exaggerates the reduction provided by the uniform coating, and by the coatings with small s_1; and (iii) the actual peak value is affected by s_1 and, hence, the edge scattering. In no case does the actual reduction in the traveling wave as indicated by the surface field fully manifest itself in the backscattering pattern.

s_1	0	0.25	0.5	0.75	1.0
surface field	16.7	16.7	16.7	16.7	16.7
$\phi = 154^{o}$	22.9	16.6	14.3	13.9	13.8
local peak	15.9	15.0	14.0	13.9	13.8

Table 3-3: Traveling wave reductions in dB at 7.5 GHz.

In an attempt to realize the full reduction which the coating is capable of, we have examined the effect of starting the one-inch taper with a non-zero thickness $d = d_1$ at the front edge. The thickness variation used was

$$d = d_1 + (d_{max} - d_1) \sin \frac{\pi s}{2s_1} \quad , \qquad 0 \leq s \leq s_1$$

and data were obtained at 7.5 GHz for

$$d = 0.005 \text{ inch}, \quad \text{implying} \quad \eta_{tip} = 0.054 - i\,0.033$$
$$= 0.010 \text{ inch}, \qquad\qquad = 0.110 - i\,0.064$$
$$= 0.015 \text{ inch}, \qquad\qquad = 0.172 - i\,0.091$$

all for $s_1 = 1$ inch. The patterns in the aspect range $140^o \leq \phi \leq 180^o$ are plotted in Figure 3-15 along with those for the coated body with $d_1 = 0$ and for the bare body. Judged from the surface field data, the value of d_1 had no effect on the traveling wave. The broadside scattering varied by no more than 0.1 dB, but the choice $d_1 = 0.01$ inch reduced the edge-on backscattering by an additional 10 dB. It also reduced the traveling wave peak by almost 2 dB more than the 0-tip coating, bringing the peak down closer to the level indicated by the surface field data, and had a significant effect on the total power (see Table 3-4). Increasing d_1 to 0.015 inch reduces the peak by a further 1 dB and also reduces the total power a little more, but the edge-on scattering is now on its way up. It would appear that this is close to the optimum coating at 7.5 GHz, but since the mechanism responsible for this type of tuning is almost certainly phase cancellation, it is questionable whether the results obtained are practially significant.

d_1	0	0.005	0.010	0.015
surface field	16.7	16.7	16.7	16.7
tr. wave peak	13.8	14.5	15.3	16.3
edge-on	5.2	9.7	15.6	12.3
total power	14.4	15.5	16.0	16.3

Table 3-4: Cross section reductions in dB at 7.5 GHz for various tip thicknesses.

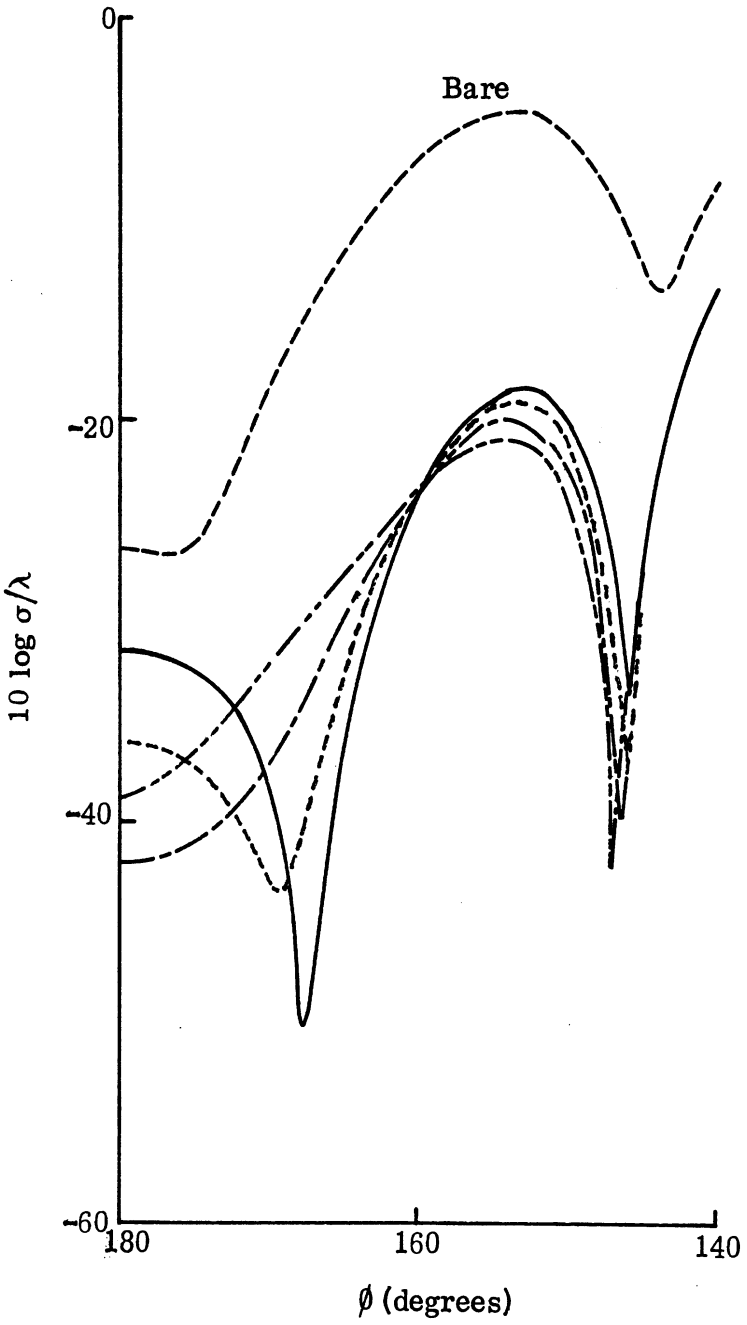

Figure 3-15: Effect of OG-C-1 coating at 7.5 GHz for s_1 = 1 inch with d_{tip} = 0 (——), 0.005 (— — —), 0.010 (— - —) and 0.015 (— - - —) inches.

We also carried out calculations for the 0-tip coatings at the highest frequency 15 GHz using a total of 150 sampling points on the body. Since the surface impedance provided by the full 50 mils of coating is now only $\eta = 0.24236 + i\,0.18578$, the performance is poorer than at 7.5 GHz. The effect on the broadside ($\phi = 90^{o}$), traveling wave peak ($\phi = 160^{o}$) and edge-on ($\phi = 180^{o}$) cross sections of the taper lengths $s_1 = 0(0.25)1.0$ inches are plotted in Figure 3-16, along with the total power reductions computed using the data at every 2^{o} from 180^{o} to 150^{o}. We remark, however, that for the smaller taper lengths the actual traveling wave peak occurs at a somewhat smaller angle than 160^{o}, and the true reduction never exceeds the 12.6 dB computed from the surface field data. Judged by both the traveling wave and the total power, the uniform ($s_1 = 0$) coating is the best, but the case $s_1 = 0.25$ inches is best as regards the edge-on return and there is no more than about 1 dB difference for any of the values of s_1 considered. The patterns of the bare and coated (with $s_1 = 1$ inch) bodies are shown in Figure 3-17.

In addition to these investigations we also examined the effect of different thickness variations, e.g. an S-shaped taper, in the vicinity of the front edge. None proved superior to the 0-tip coating and subject to the constraint on the maximum layer thickness it would appear that the optimum application of the OG-C-1 material is in a layer whose thickness d starts at zero at the front edge and rises to a maximum of 50 mils in a distance of one inch. At the four designated frequencies such a layer produces the cross sectional changes shown in Table 3-5.

f(GHz)	2.0	3.75	7.5	15.0
tr. wave peak	-0.3	-10.9	-13.8	-12.4
edge-on	3.2	-12.7	-5.2	1.1
total power	-0.4	-13.1	-14.4	-11.3

Table 3-5: Cross section changes in dB for optimum application of material OG-C-1.

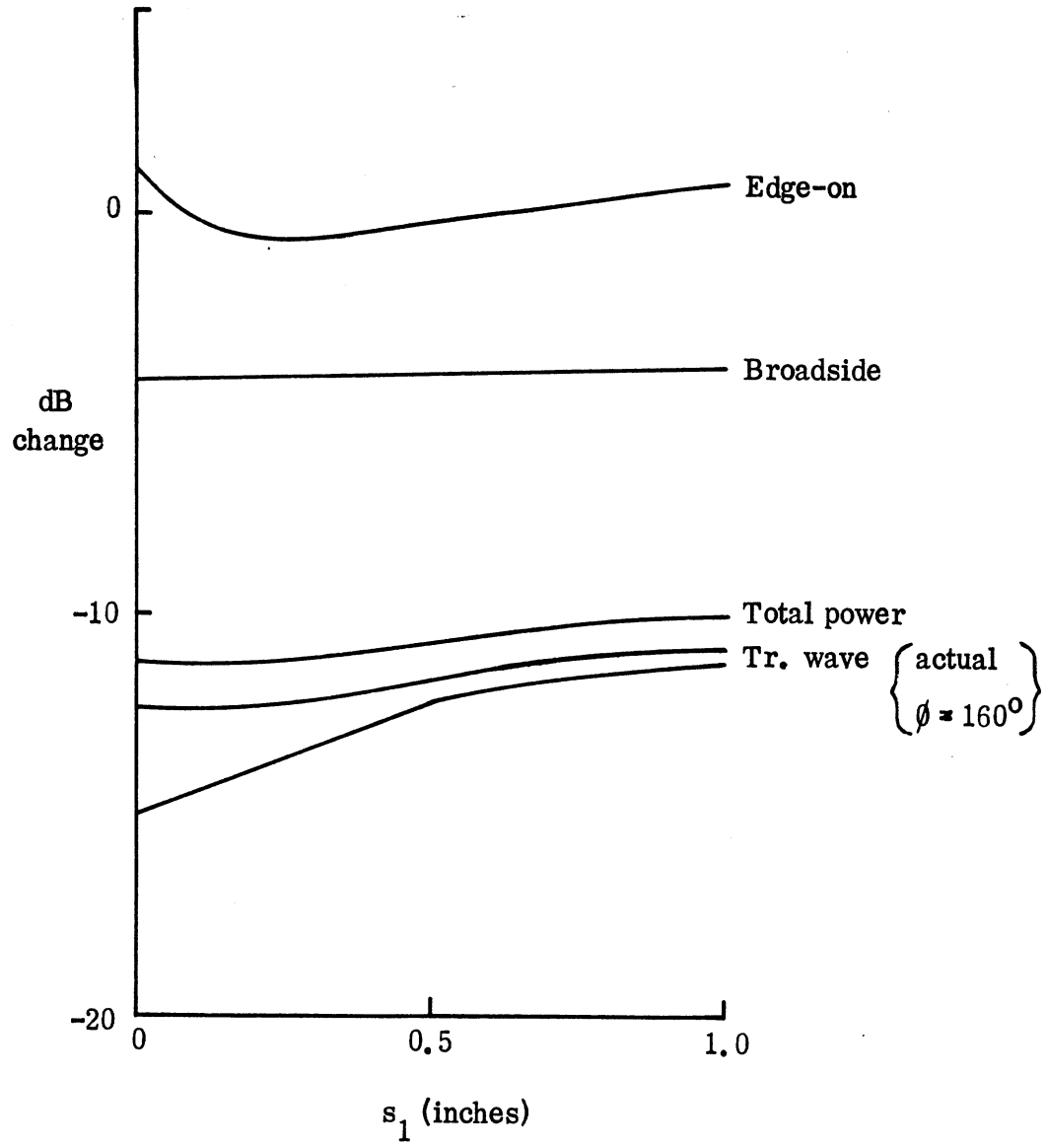

Figure 3-16: Effect of taper length for material OG-C-1 at 15 GHz.

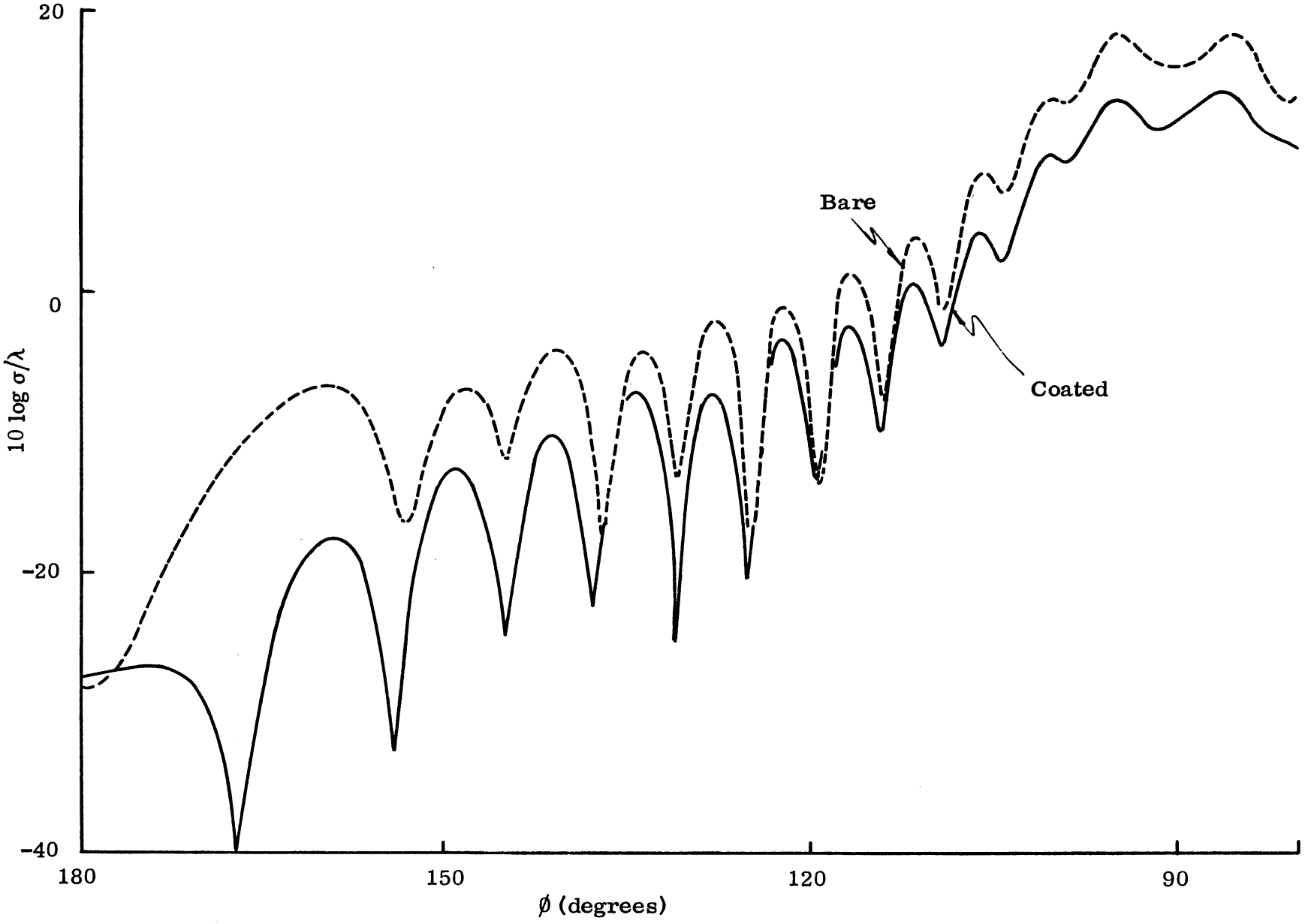

Figure 3-17: Effect of OG-C-1 coating with $s_1 = 1$ inch at 15 GHz.

Towards the end of the Contract a material was proposed whose properties were attractive as a coating material. From a knowledge of its composition, the relative permittivity and permeability were predicted at a number of frequencies and these are listed in Table 3-6. Two versions of the material were manufactured and designated TCPER-25 and TCPER-26. They had somewhat different dopings and their electromagnetic constants measured by the Avionics Laboratory are included in Table 3-6. Backscattering patterns were computed for 0-tip coatings of each material applied to the ogival cylinder. The cross section changes obtained are given in Table 3-7. Comparison with the results in Table 3-5 shows that a material having the predicted properties would have been superior to OG-C-1 as a coating, but that neither TCPER-25 nor TCPER-26 is, the poorer performance being attributable to the inflated values of the permittivity.

f (GHz)	ϵ			μ		
	'predicted'	TCPER-25	TCPER-26	'predicted'	TCPER-25	TCPER-26
2.0	36.0 + i1.0	62.4 + i55	16.4 + i0.68	6.1 + i4.0	5.4 + i4.2	5.0 + i1.77
2.5	36.0 + i1.0	80.5 + i68.2	16.0 + i0.75	6.1 + i4.0	5.6 + i5.1	4.7 + i2.16
3.75	35.0 + i2.2	66.5 + i32.3	16.3 + i0.88	4.5 + i3.8	3.0 + i3.8	3.7 + i2.39
7.5	33.0 + i2.5	36.0 + i12.2	16.1 + i0.38	3.2 + i3.6	1.8 + i2.2	2.3 + i2.10
15.0	32.0 + i3.5	28.6 + i7.8	19.0 + i3.56	2.0 + i3.4	0.2 + i0.9	1.5 + i1.16

Table 3-6: Properties of three candidate coating materials.

f (GHz)	2.0			2.5		
	'predicted'	TCPER-25	TCPER-26	'predicted'	TCPER-25	TCPER-26
tr. wave peak	-2.0	-2.9	2.0	-11.0	-5.8	-2.5
edge-on	4.0	2.2	2.9	-3.4	-8.1	1.7
total power	-2.2	-1.4	0.5	-8.2	-5.7	-0.8

f (GHz)	3.75			7.5		
	'predicted'	TCPER-25	TCPER-26	'predicted'	TCPER-25	TCPER-26
tr. wave peak	-12.5	-7.1	-8.7	-12.1		
edge-on	-20.0	-11.1	-4.0	-8.4		
total power	-15.4	-7.3	-7.9	-12.9		

Table 3-7: Cross section changes in dB for three coating materials.

CHAPTER 4

COMPUTER DATA

During the course of this study, a large volume of data has been generated using programs RAMVS and RAMD, primarily the latter. The data are all for H polarization and include the surface and backscattered fields of ogival and wedge cylinders, ogival cylinders with various impedances specified over the surface, and ogival cylinders with coatings of several materials and thickness variations. Because the cross section reduction tasks for the ogival and wedge cylinders turned out to be almost identical, most attention was given to the former shape. The data presented here are only a small fraction of the total obtained and limited to those situations for which experimental measurements have been performed.

On the following pages we show backscattering data for wedge and ogival cylinders at 2.0, 2.5, 3.75, 7.5 and 15.0 GHz, specifically

1. Bare wedge cylinder (for dimensions, see p. 6)
2. Bare ogival cylinder (for dimensions, see p. 6)
3. Bare ogival cylinder, extended size (for dimensions, see p. 46)
4. Ogival cylinder with uniform coating of OG-C-1 material, 0.050 inches thick
5. Ogival cylinder with linearly tapered coating of OG-C-1 material, 0 to 0.050 inches thick
6. Ogival cylinder with OG-C-1 coating, cylindrical (i.e. 0-tip) taper from 0.050 inches to 0 over 1 inch (see p. 57).

Then angle labelled theta is the angle ϕ of the text, with 180^{o} corresponding to edge-on incidence. The tabulated quantity is the two dimensional cross section σ/λ in dB and is related to the three dimensional cross section of an 18-inch section of the cylinder by equation (2.3).

The following table may assist in locating a particular data set.

	Model	Frequency, GHz				
		2.0	2.5	3.75	7.5	15.0
1	Bare wedge cylinder	4.1.1		4.1.2	4.1.3	4.1.4
2	Bare ogival cylinder	4.2.1		4.2.2	4.2.3	4.2.4
3	Bare ogival cylinder, extended size	4.3.1	4.3.2	4.3.3	4.3.4	4.3.5
4	Ogival cylinder with uniform coating of OG-C-1 material	4.4.1	4.4.2	4.4.3	4.4.4	4.4.5
5	Ogival cylinder with linearly tapered coating of OG-C-1 material	4.5.1		4.5.2	4.5.3	4.5.4
6	Ogival cylinder with OG-C-1 coating, cylindrical tip	4.6.1	4.6.2	4.6.3	4.6.4	4.6.5

Table 4-1: Index for location of data presented.

Table 4.1.1: Bare wedge cylinder; 2.0 GHz.

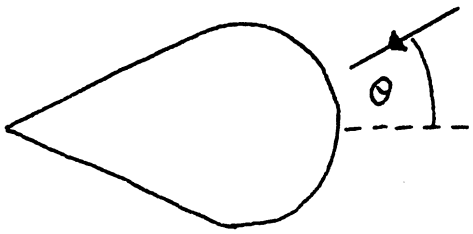

BACKSCATTERING CROSS SECTION

THETA	10*LOG(SIGMA/LAMBDA)	PHASE			
			59.00	-11.41	220.1
0.00	-5.93	202.4	60.00	-10.35	216.3
1.00	-5.93	202.4	61.00	-9.27	214.0
2.00	-5.92	202.6	62.00	-8.22	213.0
3.00	-5.90	202.8	63.00	-7.21	212.9
4.00	-5.88	203.2	64.00	-6.27	213.6
5.00	-5.85	203.6	65.00	-5.39	214.9
6.00	-5.82	204.2	66.00	-4.56	216.7
7.00	-5.78	204.8	67.00	-3.79	218.8
8.00	-5.74	205.6	68.00	-3.08	221.3
9.00	-5.69	206.4	69.00	-2.41	224.0
10.00	-5.64	207.3	70.00	-1.78	226.9
11.00	-5.58	208.3	71.00	-1.19	230.0
12.00	-5.52	209.4	72.00	-.65	233.2
13.00	-5.46	210.6	73.00	-.14	236.6
14.00	-5.40	211.8	74.00	.34	240.1
15.00	-5.33	213.2	75.00	.79	243.7
16.00	-5.27	214.6	76.00	1.21	247.3
17.00	-5.20	216.1	77.00	1.60	251.1
18.00	-5.14	217.6	78.00	1.96	254.9
19.00	-5.08	219.2	79.00	2.30	258.8
20.00	-5.02	220.9	80.00	2.61	262.7
21.00	-4.96	222.6	81.00	2.90	266.7
22.00	-4.91	224.4	82.00	3.17	270.7
23.00	-4.87	226.3	83.00	3.42	274.8
24.00	-4.83	228.2	84.00	3.64	278.9
25.00	-4.79	230.1	85.00	3.85	283.1
26.00	-4.77	232.1	86.00	4.04	287.3
27.00	-4.75	234.1	87.00	4.20	291.5
28.00	-4.75	236.2	88.00	4.35	295.7
29.00	-4.75	238.3	89.00	4.48	300.0
30.00	-4.77	240.5	90.00	4.60	304.3
31.00	-4.80	242.7	91.00	4.69	308.6
32.00	-4.85	244.9	92.00	4.77	312.9
33.00	-4.91	247.1	93.00	4.83	317.2
34.00	-4.99	249.3	94.00	4.88	321.6
35.00	-5.09	251.5	95.00	4.90	326.0
36.00	-5.21	253.8	96.00	4.92	330.4
37.00	-5.35	256.0	97.00	4.91	334.8
38.00	-5.52	258.2	98.00	4.89	339.2
39.00	-5.71	260.4	99.00	4.86	343.6
40.00	-5.94	262.5	100.00	4.81	348.1
41.00	-6.19	264.6	101.00	4.74	352.5
42.00	-6.48	266.6	102.00	4.66	357.1
43.00	-6.81	268.4	103.00	4.56	1.4
44.00	-7.18	270.1	104.00	4.45	5.9
45.00	-7.59	271.7	105.00	4.33	10.3
46.00	-8.05	272.9	106.00	4.19	14.8
47.00	-8.57	273.9	107.00	4.03	19.3
48.00	-9.15	274.4	108.00	3.86	23.8
49.00	-9.78	274.3	109.00	3.67	28.3
50.00	-10.47	273.6	110.00	3.47	32.8
51.00	-11.20	271.8	111.00	3.26	37.3
52.00	-11.95	268.8	112.00	3.03	41.8
53.00	-12.67	264.2	113.00	2.78	46.3
54.00	-13.25	258.0	114.00	2.52	50.8
55.00	-13.59	250.1	115.00	2.25	55.4
56.00	-13.56	241.4	116.00	1.96	59.9
57.00	-13.14	232.9	117.00	1.66	64.4
58.00	-12.38	225.6	118.00	1.34	69.0

Table 4.1.1 Continued

119.00	1.00	73.6
120.00	.55	78.2
121.00	.29	82.8
122.00	-.09	87.4
123.00	-.48	92.1
124.00	-.89	96.8
125.00	-1.31	101.5
126.00	-1.75	106.3
127.00	-2.20	111.1
128.00	-2.66	116.0
129.00	-3.14	121.0
130.00	-3.63	126.0
131.00	-4.14	131.1
132.00	-4.66	136.3
133.00	-5.18	141.5
134.00	-5.72	147.0
135.00	-6.27	152.5
136.00	-6.82	158.2
137.00	-7.37	164.0
138.00	-7.92	170.0
139.00	-8.46	176.2
140.00	-9.00	182.6
141.00	-9.51	189.1
142.00	-10.01	195.9
143.00	-10.47	202.8
144.00	-10.90	209.9
145.00	-11.29	217.1
146.00	-11.63	224.3
147.00	-11.91	231.6
148.00	-12.14	238.8
149.00	-12.32	246.0
150.00	-12.45	252.9
151.00	-12.53	259.6
152.00	-12.57	266.1
153.00	-12.57	272.3
154.00	-12.54	278.2
155.00	-12.49	283.8
156.00	-12.42	289.0
157.00	-12.34	293.9
158.00	-12.26	298.6
159.00	-12.16	302.9
160.00	-12.07	307.0
161.00	-11.97	310.7
162.00	-11.88	314.3
163.00	-11.79	317.5
164.00	-11.70	320.6
165.00	-11.62	323.4
166.00	-11.55	326.0
167.00	-11.48	328.4
168.00	-11.41	330.6
169.00	-11.35	332.6
170.00	-11.30	334.4
171.00	-11.25	336.0
172.00	-11.21	337.5
173.00	-11.17	338.7
174.00	-11.14	339.8
175.00	-11.11	340.8
176.00	-11.09	341.5
177.00	-11.07	342.1
178.00	-11.06	342.5
179.00	-11.05	342.8
180.00	-11.05	342.8

Table 4.1.2: Bare wedge cylinder; 3.75 GHz.

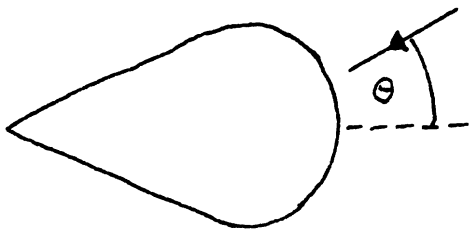

BACKSCATTERING CROSS SECTION		
THETA	10*LOG(SIGMA/LAMBDA)	PHASE
0.00	-.98	134.3
1.00	-.98	134.5
2.00	-.97	134.9
3.00	-.95	135.6
4.00	-.93	136.5
5.00	-.89	137.8
6.00	-.85	139.3
7.00	-.80	141.0
8.00	-.74	143.0
9.00	-.68	145.2
10.00	-.60	147.6
11.00	-.52	150.3
12.00	-.43	153.2
13.00	-.33	156.2
14.00	-.23	159.5
15.00	-.12	162.9
16.00	-.01	166.5
17.00	.12	170.2
18.00	.24	174.1
19.00	.37	178.1
20.00	.49	182.1
21.00	.62	186.4
22.00	.74	190.7
23.00	.85	195.1
24.00	.95	199.7
25.00	1.05	204.3
26.00	1.13	209.1
27.00	1.20	213.8
28.00	1.25	218.7
29.00	1.28	223.6
30.00	1.29	228.7
31.00	1.27	233.8
32.00	1.23	239.1
33.00	1.16	244.4
34.00	1.05	249.8
35.00	.90	255.4
36.00	.71	261.0
37.00	.47	266.8
38.00	.18	272.8
39.00	-.17	278.9
40.00	-.58	285.1
41.00	-1.08	291.6
42.00	-1.67	298.4
43.00	-2.36	305.4
44.00	-3.18	312.9
45.00	-4.15	321.0
46.00	-5.31	329.8
47.00	-6.70	339.9
48.00	-8.37	352.0
49.00	-10.36	7.7
50.00	-12.52	29.9
51.00	-14.02	61.6
52.00	-13.54	97.3
53.00	-11.49	125.5
54.00	-9.23	145.1
55.00	-7.24	159.7
56.00	-5.56	171.5
57.00	-4.17	181.7
58.00	-3.00	191.1
59.00	-2.02	199.9
60.00	-1.21	208.3
61.00	-.53	216.5
62.00	.02	224.5
63.00	.44	232.4
64.00	.76	240.2
65.00	.97	248.0
66.00	1.07	255.8
67.00	1.06	263.6
68.00	.94	271.4
69.00	.69	279.2
70.00	.30	287.1
71.00	-.26	295.0
72.00	-1.00	303.0
73.00	-1.99	311.2
74.00	-3.29	319.5
75.00	-5.06	328.2
76.00	-7.55	337.5
77.00	-11.45	348.9
78.00	-19.28	11.6
79.00	-21.12	144.3
80.00	-11.55	172.9
81.00	-6.85	185.0
82.00	-3.73	194.6
83.00	-1.43	203.5
84.00	.45	212.0
85.00	1.97	220.4
86.00	3.25	228.6
87.00	4.35	236.8
88.00	5.29	244.9
89.00	6.10	253.1
90.00	6.81	261.1
91.00	7.41	269.2
92.00	7.94	277.3
93.00	8.38	285.3
94.00	8.76	293.4
95.00	9.06	301.4
96.00	9.31	309.4
97.00	9.49	317.4
98.00	9.62	325.4
99.00	9.70	333.4
100.00	9.72	341.4
101.00	9.69	349.4
102.00	9.61	357.3
103.00	9.47	5.3
104.00	9.29	13.2
105.00	9.06	21.1
106.00	8.78	29.0
107.00	8.44	36.9
108.00	8.06	44.8
109.00	7.61	52.7
110.00	7.12	60.6
111.00	6.57	68.4
112.00	5.95	76.3
113.00	5.27	84.2
114.00	4.52	92.1
115.00	3.70	100.0
116.00	2.79	108.0
117.00	1.79	116.1
118.00	.68	124.3

Table 4.1.2 Continued

119.00	-.55	132.6
120.00	-1.93	141.3
121.00	-3.48	150.3
122.00	-5.26	160.0
123.00	-7.32	170.9
124.00	-9.76	183.8
125.00	-12.65	201.0
126.00	-15.82	226.9
127.00	-17.83	266.3
128.00	-16.82	306.2
129.00	-14.53	332.4
130.00	-12.50	349.4
131.00	-10.93	2.0
132.00	-9.74	12.3
133.00	-8.83	21.3
134.00	-8.15	29.4
135.00	-7.64	37.0
136.00	-7.28	44.1
137.00	-7.04	50.9
138.00	-6.91	57.5
139.00	-6.86	63.8
140.00	-6.90	69.8
141.00	-7.02	75.7
142.00	-7.20	81.3
143.00	-7.44	86.8
144.00	-7.75	92.1
145.00	-8.11	97.1
146.00	-8.53	102.0
147.00	-9.00	106.6
148.00	-9.52	110.9
149.00	-10.11	115.0
150.00	-10.74	118.7
151.00	-11.43	122.1
152.00	-12.18	125.1
153.00	-12.98	127.7
154.00	-13.84	129.6
155.00	-14.75	130.9
156.00	-15.71	131.4
157.00	-16.71	130.9
158.00	-17.72	129.2
159.00	-18.71	126.1
160.00	-19.66	121.5
161.00	-20.31	115.5
162.00	-20.77	108.5
163.00	-20.93	101.1
164.00	-20.80	94.1
165.00	-20.44	88.0
166.00	-19.96	83.2
167.00	-19.41	79.5
168.00	-18.85	76.8
169.00	-18.32	74.9
170.00	-17.83	73.6
171.00	-17.39	72.7
172.00	-16.99	72.2
173.00	-16.65	71.9
174.00	-16.36	71.8
175.00	-16.12	71.7
176.00	-15.92	71.7
177.00	-15.77	71.8
178.00	-15.66	71.8
179.00	-15.60	71.8
180.00	-15.58	71.9

Table 4.1.3: Bare wedge cylinder; 7.50 GHz.

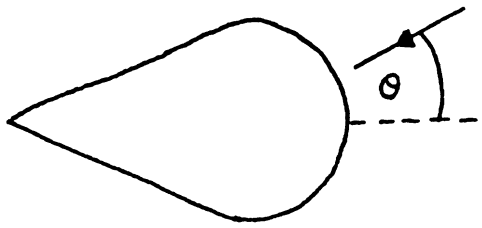

THETA	10*LOG(SIGMA/LAMBDA)	PHASE
0.00	1.21	257.8
1.00	1.21	258.0
2.00	1.21	258.[illegible]
3.00	1.22	259.[illegible]
4.00	1.23	26[illegible].[illegible]
5.00	1.24	262.5
6.00	1.25	264.6
7.00	1.25	267.0
8.00	1.24	269.9
9.00	1.22	273.2
10.00	1.19	276.9
11.00	1.14	281.1
12.00	1.06	285.7
13.00	.96	290.8
14.00	.83	296.5
15.00	.67	302.7
16.00	.48	309.6
17.00	.25	317.1
18.00	-.01	325.5
19.00	-.30	334.7
20.00	-.61	344.9
21.00	-.91	356.1
22.00	-1.19	8.5
23.00	-1.39	22.1
24.00	-1.48	36.7
25.00	-1.42	52.0
26.00	-1.20	67.8
27.00	-.81	83.5
28.00	-.30	98.9
29.00	.30	113.8
30.00	.93	128.1
31.00	1.56	141.8
32.00	2.13	155.0
33.00	2.65	167.8
34.00	3.08	180.4
35.00	3.41	192.9
36.00	3.64	205.3
37.00	3.75	217.7
38.00	3.73	230.3
39.00	3.56	243.2
40.00	3.23	256.5
41.00	2.73	270.4
42.00	2.02	285.1
43.00	1.07	301.1
44.00	-.12	319.0
45.00	-1.55	340.[illegible]
46.00	-3.06	5.9
47.00	-4.16	37.9
48.00	-4.11	73.6
49.00	-2.90	106.3
50.00	-1.24	133.2
51.00	.33	155.5
52.00	1.64	175.0
53.00	2.65	192.8
54.00	3.38	209.8
55.00	3.84	226.3
56.00	4.03	242.7
57.00	3.94	259.3
58.00	3.58	276.4
59.00	2.91	294.3
60.00	1.90	313.7
61.00	.55	335.6
62.00	-1.10	1.9
63.00	-2.68	34.9
64.00	-3.28	74.5
65.00	-2.33	113.3
66.00	-.63	145.1
67.00	1.62	170.7
68.00	2.32	192.6
69.00	3.21	212.5
70.00	3.72	231.2
71.00	3.83	249.3
72.00	3.53	267.2
73.00	2.76	285.4
74.00	1.42	304.4
75.00	-.72	325.4
76.00	-4.07	352.1
77.00	-8.78	39.2
78.00	-8.25	117.6
79.00	-3.27	161.9
80.00	.25	187.7
81.00	2.59	208.3
82.00	4.14	227.0
83.00	5.09	244.7
84.00	5.52	262.1
85.00	5.44	279.4
86.00	4.82	297.0
87.00	3.51	315.3
88.00	1.18	335.7
89.00	-2.99	3.3
90.00	-9.33	70.4
91.00	-3.52	156.4
92.00	2.35	187.5
93.00	6.08	208.5
94.00	8.71	226.7
95.00	10.68	243.7
96.00	12.18	260.1
97.00	13.33	276.2
98.00	14.19	292.1
99.00	14.80	307.7
100.00	15.19	323.2
101.00	15.39	338.5
102.00	15.39	353.8
103.00	15.21	8.9
104.00	14.84	24.0
105.00	14.29	38.9
106.00	13.54	53.7
107.00	12.58	68.4
108.00	11.39	83.1
109.00	9.92	97.4
110.00	8.14	111.6
111.00	5.93	125.5
112.00	3.13	139.0
113.00	-.63	151.5
114.00	-6.34	161.1
115.00	-18.68	142.8
116.00	-12.18	36.2
117.00	-6.18	48.6
118.00	-3.46	51.5

Table 4.1.3 Continued

119.00	-2.08	63.7
120.00	-1.49	76.2
121.00	-1.47	88.8
122.00	-1.93	101.2
123.00	-2.83	113.2
124.00	-4.20	124.8
125.00	-6.12	135.5
126.00	-8.79	144.4
127.00	-12.59	148.9
128.00	-18.15	138.4
129.00	-25.68	85.5
130.00	-15.84	60.0
131.00	-12.42	60.0
132.00	-10.37	67.7
133.00	-9.15	77.0
134.00	-8.51	87.2
135.00	-8.31	97.9
136.00	-8.49	108.9
137.00	-9.01	119.9
138.00	-9.89	131.1
139.00	-11.14	142.4
140.00	-12.84	154.0
141.00	-15.15	166.1
142.00	-18.39	179.5
143.00	-23.44	197.7
144.00	-32.48	249.6
145.00	-27.61	359.4
146.00	-21.71	15.1
147.00	-18.50	29.1
148.00	-16.49	40.4
149.00	-15.17	50.5
150.00	-14.30	59.9
151.00	-13.76	68.7
152.00	-13.49	77.1
153.00	-13.44	84.9
154.00	-13.57	92.3
155.00	-13.87	99.1
156.00	-14.33	105.2
157.00	-14.93	110.6
158.00	-15.66	115.1
159.00	-16.51	118.4
160.00	-17.46	120.3
161.00	-18.46	120.3
162.00	-19.43	118.3
163.00	-20.24	113.9
164.00	-20.73	107.7
165.00	-20.83	100.7
166.00	-20.46	94.3
167.00	-19.84	89.3
168.00	-19.08	86.0
169.00	-18.31	84.2
170.00	-17.56	83.5
171.00	-16.89	83.5
172.00	-16.29	84.0
173.00	-15.78	84.7
174.00	-15.34	85.6
175.00	-14.98	86.5
176.00	-14.69	87.3
177.00	-14.47	88.0
178.00	-14.31	88.6
179.00	-14.22	88.9
180.00	-14.19	89.0

Table 4.1.4: Bare wedge cylinder; 15.0 GHz.

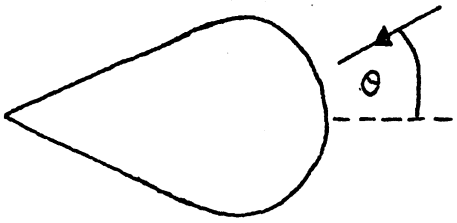

BACKSCATTERING CROSS SECTION		
THETA	10*LOG(SIGMA/LAMBDA)	PHASE
0.00	4.31	132.6
1.00	4.33	133.1
2.00	4.37	134.8
3.00	4.45	137.5
4.00	4.55	141.2
5.00	4.68	145.9
6.00	4.83	151.4
7.00	4.99	157.8
8.00	5.16	165.0
9.00	5.32	172.9
10.00	5.46	181.4
11.00	5.58	190.7
12.00	5.65	200.6
13.00	5.66	211.3
14.00	5.61	222.8
15.00	5.47	235.3
16.00	5.25	248.8
17.00	4.95	263.6
18.00	4.57	280.0
19.00	4.15	298.3
20.00	3.75	318.7
21.00	3.49	341.2
22.00	3.46	5.5
23.00	3.74	30.6
24.00	4.29	55.5
25.00	4.99	79.4
26.00	5.72	102.2
27.00	6.35	124.1
28.00	6.81	145.3
29.00	7.13	166.5
30.00	6.98	187.8
31.00	6.60	210.0
32.00	5.85	233.6
33.00	4.68	259.5
34.00	3.11	289.9
35.00	1.42	327.6
36.00	.58	13.7
37.00	1.45	60.4
38.00	3.17	99.8
39.00	4.73	132.7
40.00	5.77	162.4
41.00	6.22	190.8
42.00	6.07	219.5
43.00	5.29	250.1
44.00	3.88	284.7
45.00	2.12	327.0
46.00	1.14	19.6
47.00	2.11	73.2
48.00	3.98	117.8
49.00	5.47	155.3
50.00	6.26	189.7
51.00	6.29	223.9
52.00	5.57	260.2
53.00	4.21	301.8
54.00	2.88	352.8
55.00	3.06	50.4
56.00	4.73	102.1
57.00	6.43	144.9
58.00	7.45	183.0
59.00	7.63	219.5
60.00	6.94	256.9
61.00	5.35	298.5
62.00	3.21	349.6
63.00	2.22	53.1
64.00	3.60	113.6
65.00	5.34	161.8
66.00	6.18	203.3
67.00	5.86	243.1
68.00	4.24	285.4
69.00	1.31	338.2
70.00	-.55	54.0
71.00	2.17	125.1
72.00	4.81	174.7
73.00	6.08	216.1
74.00	5.89	256.0
75.00	4.19	299.0
76.00	.97	354.6
77.00	-.46	76.4
78.00	2.85	145.8
79.00	5.52	193.1
80.00	6.51	233.3
81.00	5.82	272.2
82.00	3.12	314.7
83.00	-2.35	18.3
84.00	-1.67	126.8
85.00	3.69	186.0
86.00	6.19	226.8
87.00	6.50	264.0
88.00	4.56	302.2
89.00	-1.29	351.9
90.00	-3.74	127.7
91.00	4.88	199.3
92.00	8.69	228.2
93.00	10.18	263.0
94.00	9.45	297.7
95.00	5.97	336.4
96.00	-3.71	67.7
97.00	7.09	184.0
98.00	13.58	223.4
99.00	17.20	256.5
100.00	19.38	287.7
101.00	20.59	318.1
102.00	21.01	347.9
103.00	20.73	17.2
104.00	19.74	45.9
105.00	17.98	74.0
106.00	15.26	101.2
107.00	11.15	126.3
108.00	4.37	143.7
109.00	-5.94	95.6
110.00	1.69	58.8
111.00	4.69	76.0
112.00	4.90	97.9
113.00	3.20	119.2
114.00	-.50	135.3
115.00	-7.06	128.0
116.00	-6.81	78.7
117.00	-2.50	78.0
118.00	-.85	93.7

Table 4.1.4 Continued

119.00	-1.38	111.9
120.00	-2.94	128.4
121.00	-6.58	136.8
122.00	-10.86	119.2
123.00	-9.29	90.2
124.00	-6.33	91.5
125.00	-5.09	104.4
126.00	-5.35	119.8
127.00	-7.01	133.6
128.00	-10.12	140.4
129.00	-13.81	127.5
130.00	-13.34	100.3
131.00	-11.62	95.9
132.00	-9.09	104.6
133.00	-8.85	117.0
134.00	-9.75	128.8
135.00	-11.67	136.6
136.00	-14.20	134.7
137.00	-15.55	120.3
138.00	-14.49	109.4
139.00	-13.04	111.0
140.00	-12.39	119.6
141.00	-12.74	130.8
142.00	-14.18	141.6
143.00	-16.91	148.2
144.00	-21.97	141.2
145.00	-22.28	103.8
146.00	-18.50	86.1
147.00	-15.66	89.7
148.00	-13.98	100.1
149.00	-13.25	112.9
150.00	-13.27	126.4
151.00	-13.97	140.1
152.00	-15.36	153.2
153.00	-17.55	165.1
154.00	-20.84	174.1
155.00	-25.91	174.6
156.00	-32.19	137.5
157.00	-28.41	89.5
158.00	-24.48	85.3
159.00	-22.31	91.1
160.00	-21.36	99.2
161.00	-21.22	107.0
162.00	-21.69	113.9
163.00	-22.71	118.6
164.00	-24.15	119.4
165.00	-25.72	114.0
166.00	-26.61	101.4
167.00	-26.01	87.3
168.00	-24.41	78.9
169.00	-22.57	76.6
170.00	-21.15	78.1
171.00	-19.98	81.5
172.00	-18.99	85.9
173.00	-18.29	90.6
174.00	-17.45	95.2
175.00	-16.95	99.4
176.00	-16.56	103.1
177.00	-16.27	106.1
178.00	-16.07	108.3
179.00	-15.96	109.6
180.00	-15.92	110.1

Table 4.2.1: Bare ogival cylinder; 2.0 GHz.

BACKSCATTERING CROSS SECTION

THETA	10*LOG(SIGMA/LAMBDA)	PHASE
0.00	-29.35	108.6
1.00	-29.29	108.4
2.00	-29.12	108.1
3.00	-27.83	107.5
4.00	-27.44	106.8
5.00	-26.96	105.9
6.00	-26.42	105.0
7.00	-25.81	104.0
8.00	-25.17	102.9
9.00	-24.50	101.9
10.00	-23.81	100.8
11.00	-23.11	99.8
12.00	-22.41	98.8
13.00	-21.72	97.9
14.00	-21.04	96.9
15.00	-20.38	95.9
16.00	-19.73	95.0
17.00	-19.10	94.0
18.00	-18.50	93.1
19.00	-17.91	92.1
20.00	-17.35	91.1
21.00	-16.81	90.1
22.00	-16.29	89.0
23.00	-15.80	87.9
24.00	-15.32	86.8
25.00	-14.87	85.6
26.00	-14.44	84.3
27.00	-14.04	83.0
28.00	-13.65	81.6
29.00	-13.28	80.1
30.00	-12.93	78.6
31.00	-12.60	76.9
32.00	-12.29	75.1
33.00	-11.99	73.2
34.00	-11.70	71.2
35.00	-11.43	69.1
36.00	-11.17	66.8
37.00	-10.91	64.4
38.00	-10.66	61.8
39.00	-10.41	59.1
40.00	-10.16	56.2
41.00	-9.91	53.2
42.00	-9.64	50.0
43.00	-9.37	46.7

Table 4.2.1 Continued

44.00	-3.07	43.3
45.00	-3.76	39.8
46.00	-4.43	36.2
47.00	-5.08	32.6
48.00	-5.70	29.0
49.00	-6.30	25.4
50.00	-6.88	21.9
51.00	-7.43	18.3
52.00	-7.97	14.9
53.00	-8.49	11.7
54.00	-8.99	8.6
55.00	-9.49	5.6
56.00	-9.99	2.8
57.00	-10.49	.1
58.00	-2.97	357.7
59.00	-2.46	355.3
60.00	-1.96	353.2
61.00	-1.47	351.1
62.00	-.99	349.3
63.00	-.52	347.5
64.00	-.06	345.9
65.00	.38	344.4
66.00	.81	343.0
67.00	1.22	341.7
68.00	1.62	340.5
69.00	2.00	339.4
70.00	2.36	338.4
71.00	2.71	337.4
72.00	3.04	336.5
73.00	3.35	335.7
74.00	3.64	335.0
75.00	3.92	334.3
76.00	4.18	333.7
77.00	4.42	333.2
78.00	4.64	332.7
79.00	4.84	332.2
80.00	5.03	331.8
81.00	5.20	331.4
82.00	5.35	331.1
83.00	5.48	330.8
84.00	5.60	330.6
85.00	5.69	330.4
86.00	5.77	330.2
87.00	5.83	330.1
88.00	5.88	330.0
89.00	5.90	329.9
90.00	5.91	329.9

Table 4.2.2: Bare ogival cylinder; 3.75 GHz.

BACKSCATTERING CROSS SECTION

THETA	10*LOG(SIGMA/LAMBDA)	PHASE
0.00	-21.71	275.5
1.00	-21.66	275.9
2.00	-21.62	277.0
3.00	-21.29	278.8
4.00	-20.96	281.2
5.00	-20.54	283.9
6.00	-20.02	287.0
7.00	-19.42	290.1
8.00	-18.74	293.1
9.00	-18.02	296.0
10.00	-17.25	298.6
11.00	-16.46	301.0
12.00	-15.65	303.1
13.00	-14.85	304.9
14.00	-14.06	306.4
15.00	-13.28	307.6
16.00	-12.53	308.7
17.00	-11.80	309.5
18.00	-11.10	310.1
19.00	-10.43	310.6
20.00	-9.80	310.9
21.00	-9.19	311.0
22.00	-8.62	311.1
23.00	-8.09	311.0
24.00	-7.59	310.8
25.00	-7.13	310.5
26.00	-6.71	310.1
27.00	-6.33	309.6
28.00	-5.99	309.1
29.00	-5.69	308.4
30.00	-5.44	307.6
31.00	-5.23	306.7
32.00	-5.06	305.6
33.00	-4.95	304.5
34.00	-4.89	303.1
35.00	-4.89	301.6
36.00	-4.95	299.9
37.00	-5.07	297.9
38.00	-5.25	295.7
39.00	-5.50	293.0
40.00	-5.83	289.8
41.00	-6.22	286.1
42.00	-6.69	281.5
43.00	-7.18	276.1

Table 4.2.2 Continued

44.00	-7.73	259.4
45.00	-8.19	251.4
46.00	-8.58	251.9
47.00	-8.76	241.3
48.00	-8.66	230.1
49.00	-8.27	219.1
50.00	-7.63	209.1
51.00	-6.85	200.5
52.00	-6.01	193.4
53.00	-5.18	187.5
54.00	-4.41	183.0
55.00	-3.72	179.3
56.00	-3.12	176.4
57.00	-2.64	174.2
58.00	-2.27	172.6
59.00	-2.02	171.5
60.00	-1.90	170.9
61.00	-1.92	170.8
62.00	-2.09	171.3
63.00	-2.43	172.5
64.00	-2.95	174.7
65.00	-3.59	178.2
66.00	-4.65	183.7
67.00	-5.81	192.3
68.00	-7.00	205.7
69.00	-7.71	225.0
70.00	-7.25	247.4
71.00	-5.52	266.7
72.00	-3.53	280.1
73.00	-1.48	288.9
74.00	.38	294.8
75.00	2.22	298.9
76.00	3.46	301.7
77.00	4.72	303.9
78.00	5.84	305.4
79.00	6.81	306.7
80.00	7.67	307.6
81.00	8.42	308.4
82.00	9.08	309.0
83.00	9.64	309.4
84.00	10.12	309.8
85.00	10.52	310.1
86.00	10.84	310.3
87.00	11.08	310.5
88.00	11.26	310.6
89.00	11.36	310.7
90.00	11.40	310.7

Table 4.2.3: Bare ogival cylinder; 7.5 GHz.

BACKSCATTERING CROSS SECTION

THETA	10*LOG(SIGMA/LAMBDA)	PHASE
0.00	-21.93	101.0
1.00	-21.85	101.8
2.00	-21.69	103.9
3.00	-21.16	107.3
4.00	-20.54	111.3
5.00	-19.76	115.7
6.00	-18.83	120.0
7.00	-17.80	123.9
8.00	-16.72	127.2
9.00	-15.62	129.9
10.00	-14.54	132.0
11.00	-13.49	133.6
12.00	-12.43	134.7
13.00	-11.54	135.4
14.00	-10.65	135.7
15.00	-9.94	135.7
16.00	-9.10	135.4
17.00	-8.43	134.8
18.00	-7.84	133.9
19.00	-7.37	132.8
20.00	-6.90	131.4
21.00	-6.56	129.8
22.00	-6.31	127.8
23.00	-6.15	125.6
24.00	-6.11	122.9
25.00	-6.16	119.7
26.00	-6.33	115.9
27.00	-6.61	111.4
28.00	-7.00	105.9
29.00	-7.48	99.2
30.00	-8.00	91.0
31.00	-8.51	81.1
32.00	-8.99	69.5
33.00	-9.32	56.7
34.00	-9.46	43.7
35.00	-9.45	31.5
36.00	-9.31	20.9
37.00	-9.08	11.9
38.00	-8.87	4.4
39.00	-8.77	358.0
40.00	-8.86	352.5
41.00	-9.31	347.4
42.00	-9.24	342.3
43.00	-9.15	336.5

Table 4.2.3 Continued

44.00	-12.55	328.2
45.00	-17.26	309.6
46.00	-21.59	241.4
47.00	-14.99	199.0
48.00	-10.12	175.0
49.00	-6.92	168.7
50.00	-4.63	164.9
51.00	-3.13	162.2
52.00	-2.17	160.1
53.00	-1.71	158.3
54.00	-1.74	156.5
55.00	-2.23	154.9
56.00	-3.60	152.8
57.00	-5.99	149.8
58.00	-10.07	143.1
59.00	-15.07	127.4
60.00	-13.37	4.2
61.00	-7.00	350.2
62.00	-3.32	346.7
63.00	-1.07	345.8
64.00	.27	346.3
65.00	.99	347.9
66.00	.85	350.9
67.00	.10	356.2
68.00	-1.44	6.1
69.00	-3.66	25.8
70.00	-4.90	62.8
71.00	-2.79	99.5
72.00	1.01	119.6
73.00	3.76	130.5
74.00	5.77	137.6
75.00	7.17	143.4
76.00	8.06	148.8
77.00	8.50	154.8
78.00	8.54	162.0
79.00	8.28	171.6
80.00	7.89	184.5
81.00	7.71	201.2
82.00	8.19	220.1
83.00	9.33	237.4
84.00	10.92	250.7
85.00	12.45	260.0
86.00	13.76	266.7
87.00	14.79	270.5
88.00	15.52	273.2
89.00	15.95	274.6
90.00	16.10	275.1

Table 4.2.4: Bare ogival cylinder; 15.0 GHz.

BACKSCATTERING CROSS SECTION

THETA	10*LOG(SIGMA/LAMBDA)	PHASE
0.00	-23.25	111.0
1.00	-22.92	111.7
2.00	-22.06	113.4
3.00	-20.64	115.5
4.00	-18.86	117.4
5.00	-17.40	118.7
6.00	-16.77	119.3
7.00	-16.23	119.2
8.00	-15.87	118.6
9.00	-11.56	117.4
10.00	-10.45	115.7
11.00	-9.48	113.5
12.00	-8.70	110.8
13.00	-8.06	107.5
14.00	-7.60	103.6
15.00	-7.29	98.8
16.00	-7.15	93.1
17.00	-7.16	86.1
18.00	-7.30	77.7
19.00	-7.49	67.6
20.00	-7.68	55.8
21.00	-7.74	42.6
22.00	-7.65	28.7
23.00	-7.42	15.1
24.00	-7.18	2.4
25.00	-7.12	350.9
26.00	-7.35	339.8
27.00	-8.12	328.4
28.00	-9.62	314.9
29.00	-12.22	294.5
30.00	-14.43	256.5
31.00	-12.90	208.1
32.00	-9.39	179.5
33.00	-6.58	164.0
34.00	-4.81	153.4
35.00	-3.97	144.6
36.00	-4.11	135.1
37.00	-4.96	123.4
38.00	-6.80	105.4
39.00	-8.71	74.4
40.00	-8.25	34.9
41.00	-6.09	7.5
42.00	-4.32	351.8
43.00	-3.37	341.5

Table 4.2.4 Continued

44.00	-4.35	332.6
45.00	-8.33	326.5
46.00	-16.20	277.5
47.00	-11.24	182.0
48.00	-5.21	153.6
49.00	-2.61	156.2
50.00	-2.11	151.0
51.00	-3.70	144.9
52.00	-8.59	131.6
53.00	-15.77	43.2
54.00	-5.29	350.5
55.00	-2.19	342.1
56.00	-1.10	339.2
57.00	-2.56	336.6
58.00	-3.35	341.5
59.00	-17.42	134.9
60.00	-3.87	151.4
61.00	.02	154.5
62.00	.74	157.8
63.00	-1.42	164.1
64.00	-3.86	180.9
65.00	-6.74	305.4
66.00	.44	326.3
67.00	2.95	335.5
68.00	2.69	346.5
69.00	-.32	0.6
70.00	-2.49	73.3
71.00	-2.63	121.2
72.00	5.02	140.5
73.00	7.01	155.6
74.00	5.99	176.4
75.00	4.29	216.3
76.00	6.25	256.3
77.00	8.68	295.9
78.00	11.70	315.0
79.00	12.29	334.1
80.00	13.05	359.3
81.00	12.41	32.5
82.00	14.28	62.2
83.00	16.19	84.7
84.00	17.43	100.5
85.00	17.80	114.6
86.00	17.48	130.0
87.00	16.98	148.0
88.00	16.85	166.1
89.00	17.11	179.1
90.00	17.29	193.6

Table 4.3.1: Bare ogival cylinder, extended size; 2.0 GHz.

BACKSCATTERING CROSS SECTION		
THETA	10*LOG(SIGMA/LAMBDA)	PHASE
80.00	5.07	329.6
82.00	5.44	328.9
84.00	5.73	328.3
86.00	5.93	327.9
88.00	6.05	327.7
90.00	6.09	327.6
92.00	6.05	327.7
94.00	5.93	327.9
96.00	5.73	328.3
98.00	5.44	328.9
100.00	5.07	329.6
102.00	4.62	330.6
104.00	4.08	331.8
106.00	3.46	333.2
108.00	2.75	335.0
110.00	1.95	337.1
112.00	1.07	339.7
114.00	0.10	342.8
116.00	-0.94	346.5
118.00	-2.05	351.0
120.00	-3.20	356.4
122.00	-4.37	2.8
124.00	-5.50	10.4
126.00	-6.54	19.0
128.00	-7.41	28.4
130.00	-8.09	38.1
132.00	-8.57	47.5
134.00	-8.89	56.2
136.00	-9.11	63.9
138.00	-9.28	70.6
140.00	-9.47	76.1
142.00	-9.69	80.8
144.00	-9.98	84.8
146.00	-10.35	88.1
148.00	-10.80	90.8
150.00	-11.33	93.2
152.00	-11.96	95.2
154.00	-12.67	96.9
156.00	-13.47	98.3
158.00	-14.35	99.5
160.00	-15.31	100.5
162.00	-16.35	101.3
164.00	-17.45	101.9
166.00	-18.61	102.3
168.00	-19.80	102.6
170.00	-20.98	102.7
172.00	-22.11	102.7
174.00	-23.12	102.6
176.00	-23.93	102.5
178.00	-24.46	102.4
180.00	-24.65	102.3

Table 4.3.2: Bare ogival cylinder, extended size; 2.5 GHz.

BACKSCATTERING CROSS SECTION		
THETA	10*LOG(SIGMA/LAMBDA)	PHASE
80.00	5.44	322.3
82.00	6.13	321.8
84.00	6.65	321.5
86.00	7.01	321.3
88.00	7.23	321.1
90.00	7.30	321.1
92.00	7.23	321.1
94.00	7.01	321.3
96.00	6.65	321.5
98.00	6.13	321.8
100.00	5.44	322.3
102.00	4.57	322.9
104.00	3.49	323.8
106.00	2.18	324.9
108.00	0.56	326.5
110.00	-1.43	328.9
112.00	-3.96	332.6
114.00	-7.29	339.5
116.00	-11.87	355.3
118.00	-16.50	40.4
120.00	-13.92	93.9
122.00	-10.00	113.7
124.00	-7.39	121.8
126.00	-5.67	126.2
128.00	-4.52	129.0
130.00	-3.77	131.0
132.00	-3.31	132.5
134.00	-3.09	133.7
136.00	-3.06	134.8
138.00	-3.20	135.6
140.00	-3.48	136.4
142.00	-3.89	137.0
144.00	-4.43	137.5
146.00	-5.07	137.8
148.00	-5.82	138.1
150.00	-6.67	138.1
152.00	-7.61	137.9
154.00	-8.65	137.5
156.00	-9.77	136.7
158.00	-10.99	135.5
160.00	-12.28	133.8
162.00	-13.64	131.4
164.00	-15.05	128.2
166.00	-16.47	124.0
168.00	-17.84	118.9
170.00	-19.09	112.8
172.00	-20.14	106.2
174.00	-20.93	99.7
176.00	-21.45	94.4
178.00	-21.73	90.9
180.00	-21.82	89.7

Table 4.3.3: Bare ogival cylinder, extended size; 3.75 GHz.

BACKSCATTERING CROSS SECTION

THETA	10*LOG(SIGMA/LAMBDA)	PHASE
80.00	7.68	303.8
82.00	9.19	305.5
84.00	10.31	306.6
86.00	11.07	307.2
88.00	11.52	307.6
90.00	11.67	307.7
92.00	11.52	307.6
94.00	11.07	307.2
96.00	10.31	306.6
98.00	9.19	305.5
100.00	7.68	303.8
102.00	5.70	301.1
104.00	3.11	296.3
106.00	-0.25	287.2
108.00	-4.34	267.3
110.00	-7.03	227.7
112.00	-5.58	191.9
114.00	-3.46	175.4
116.00	-2.20	168.5
118.00	-1.76	165.8
120.00	-2.01	165.6
122.00	-2.88	167.5
124.00	-4.39	171.9
126.00	-6.57	180.3
128.00	-9.31	196.7
130.00	-11.52	226.5
132.00	-11.02	261.4
134.00	-8.85	284.0
136.00	-6.89	296.2
138.00	-5.49	303.5
140.00	-4.58	308.2
142.00	-4.07	311.6
144.00	-3.88	314.2
146.00	-3.96	316.3
148.00	-4.28	318.0
150.00	-4.79	319.3
152.00	-5.50	320.4
154.00	-6.37	321.2
156.00	-7.40	321.7
158.00	-8.59	321.7
160.00	-9.93	321.2
162.00	-11.41	320.1
164.00	-13.02	318.0
166.00	-14.75	314.8
168.00	-16.54	310.2
170.00	-18.30	303.7
172.00	-19.89	295.6
174.00	-21.13	286.6
176.00	-21.92	278.5
178.00	-22.33	272.8
180.00	-22.44	270.8

Table 4.3.4: Bare ogival cylinder, extended size; 7.5 GHz.

BACKSCATTERING CROSS SECTION		
THETA	10*LOG(SIGMA/LAMBDA)	PHASE
80.00	9.21	174.0
81.00	9.00	188.2
82.00	9.15	205.2
83.00	9.92	222.5
84.00	11.18	237.2
85.00	12.59	248.1
86.00	13.87	255.8
87.00	14.91	260.9
88.00	15.67	264.2
89.00	16.12	266.0
90.00	16.27	266.5
91.00	16.12	266.0
92.00	15.67	264.2
93.00	14.91	260.9
94.00	13.87	255.8
95.00	12.59	248.1
96.00	11.18	237.2
97.00	9.92	222.5
98.00	9.15	205.2
99.00	9.00	188.2
100.00	9.21	174.0
101.00	9.43	163.0
102.00	9.42	154.6
103.00	9.05	147.8
104.00	8.25	141.7
105.00	6.95	135.5
106.00	5.04	128.2
107.00	2.42	117.6
108.00	-0.91	98.8
109.00	-3.65	64.0
110.00	-2.98	35.2
111.00	-0.84	3.0
112.00	0.71	351.7
113.00	1.43	345.1
114.00	1.40	340.9
115.00	0.63	337.7
116.00	-0.97	335.0
117.00	-3.68	332.0
118.00	-8.42	326.5
119.00	-10.28	295.8
120.00	-13.53	176.2
121.00	-6.86	165.4
122.00	-3.66	162.7
123.00	-1.90	161.8
124.00	-1.02	161.8

Table 4.3.4 Continued

125.00	-0.78	162.4
126.00	-1.10	163.5
127.00	-1.95	165.3
128.00	-3.37	168.0
129.00	-5.48	172.3
130.00	-8.53	179.9
131.00	-12.95	196.9
132.00	-17.33	243.1
133.00	-14.77	296.2
134.00	-11.10	316.9
135.00	-8.82	326.5
136.00	-7.53	332.7
137.00	-6.95	337.8
138.00	-6.92	342.7
139.00	-7.37	348.2
140.00	-8.28	355.0
141.00	-9.63	4.1
142.00	-11.32	17.4
143.00	-12.97	37.6
144.00	-13.60	64.4
145.00	-12.65	90.1
146.00	-10.92	108.3
147.00	-9.22	120.3
148.00	-7.83	128.5
149.00	-6.74	134.4
150.00	-5.93	139.0
151.00	-5.36	142.7
152.00	-4.98	145.9
153.00	-4.78	148.7
154.00	-4.73	151.1
155.00	-4.82	153.4
156.00	-5.03	155.4
157.00	-5.34	157.3
158.00	-5.76	159.1
159.00	-6.28	160.7
160.00	-6.89	162.2
161.00	-7.59	163.6
162.00	-8.38	164.8
163.00	-9.25	165.8
164.00	-10.22	166.6
165.00	-11.28	167.1
166.00	-12.43	167.2
167.00	-13.69	166.9
168.00	-15.06	166.1
169.00	-16.55	164.5
170.00	-18.16	162.0
171.00	-19.87	158.0
172.00	-21.66	152.2
173.00	-23.43	144.0
174.00	-24.99	133.1
175.00	-26.12	120.3
176.00	-26.68	107.5
177.00	-26.77	96.7
178.00	-26.64	89.1
179.00	-26.48	84.7
180.00	-26.41	83.3

Table 4.3.5: Bare ogival cylinder, extended size; 15.0 GHz.

BACKSCATTERING CROSS SECTION

THETA	10*LOG(SIGMA/LAMBDA)	PHASE
80.00	13.84	334.9
81.00	13.62	2.4
82.00	14.25	35.7
83.00	16.02	63.9
84.00	17.62	83.4
85.00	18.35	98.2
86.00	18.18	111.9
87.00	17.38	127.1
88.00	16.54	144.0
89.00	16.17	158.2
90.00	16.13	163.7
91.00	16.17	158.2
92.00	16.54	144.0
93.00	17.38	127.1
94.00	18.18	111.9
95.00	18.35	98.2
96.00	17.62	83.4
97.00	16.02	63.9
98.00	14.25	35.7
99.00	13.62	2.4
100.00	13.84	334.9
101.00	13.45	314.0
102.00	11.75	293.5
103.00	8.83	264.4
104.00	6.95	219.5
105.00	7.90	180.8
106.00	8.42	158.2
107.00	6.98	140.8
108.00	3.02	116.7
109.00	-1.30	57.3
110.00	1.91	2.9
111.00	3.98	342.8
112.00	3.17	330.1
113.00	-.90	312.8
114.00	-7.61	248.0
115.00	-1.93	182.8
116.00	1.28	168.1
117.00	1.20	161.9
118.00	-2.08	157.6
119.00	-13.07	147.2
120.00	-8.86	344.5
121.00	-2.35	339.9
122.00	-1.03	338.7
123.00	-2.79	338.3
124.00	-9.16	338.1
125.00	-18.95	162.7

Table 4.3.5 Continued

126.00	-5.69	161.8
127.00	-2.33	163.7
128.00	-1.94	167.2
129.00	-3.88	174.0
130.00	-8.75	192.4
131.00	-13.41	264.4
132.00	-7.69	313.9
133.00	-4.67	327.9
134.00	-4.14	336.1
135.00	-5.71	344.4
136.00	-9.99	359.4
137.00	-17.12	61.3
138.00	-10.89	133.1
139.00	-6.35	150.4
140.00	-4.39	159.9
141.00	-3.98	168.6
142.00	-4.74	179.0
143.00	-6.46	194.0
144.00	-8.65	218.0
145.00	-9.75	252.0
146.00	-8.87	282.9
147.00	-7.61	303.3
148.00	-6.99	317.0
149.00	-7.21	328.0
150.00	-8.34	338.8
151.00	-10.47	352.1
152.00	-13.67	13.8
153.00	-16.49	55.8
154.00	-14.85	103.0
155.00	-11.70	128.3
156.00	-9.41	142.1
157.00	-7.94	151.7
158.00	-7.07	159.4
159.00	-6.66	166.3
160.00	-6.58	172.9
161.00	-6.77	179.3
162.00	-7.18	185.8
163.00	-7.76	192.4
164.00	-8.49	199.0
165.00	-9.32	205.7
166.00	-10.27	212.5
167.00	-11.30	219.2
168.00	-12.43	225.9
169.00	-13.66	232.5
170.00	-15.01	239.1
171.00	-16.49	245.8
172.00	-18.11	252.8
173.00	-19.88	260.4
174.00	-21.76	269.1
175.00	-23.68	279.3
176.00	-25.47	291.4
177.00	-26.88	304.5
178.00	-27.74	316.5
179.00	-28.12	324.7
180.00	-28.21	327.6

Table 4.4.1: Ogival cylinder with uniform coating of OG-C-1 material; 2.0 GHz.

BACKSCATTERING CROSS SECTION		
THETA	10*LOG(SIGMA/LAMBDA)	PHASE
80.00	1.25	8.6
82.00	1.62	7.6
84.00	1.91	6.9
86.00	2.12	6.4
88.00	2.24	6.1
90.00	2.28	6.0
92.00	2.24	6.1
94.00	2.12	6.4
96.00	1.91	6.9
98.00	1.62	7.6
100.00	1.25	8.6
102.00	0.79	9.9
104.00	0.25	11.5
106.00	-0.37	13.5
108.00	-1.08	15.9
110.00	-1.86	18.8
112.00	-2.72	22.4
114.00	-3.64	26.6
116.00	-4.59	31.7
118.00	-5.56	37.7
120.00	-6.50	44.6
122.00	-7.35	52.5
124.00	-8.09	61.0
126.00	-8.66	69.8
128.00	-9.07	78.5
130.00	-9.34	86.6
132.00	-9.52	93.9
134.00	-9.66	100.2
136.00	-9.80	105.6
138.00	-9.98	110.1
140.00	-10.22	113.8
142.00	-10.53	116.9
144.00	-10.93	119.5
146.00	-11.42	121.5
148.00	-12.02	123.0
150.00	-12.71	124.1
152.00	-13.51	124.8
154.00	-14.43	125.0
156.00	-15.46	124.6
158.00	-16.61	123.7
160.00	-17.88	122.1
162.00	-19.27	119.5
164.00	-20.76	115.7
166.00	-22.32	110.5
168.00	-23.87	103.5
170.00	-25.28	94.8
172.00	-26.38	84.9
174.00	-27.10	75.1
176.00	-27.45	67.2
178.00	-27.58	62.1
180.00	-27.61	60.3

Table 4.4.2: Ogival cylinder with uniform coating of OG-C-1 material; 2.5 GHz.

BACKSCATTERING CROSS SECTION		
THETA	10*LOG(SIGMA/LAMBDA)	PHASE
80.00	-0.24	0.5
82.00	0.41	0.4
84.00	0.91	0.4
86.00	1.25	0.4
88.00	1.46	0.3
90.00	1.53	0.3
92.00	1.46	0.3
94.00	1.25	0.4
96.00	0.91	0.4
98.00	0.41	0.4
100.00	-0.24	0.5
102.00	-1.07	0.5
104.00	-2.09	0.5
106.00	-3.34	0.4
108.00	-4.87	0.2
110.00	-6.76	359.7
112.00	-9.16	358.7
114.00	-12.38	356.5
116.00	-17.13	350.6
118.00	-25.57	322.1
120.00	-24.02	223.4
122.00	-17.38	204.0
124.00	-13.87	199.5
126.00	-11.68	198.0
128.00	-10.21	197.6
130.00	-9.20	197.8
132.00	-8.51	198.2
134.00	-8.07	198.9
136.00	-7.81	199.6
138.00	-7.72	200.4
140.00	-7.76	201.2
142.00	-7.92	202.0
144.00	-8.17	202.6
146.00	-8.52	203.2
148.00	-8.94	203.6
150.00	-9.44	203.9
152.00	-10.00	203.9
154.00	-10.62	203.6
156.00	-11.28	203.0
158.00	-11.98	202.0
160.00	-12.71	200.7
162.00	-13.44	198.9
164.00	-14.16	196.8
166.00	-14.84	194.3
168.00	-15.48	191.5
170.00	-16.03	188.7
172.00	-16.49	186.0
174.00	-16.85	183.5
176.00	-17.11	181.6
178.00	-17.26	180.4
180.00	-17.31	180.0

Table 4.4.3: Ogival cylinder with uniform coating of OG-C-1 material; 3.75 GHz.

BACKSCATTERING CROSS SECTION		
THETA	10*LOG(SIGMA/LAMBDA)	PHASE
80.00	-1.60	345.6
82.00	-0.32	346.2
84.00	0.63	346.6
86.00	1.29	346.9
88.00	1.68	347.0
90.00	1.80	347.0
92.00	1.68	347.0
94.00	1.29	346.9
96.00	0.63	346.6
98.00	-0.32	346.2
100.00	-1.60	345.6
102.00	-3.27	344.5
104.00	-5.41	342.7
106.00	-8.21	339.4
108.00	-11.94	332.5
110.00	-17.02	314.6
112.00	-21.10	265.1
114.00	-18.31	220.5
116.00	-15.35	205.4
118.00	-13.74	200.0
120.00	-13.09	197.9
122.00	-13.15	197.6
124.00	-13.83	198.2
126.00	-15.13	199.6
128.00	-17.15	201.6
130.00	-20.20	204.4
132.00	-25.21	209.0
134.00	-37.50	229.0
136.00	-31.03	17.8
138.00	-23.90	26.5
140.00	-20.44	30.8
142.00	-18.33	34.2
144.00	-16.94	37.2
146.00	-16.03	40.0
148.00	-15.44	42.5
150.00	-15.12	44.7
152.00	-14.99	46.6
154.00	-15.03	48.1
156.00	-15.21	49.3
158.00	-15.50	50.0
160.00	-15.89	50.3
162.00	-16.36	50.1
164.00	-16.87	49.4
166.00	-17.41	48.2
168.00	-17.95	46.7
170.00	-18.46	44.9
172.00	-18.91	42.9
174.00	-19.28	41.1
176.00	-19.55	39.6
178.00	-19.72	38.6
180.00	-19.78	38.3

Table 4.4.4: Ogival cylinder with uniform coating of OG-C-1 material; 7.5 GHz.

BACKSCATTERING CROSS SECTION

THETA	10*LOG(SIGMA/LAMBDA)	PHASE
80.00	-0.86	144.3
82.00	-1.12	177.7
84.00	1.26	212.3
86.00	4.31	230.9
88.00	6.26	238.9
90.00	6.90	241.1
92.00	6.26	238.9
94.00	4.31	230.9
96.00	1.26	212.3
98.00	-1.12	177.7
100.00	-0.86	144.3
102.00	-0.50	125.6
104.00	-1.78	114.5
106.00	-5.48	103.5
108.00	-13.36	73.1
110.00	-13.50	337.7
112.00	-8.69	315.2
114.00	-8.05	310.3
116.00	-10.45	310.5
118.00	-17.37	317.4
120.00	-26.42	93.4
122.00	-15.52	122.1
124.00	-13.12	130.4
126.00	-13.70	140.5
128.00	-16.38	159.1
130.00	-19.48	197.9
132.00	-18.88	243.7
134.00	-17.24	269.1
136.00	-17.12	284.7
138.00	-18.69	299.5
140.00	-21.82	322.2
142.00	-24.60	5.0
144.00	-23.28	48.4
146.00	-21.30	70.2
148.00	-20.65	81.7
150.00	-21.36	89.7
152.00	-23.52	97.3
154.00	-27.63	109.2
156.00	-34.63	147.9
158.00	-32.45	228.4
160.00	-27.17	250.0
162.00	-24.38	256.5
164.00	-22.89	259.1
166.00	-22.16	259.8
168.00	-21.90	259.3
170.00	-21.95	258.2
172.00	-22.17	256.5
174.00	-22.45	254.6
176.00	-22.71	252.9
178.00	-22.89	251.7
180.00	-22.96	251.3

Table 4.4.5: Ogival cylinder with uniform coating of OG-C-1 material; 15.0 GHz.

BACKSCATTERING CROSS SECTION

THETA	10*LOG(SIGMA/LAMBDA)	PHASE
80.00	9.77	313.1
81.00	9.56	340.1
82.00	10.19	13.1
83.00	11.96	41.1
84.00	13.56	60.4
85.00	14.28	75.0
86.00	14.08	88.6
87.00	13.26	103.8
88.00	12.39	120.9
89.00	12.01	135.2
90.00	11.97	140.8
91.00	12.01	135.2
92.00	12.39	120.9
93.00	13.26	103.8
94.00	14.08	88.6
95.00	14.28	75.0
96.00	13.56	60.4
97.00	11.96	41.1
98.00	10.19	13.1
99.00	9.56	340.1
100.00	9.77	313.1
101.00	9.35	293.0
102.00	7.52	273.9
103.00	4.17	246.0
104.00	1.66	197.4
105.00	2.98	154.3
106.00	3.91	131.2
107.00	2.72	114.1
108.00	-.97	90.3
109.00	-4.98	33.9
110.00	-2.11	341.0
111.00	-.08	320.9
112.00	-.82	309.1
113.00	-4.82	295.1
114.00	-13.59	237.9
115.00	-7.47	155.2
116.00	-3.66	140.4
117.00	-3.57	133.7
118.00	-6.84	126.6
119.00	-17.08	95.0
120.00	-11.59	336.3
121.00	-5.87	326.0
122.00	-4.46	325.0
123.00	-5.64	328.1
124.00	-9.68	339.1
125.00	-16.63	30.2
126.00	-12.41	100.3

Table 4.4.5 Continued

127.00	-8.88	116.7
128.00	-8.53	123.4
129.00	-11.03	128.2
130.00	-18.97	136.5
131.00	-21.53	298.7
132.00	-12.03	309.7
133.00	-9.00	314.6
134.00	-8.41	319.8
135.00	-9.60	327.4
136.00	-12.61	341.5
137.00	-17.05	16.5
138.00	-16.93	75.3
139.00	-13.65	105.4
140.00	-12.00	119.7
141.00	-11.96	130.4
142.00	-13.32	142.3
143.00	-16.01	160.9
144.00	-18.97	196.7
145.00	-18.45	242.5
146.00	-15.98	269.6
147.00	-14.37	284.0
148.00	-13.88	293.7
149.00	-14.37	302.2
150.00	-15.80	311.5
151.00	-18.22	324.3
152.00	-21.47	346.3
153.00	-23.82	25.2
154.00	-22.71	63.9
155.00	-20.65	85.7
156.00	-19.35	98.1
157.00	-18.88	106.5
158.00	-19.14	113.4
159.00	-20.05	120.2
160.00	-21.60	129.1
161.00	-23.80	139.0
162.00	-26.53	156.2
163.00	-28.87	184.7
164.00	-28.93	218.7
165.00	-27.27	242.5
166.00	-25.61	255.8
167.00	-24.43	263.5
168.00	-23.71	268.1
169.00	-23.36	271.0
170.00	-23.31	272.5
171.00	-23.48	273.2
172.00	-23.82	273.1
173.00	-24.29	272.3
174.00	-24.83	271.1
175.00	-25.40	269.3
176.00	-25.94	267.4
177.00	-26.41	265.4
178.00	-26.77	263.8
179.00	-26.99	262.6
180.00	-27.07	262.2

Table 4.5.1: Ogival cylinder with linearly tapered coating of OG-C-1 material; 2.0 GHz.

BACKSCATTERING CROSS SECTION		
THETA	10*LOG(SIGMA/LAMBDA)	PHASE
80.00	1.80	10.0
82.00	1.75	7.9
84.00	1.63	5.9
86.00	1.46	3.9
88.00	1.23	2.0
90.00	0.92	0.2
92.00	0.55	358.4
94.00	0.10	356.8
96.00	-0.42	355.1
98.00	-1.04	353.6
100.00	-1.75	352.2
102.00	-2.57	351.0
104.00	-3.51	349.9
106.00	-4.60	349.0
108.00	-5.85	348.3
110.00	-7.32	348.1
112.00	-9.06	348.5
114.00	-11.17	349.8
116.00	-13.79	352.9
118.00	-17.21	0.1
120.00	-21.69	18.9
122.00	-24.71	66.4
124.00	-21.59	107.8
126.00	-18.10	123.3
128.00	-15.65	129.6
130.00	-13.92	132.6
132.00	-12.69	134.1
134.00	-11.80	134.7
136.00	-11.17	134.9
138.00	-10.74	134.8
140.00	-10.48	134.4
142.00	-10.35	133.8
144.00	-10.34	133.1
146.00	-10.44	132.2
148.00	-10.62	131.2
150.00	-10.88	130.0
152.00	-11.20	128.6
154.00	-11.57	127.1
156.00	-11.99	125.4
158.00	-12.44	123.5
160.00	-12.90	121.5
162.00	-13.37	119.2
164.00	-13.83	116.9
166.00	-14.26	114.6
168.00	-14.66	112.2
170.00	-15.01	110.0
172.00	-15.31	108.0
174.00	-15.54	106.3
176.00	-15.71	105.0
178.00	-15.81	104.2
180.00	-15.84	103.9

Table 4.5.2: Ogival cylinder with linearly tapered coating of OG-C-1 material; 3.75 GHz.

BACKSCATTERING CROSS SECTION

THETA	10*LOG(SIGMA/LAMBDA)	PHASE
80.00	-0.20	14.4
82.00	0.64	359.3
84.00	1.66	346.4
86.00	2.67	336.0
88.00	3.51	327.6
90.00	4.13	320.7
92.00	4.48	314.9
94.00	4.54	309.9
96.00	4.31	305.2
98.00	3.76	300.6
100.00	2.88	295.9
102.00	1.64	290.7
104.00	0.01	284.3
106.00	-2.07	276.0
108.00	-4.58	263.9
110.00	-7.29	245.2
112.00	-9.29	218.0
114.00	-9.55	189.3
116.00	-8.78	168.1
118.00	-8.07	154.4
120.00	-7.82	144.9
122.00	-8.10	137.4
124.00	-8.91	130.7
126.00	-10.24	123.5
128.00	-12.13	114.6
130.00	-14.53	101.6
132.00	-17.08	80.7
134.00	-18.49	50.8
136.00	-17.83	22.7
138.00	-16.35	4.7
140.00	-15.11	354.2
142.00	-14.32	347.8
144.00	-13.94	343.7
146.00	-13.91	341.0
148.00	-14.19	339.1
150.00	-14.73	337.8
152.00	-15.50	336.8
154.00	-16.47	336.0
156.00	-17.64	335.2
158.00	-18.99	334.3
160.00	-20.51	333.2
162.00	-22.18	331.5
164.00	-24.00	329.0
166.00	-25.94	325.3
168.00	-27.93	320.0
170.00	-29.86	312.8
172.00	-31.54	303.6
174.00	-32.79	293.5
176.00	-33.52	284.6
178.00	-33.85	278.6
180.00	-33.96	276.5

Table 4.5.3: Ogival cylinder with linearly tapered coating of OG-C-1 material; 7.5 GHz.

BACKSCATTERING CROSS SECTION

THETA	10*LOG(SIGMA/LAMBDA)	PHASE
80.00	6.60	126.2
81.00	5.77	129.1
82.00	4.21	134.1
83.00	1.74	144.3
84.00	-1.50	168.2
85.00	-2.24	213.4
86.00	1.19	245.6
87.00	4.50	258.7
88.00	6.86	264.1
89.00	8.46	266.1
90.00	9.48	266.3
91.00	10.02	265.1
92.00	10.14	262.8
93.00	9.89	259.2
94.00	9.28	254.1
95.00	8.37	247.0
96.00	7.22	237.1
97.00	6.02	224.0
98.00	5.07	207.5
99.00	4.63	189.4
100.00	4.70	172.7
101.00	4.97	158.9
102.00	5.14	147.9
103.00	5.03	138.8
104.00	4.54	130.9
105.00	3.62	123.0
106.00	2.20	114.4
107.00	.23	103.2
108.00	-2.20	86.7
109.00	-4.47	60.8
110.00	-5.08	28.2
111.00	-3.92	1.9
112.00	-2.55	345.4
113.00	-1.66	334.8
114.00	-1.38	327.2
115.00	-1.71	320.9
116.00	-2.65	315.0
117.00	-4.30	308.2
118.00	-6.80	298.6
119.00	-10.34	291.1
120.00	-13.76	243.0
121.00	-12.55	196.0
122.00	-9.42	172.4
123.00	-7.20	161.6
124.00	-5.91	155.5
125.00	-5.34	151.7
126.00	-5.36	149.0

Table 4.5.3 Continued

127.00	-5.94	147.0
128.00	-7.09	145.5
129.00	-8.93	144.3
130.00	-11.70	143.3
131.00	-16.15	142.6
132.00	-25.60	142.7
133.00	-27.16	319.4
134.00	-17.84	319.8
135.00	-14.10	317.4
136.00	-12.09	319.0
137.00	-11.01	318.5
138.00	-10.57	317.9
139.00	-10.62	317.3
140.00	-11.12	316.5
141.00	-12.05	315.5
142.00	-13.46	314.0
143.00	-15.43	311.6
144.00	-18.18	307.4
145.00	-22.15	298.2
146.00	-27.87	270.3
147.00	-28.71	202.4
148.00	-23.73	171.5
149.00	-20.42	161.8
150.00	-18.34	157.5
151.00	-17.01	155.2
152.00	-16.17	153.9
153.00	-15.70	153.1
154.00	-15.52	152.6
155.00	-15.57	152.3
156.00	-15.82	152.1
157.00	-16.25	152.0
158.00	-16.84	151.8
159.00	-17.58	151.6
160.00	-18.47	151.3
161.00	-19.51	150.8
162.00	-20.70	150.1
163.00	-22.03	148.9
164.00	-23.52	147.1
165.00	-25.19	144.4
166.00	-27.02	140.3
167.00	-29.00	134.1
168.00	-31.04	124.8
169.00	-32.87	111.2
170.00	-34.07	93.9
171.00	-34.29	76.2
172.00	-33.75	61.6
173.00	-32.92	51.4
174.00	-32.02	44.6
175.00	-31.37	40.1
176.00	-30.80	37.1
177.00	-30.37	35.2
178.00	-30.07	34.1
179.00	-29.90	33.4
180.00	-29.84	33.2

Table 4.5.4: Ogival cylinder with linearly tapered coating of OG-C-1 material; 15.0 GHz.

BACKSCATTERING CROSS SECTION

THETA	10*LOG(SIGMA/LAMBDA)	PHASE
80.00	9.96	319.3
81.00	9.26	343.6
82.00	9.39	20.6
83.00	11.82	52.6
84.00	14.24	70.4
85.00	15.49	80.3
86.00	15.43	87.2
87.00	14.09	93.9
88.00	11.54	104.0
89.00	8.50	122.3
90.00	7.14	144.8
91.00	7.80	152.1
92.00	9.15	141.7
93.00	10.95	124.4
94.00	12.63	108.2
95.00	13.55	93.9
96.00	13.44	79.0
97.00	12.35	60.1
98.00	10.85	33.2
99.00	10.19	.1
100.00	10.48	330.9
101.00	10.40	308.4
102.00	9.13	287.8
103.00	6.56	261.3
104.00	4.12	219.6
105.00	4.47	175.8
106.00	5.32	147.6
107.00	4.58	126.6
108.00	1.87	101.3
109.00	-1.34	54.9
110.00	-.15	2.9
111.00	1.70	335.8
112.00	1.43	318.6
113.00	-1.34	299.3
114.00	-6.40	256.5
115.00	-5.30	187.6
116.00	-1.99	159.1
117.00	-1.50	144.7
118.00	-3.81	130.0
119.00	-9.54	95.2
120.00	-9.05	13.2
121.00	-4.08	344.7
122.00	-2.38	334.7
123.00	-3.16	323.9
124.00	-6.71	324.0
125.00	-16.86	312.7
126.00	-15.30	152.6

Table 4.5.4 Continued

127.00	-8.28	144.4
128.00	-6.77	140.5
129.00	-8.22	135.8
130.00	-13.47	124.1
131.00	-21.41	28.8
132.00	-11.43	339.4
133.00	-7.56	332.2
134.00	-6.45	329.5
135.00	-7.26	328.2
136.00	-10.17	327.9
137.00	-17.07	328.9
138.00	-28.38	138.1
139.00	-14.54	145.2
140.00	-10.93	146.5
141.00	-9.98	147.8
142.00	-10.80	149.8
143.00	-13.48	153.7
144.00	-19.30	165.6
145.00	-27.24	255.1
146.00	-17.90	306.7
147.00	-13.74	315.0
148.00	-11.94	318.4
149.00	-11.50	320.5
150.00	-12.11	322.1
151.00	-13.75	323.6
152.00	-16.66	325.1
153.00	-21.80	327.5
154.00	-35.43	339.9
155.00	-27.66	140.5
156.00	-21.17	144.5
157.00	-18.42	146.2
158.00	-17.18	147.5
159.00	-16.83	148.6
160.00	-17.16	149.6
161.00	-18.06	150.6
162.00	-19.52	151.5
163.00	-21.62	152.4
164.00	-24.54	153.2
165.00	-28.81	153.8
166.00	-36.41	153.4
167.00	-49.36	347.1
168.00	-34.56	339.5
169.00	-30.21	339.7
170.00	-27.96	340.4
171.00	-26.66	341.1
172.00	-25.92	342.0
173.00	-25.53	342.8
174.00	-25.37	343.5
175.00	-25.37	344.2
176.00	-25.46	344.9
177.00	-25.58	345.4
178.00	-25.70	345.8
179.00	-25.78	346.1
180.00	-25.81	346.1

Table 4.6.1: Ogival cylinder with OG-C-1 coating, cylindrical tip; 2.0 GHz.

BACKSCATTERING CROSS SECTION		
THETA	10*LOG(SIGMA/LAMBDA)	PHASE
80.00	1.35	4.0
82.00	1.72	2.7
84.00	2.00	1.6
86.00	2.20	0.8
88.00	2.30	0.3
90.00	2.31	360.0
92.00	2.23	359.9
94.00	2.06	360.0
96.00	1.80	0.4
98.00	1.44	1.0
100.00	0.99	2.0
102.00	0.44	3.3
104.00	-0.20	5.0
106.00	-0.95	7.2
108.00	-1.79	9.9
110.00	-2.72	13.4
112.00	-3.73	17.8
114.00	-4.80	23.2
116.00	-5.88	29.9
118.00	-6.91	37.9
120.00	-7.81	47.3
122.00	-8.51	57.5
124.00	-8.94	67.9
126.00	-9.14	77.8
128.00	-9.16	86.5
130.00	-9.09	94.0
132.00	-9.00	100.1
134.00	-8.95	105.0
136.00	-8.97	108.9
138.00	-9.07	112.0
140.00	-9.27	114.4
142.00	-9.56	116.1
144.00	-9.95	117.4
146.00	-10.44	118.2
148.00	-11.02	118.5
150.00	-11.70	118.3
152.00	-12.47	117.6
154.00	-13.34	116.3
156.00	-14.28	114.4
158.00	-15.29	111.7
160.00	-16.35	108.1
162.00	-17.43	103.5
164.00	-18.47	97.8
166.00	-19.42	91.1
168.00	-20.20	83.7
170.00	-20.77	76.2
172.00	-21.13	69.2
174.00	-21.32	63.3
176.00	-21.39	58.9
178.00	-21.41	56.2
180.00	-21.41	55.3

Table 4.6.2: Ogival cylinder with OG-C-1 coating, cylindrical tip; 2.5 GHz.

BACKSCATTERING CROSS SECTION		
THETA	10*LOG(SIGMA/LAMBDA)	PHASE
80.00	0.31	2.0
82.00	0.94	1.2
84.00	1.41	0.5
86.00	1.72	359.8
88.00	1.88	359.2
90.00	1.89	358.7
92.00	1.76	358.2
94.00	1.48	357.8
96.00	1.04	357.4
98.00	0.44	357.1
100.00	-0.33	356.8
102.00	-1.30	356.6
104.00	-2.50	356.4
106.00	-3.96	356.3
108.00	-5.78	356.1
110.00	-8.07	356.0
112.00	-11.10	355.6
114.00	-15.49	354.7
116.00	-23.68	350.1
118.00	-30.36	196.6
120.00	-18.99	184.1
122.00	-14.70	183.0
124.00	-12.25	183.1
126.00	-10.68	183.7
128.00	-9.64	184.5
130.00	-8.97	185.5
132.00	-8.56	186.7
134.00	-8.37	188.0
136.00	-8.35	189.4
138.00	-8.47	190.8
140.00	-8.72	192.3
142.00	-9.07	193.9
144.00	-9.52	195.4
146.00	-10.05	196.9
148.00	-10.66	198.3
150.00	-11.34	199.6
152.00	-12.09	200.7
154.00	-12.90	201.5
156.00	-13.77	202.1
158.00	-14.69	202.3
160.00	-15.66	202.0
162.00	-16.66	201.3
164.00	-17.68	200.0
166.00	-18.70	198.1
168.00	-19.67	195.7
170.00	-20.58	192.8
172.00	-21.36	189.8
174.00	-22.00	186.8
176.00	-22.47	184.2
178.00	-22.75	182.6
180.00	-22.84	182.0

Table 4.6.3: Ogival cylinder with OG-C-1 coating, cylindrical tip; 3.75 GHz.

BACKSCATTERING CROSS SECTION		
THETA	10*LOG(SIGMA/LAMBDA)	PHASE
80.00	-1.07	353.6
82.00	0.42	352.2
84.00	1.50	350.7
86.00	2.23	349.2
88.00	2.64	347.6
90.00	2.75	345.9
92.00	2.56	344.2
94.00	2.06	342.5
96.00	1.24	340.6
98.00	0.07	338.5
100.00	-1.53	336.2
102.00	-3.63	333.2
104.00	-6.43	329.1
106.00	-10.28	322.2
108.00	-15.92	305.9
110.00	-21.94	248.7
112.00	-18.02	192.1
114.00	-14.59	176.1
116.00	-13.02	169.5
118.00	-12.63	165.7
120.00	-13.17	163.0
122.00	-14.58	160.7
124.00	-17.07	157.9
126.00	-21.30	152.9
128.00	-29.84	132.3
130.00	-29.84	15.7
132.00	-22.13	356.8
134.00	-18.55	353.0
136.00	-16.55	352.1
138.00	-15.43	352.4
140.00	-14.89	353.4
142.00	-14.78	355.0
144.00	-15.01	357.1
146.00	-15.52	359.7
148.00	-16.26	2.9
150.00	-17.20	6.8
152.00	-18.31	11.2
154.00	-19.55	16.3
156.00	-20.88	22.0
158.00	-22.28	28.4
160.00	-23.71	35.1
162.00	-25.15	42.1
164.00	-26.59	49.2
166.00	-28.02	56.1
168.00	-29.44	62.7
170.00	-30.83	69.0
172.00	-32.15	74.7
174.00	-33.35	79.8
176.00	-34.32	84.0
178.00	-34.96	86.7
180.00	-35.18	87.7

Table 4.6.4: Ogival cylinder with OG-C-1 coating, cylindrical tip; 7.5 GHz.

BACKSCATTERING CROSS SECTION		
THETA	10*LOG(SIGMA/LAMBDA)	PHASE
80.00	1.32	153.6
82.00	1.27	170.2
84.00	1.24	187.1
86.00	2.80	204.9
88.00	4.92	221.4
90.00	6.18	237.9
92.00	6.22	247.5
94.00	4.98	240.3
96.00	2.67	222.9
98.00	0.69	191.0
100.00	0.85	157.0
102.00	1.43	134.6
104.00	0.70	118.9
106.00	-1.94	101.7
108.00	-6.50	68.4
110.00	-7.66	6.9
112.00	-4.87	332.1
114.00	-4.05	316.2
116.00	-5.61	303.5
118.00	-9.93	283.6
120.00	-15.10	223.0
122.00	-11.09	166.8
124.00	-8.41	150.0
126.00	-8.36	142.1
128.00	-10.64	135.0
130.00	-16.31	126.5
132.00	-28.86	40.3
134.00	-17.36	331.0
136.00	-13.56	323.5
138.00	-12.75	320.1
140.00	-13.84	317.3
142.00	-16.80	313.6
144.00	-22.68	304.0
146.00	-32.97	283.6
148.00	-24.13	162.2
150.00	-20.09	153.9
152.00	-18.63	151.5
154.00	-18.52	150.8
156.00	-19.37	150.8
158.00	-21.03	151.3
160.00	-23.50	152.1
162.00	-26.95	153.1
164.00	-31.95	154.1
166.00	-40.88	154.0
168.00	-49.09	344.4
170.00	-38.03	341.7
172.00	-34.58	342.8
174.00	-32.93	344.2
176.00	-32.09	345.5
178.00	-31.69	346.3
180.00	-31.58	346.6

Table 4.6.5: Ogival cylinder with OG-C-1 coating, cylindrical tip; 15.0 GHz.

BACKSCATTERING CROSS SECTION

THETA	10*LOG(SIGMA/LAMBDA)	PHASE
80.00	10.06	321.5
81.00	10.76	342.8
82.00	11.05	7.5
83.00	11.65	34.4
84.00	12.68	58.7
85.00	13.60	78.1
86.00	14.00	93.9
87.00	13.85	107.9
88.00	13.31	120.4
89.00	12.62	130.3
90.00	11.96	134.2
91.00	11.50	129.5
92.00	11.63	117.0
93.00	12.45	101.9
94.00	13.33	88.6
95.00	13.63	76.8
96.00	13.03	63.8
97.00	11.54	46.0
98.00	9.82	19.2
99.00	9.22	346.5
100.00	9.58	319.3
101.00	9.41	299.3
102.00	7.89	280.7
103.00	4.86	254.9
104.00	2.14	209.7
105.00	3.12	164.7
106.00	4.26	139.5
107.00	3.46	121.6
108.00	.36	98.8
109.00	-3.63	49.8
110.00	-1.75	353.8
111.00	.51	329.7
112.00	.23	315.8
113.00	-2.93	300.6
114.00	-9.86	257.5
115.00	-7.36	173.0
116.00	-3.14	150.2
117.00	-2.54	140.0
118.00	-5.05	129.8
119.00	-12.29	100.0
120.00	-11.23	358.2
121.00	-5.18	336.0
122.00	-3.34	330.3
123.00	-4.14	328.5
124.00	-7.91	330.2
125.00	-18.13	351.1
126.00	-14.55	120.3

Table 4.6.5 Continued

127.00	-8.51	130.1
128.00	-7.21	131.7
129.00	-6.81	130.8
130.00	-14.43	124.8
131.00	-24.93	7.8
132.00	-12.08	328.7
133.00	-8.10	325.7
134.00	-6.97	325.8
135.00	-7.74	327.6
136.00	-10.54	332.0
137.00	-16.73	346.6
138.00	-22.84	81.3
139.00	-14.60	124.5
140.00	-11.25	133.4
141.00	-10.32	138.4
142.00	-11.06	143.1
143.00	-13.51	149.9
144.00	-18.41	165.4
145.00	-24.49	229.5
146.00	-18.78	288.5
147.00	-14.78	302.9
148.00	-12.99	309.2
149.00	-12.56	313.3
150.00	-13.20	316.7
151.00	-14.89	320.4
152.00	-17.90	325.3
153.00	-23.16	335.8
154.00	-32.59	30.6
155.00	-26.10	113.9
156.00	-21.10	127.8
157.00	-18.72	133.2
158.00	-17.64	136.6
159.00	-17.39	139.3
160.00	-17.78	141.7
161.00	-18.72	144.1
162.00	-20.22	146.6
163.00	-22.31	149.7
164.00	-25.19	154.0
165.00	-29.23	161.4
166.00	-35.40	180.6
167.00	-40.30	252.5
168.00	-34.68	299.4
169.00	-31.02	311.9
170.00	-28.98	317.5
171.00	-27.80	320.9
172.00	-27.14	323.3
173.00	-26.83	325.2
174.00	-26.75	326.7
175.00	-26.82	327.9
176.00	-26.97	328.9
177.00	-27.15	329.7
178.00	-27.31	330.3
179.00	-27.42	330.7
180.00	-27.46	330.8

CHAPTER 5

CONCLUSIONS

Our analyses of the types of scattering contributions that the ogival and wedge cylinders present has shown how it is possible to specify the impedances that would be most effective in reducing the scattering; and given the impedances it is then possible to define an impedance variation over the surface that would be optimum in reducing the backscattering cross section over a given range of aspects subject to some constraints or (say) the maximum allowed value of Re. η. This knowledge can be used to specify the desired properties of a coating material and program RAMD then enables us to compute the cross section reduction that would be realized with any actual coating material.

Of the materials available for assessment, that designated OG-C-1 proved most effective, and the optimum application of it has been determined. The resulting coating should produce approximately 10 dB cross section reduction at near edge-on aspects and over most of the frequency band, but though the performance is quite impressive considering the small thickness ($\leq$ 50 mils) of material allowed and the broad range of frequencies to be covered, it is not felt to be the best that is attainable. Indeed, no use has been made of the existing technology of 'thin film' materials, and judged by the capability that existed even in the late 1960's, thin films would appear to have just the properties which are desired for this type of application.

CHAPTER 6

REFERENCES

1. Bowman, J.J., T.B.A. Senior and P.L.E. Uslenghi (1969), "Electromagnetic and acoustic scattering by simple shapes", North-Holland Publishing Co., Amsterdam.

2. Knott, E.F. and T.B.A. Senior (1973), "Non-specular radar cross section study", The University of Michigan Radiation Laboratory Report No. 011062-1-T.

3. Knott, E.F. and T.B.A. Senior (1974), "Non-specular radar cross section study", The University of Michigan Radiation Laboratory Report No. 011764-1-T.

4. Knott, E.F., V.V. Liepa and T.B.A. Senior (1973), "Non-specular radar cross section study", The University of Michigan Radiation Laboratory Report No. 011062-1-F.

5. Liepa, V.V., E.F. Knott and T.B.A. Senior (1974), "Scattering from two-dimensional bodies with absorber sheets", The University of Michigan Radiation Laboratory Report No. 011764-2-T.

6. Maliuzhinets, G.D. (1959), "Excitation, reflection and transmission of surface waves from a wedge with given face impedances", Sov. Phys.-Dokl. 3 (4), 752-755.

7. Senior, T.B.A. (1960), "Impedance boundary conditions for imperfectly conducting surfaces", Appl. Sci. Res. 8 B, 418-436.

8. Senior, T.B.A. (1962), "A note on impedance boundary conditions", Can. J. Phys. 40, 663-665.

9. Senior, T.B.A. and E.F. Knott (1968), "Research on resonant region radar camouflage techniques, The University of Michigan Radiation Laboratory Report No. 8077-9-T (CONFIDENTIAL).

10. Senior, T.B.A. (1972), "The diffraction matrix for a discontinuity in curvature", IEEE Trans. AP-20 (3), 326-333.

11. Senior, T.B.A. (1976), "Cell curvature effects", The University of Michigan Radiation Laboratory Memorandum No. 014518-502-M.

12. Senior, T.B.A. (1977), unpublished notes.

APPENDIX A

COMPUTER PROGRAM RAMVS (as of August 1976)

Program RAMVS was developed during the latter stages of Contract F33615-73-C-1174 to compute the field scattered by a two dimensional body in the presence of (lossy) electric and magnetic sheets. With an impedance boundary condition imposed at the surface of the body and the usual transition conditions at the thin sheets, the program solves the set of three coupled integral equations for the currents induced. The electric and magnetic sheets can be superposed to simulate the effect of a thin layer of absorber of arbitrary permittivity and permeability and it had been our hope to do this for an absorbing coating applied to a body.

The original program was documented by Liepa et al (1974), but since that time a number of minor errors have been found and corrected and we have also modified the expression for the self cell contribution by including higher order terms. In order to save space we will not repeat the entire formulation of the present RAMVS, but will list the differences from the version in Liepa et al by citing the equations from that reference:

on p. 10, equation (2.8) should read

$$H_s^i(s_1) = \frac{i}{4}\int_{C_1} J_z(s')(\hat{n}\cdot\hat{r})H_1^{(1)}(kr)\,d(ks') + Z_m(s_1)J_s^*(s_1)\textcircled{Y_o}$$

$$+ \ldots .$$

The free space impedance circled was left out.

on p. 14, equation (2.18) should read

$$A_1 J_z(s_1) = \ldots .$$

$$+ \textcircled{\frac{1}{4}}\int_{\pm 2\Delta} J_z(s')H_0^{(1)}(kr)\,d(ks') + \textcircled{\frac{1}{4}}\int_{C_1-(\Delta\mp 2\Delta)} J_z(s_1')H_0^{(1)}(kr)\,d(ks'),$$

the factor $\frac{1}{4}$ having been omitted;

on p. 17, equation (2.22) should be

$$A_5 J_s^*(s_1) = \left\{ Z_m(s_1) + \frac{iY_0}{\pi^2 \Delta/\lambda} + Y_0 \frac{\Delta(s_1)}{② \lambda} \left[\frac{\pi}{2} + i \left(\ell n \frac{\Delta(s_1)}{\lambda} + 0.02879837 \right) \right] \right\}_\Delta J_s^*(s_1)$$
$$+ \ldots .$$

The factor 2 appears in the denominator as the result of retaining higher order terms in the expansions of the Hankel functions.

on p. 33, the equations at the top of the page should be

$$\left(\frac{ZE}{\lambda}\right) = \frac{i}{2\pi(\epsilon_r - 1)\Delta} = \frac{i}{2\pi(4. + i3.)(.05)} = 0.382 + i\,0.509$$

$$\left(\frac{ZM}{\lambda}\right) = \frac{i}{2\pi(\mu_r - 1)\Delta} = \frac{i}{2\pi(1. + i1.)(.05)} = 1.59 + i1.59$$

The use of electric and magnetic impedances which are normalized with respect to the wavelength somewhat simplifies the computer code and eliminates one hand computation in preparing the input data. In addition, quite extensive changes have been made in the RAMVS source code to incorporate the above modifications and to make such other corrections found necessary, and instead of citing them individually, we include the complete program listing later in this Appendix.

This latest version of the program has been applied to perfectly conducting cylinders, cylinders with specific surface impedance variations, and thin electric and magnetic cylindrical shells. It presumably works (but has not been used) for cylinders surrounded by electric and/or magnetic sheets provided the sheets are not too close to the cylinder or to each other. It has been shown to work for single and multiple (but well separated) sheets extending outwards (like fins) from an ogival cylinder.

The words "not too close to" and "well separated" hint at the difficulty experienced in trying to use the program as a tool in our present work. By placing one or more sheets close to the surface of the perfectly conducting ogival or wedge cylinder, we had hoped to simulate the effect of an absorbing coating whose electric and magnetic properties could vary in depth as well as along the surface, and would be explicit in the specification of the sheets. Unfortunately, the program now ran into difficulties. Because of the formulation used here and in most other programs based on discrete sampling to derive a system of simultaneous equations from an integral equation, RAMVS fails when the distance between two surfaces becomes comparable to the cell size or sampling distance. This was recognized when we examined the effect of changes in cell size on the solution for a sheet close to the surface of the body, and though we immediately began an intensive investigation in an attempt to work around the difficulty, our endeavors were not successful.

In the hope that there was a cell size or sampling distance that would be adequate to produce the desired accuracy, a numerical experiment was performed using an ogival cylinder surrounded by an absorber sheet. As the sheet-body spacing h and the cell sizes were varied, the changes in the backscattering cross section averaged over 30° about edge-on were recorded, the expectation being that when the sampling rate was sufficient, the results would be substantially independent of any further decrease in the cell size. To minimize the computer costs, we chose a wavelength of 10.7 inches for which the ogival cylinder is only about 0.44λ in length, with 12 (i.e. 6 times 2) sampling points on the sheet and either 12 or 16 on the cylinder. The sheet-body spacings considered were $h = 0.5(0.25)1.5$ inches. Figure A-1 shows the changes in the average cross section as a function of h/Δ where Δ is the cell size on the cylinder for either 12 or 16 sampling points there. From the amplitude and phase data, it is evident that the accuracy rapidly diminishes for $h/\Delta \lesssim 0.8$ and, in effect, the program fails if $h < 0.8\Delta$. For $h \gtrsim \Delta$, the differences of 0.5 dB in amplitude and 0.5° in phase could doubtless be reduced were more sampling points used.

Having determined the minimum (practical) spacing h in terms of the cell size, program RAMVS was now run for a sheet spaced 0.2 inches from the surface

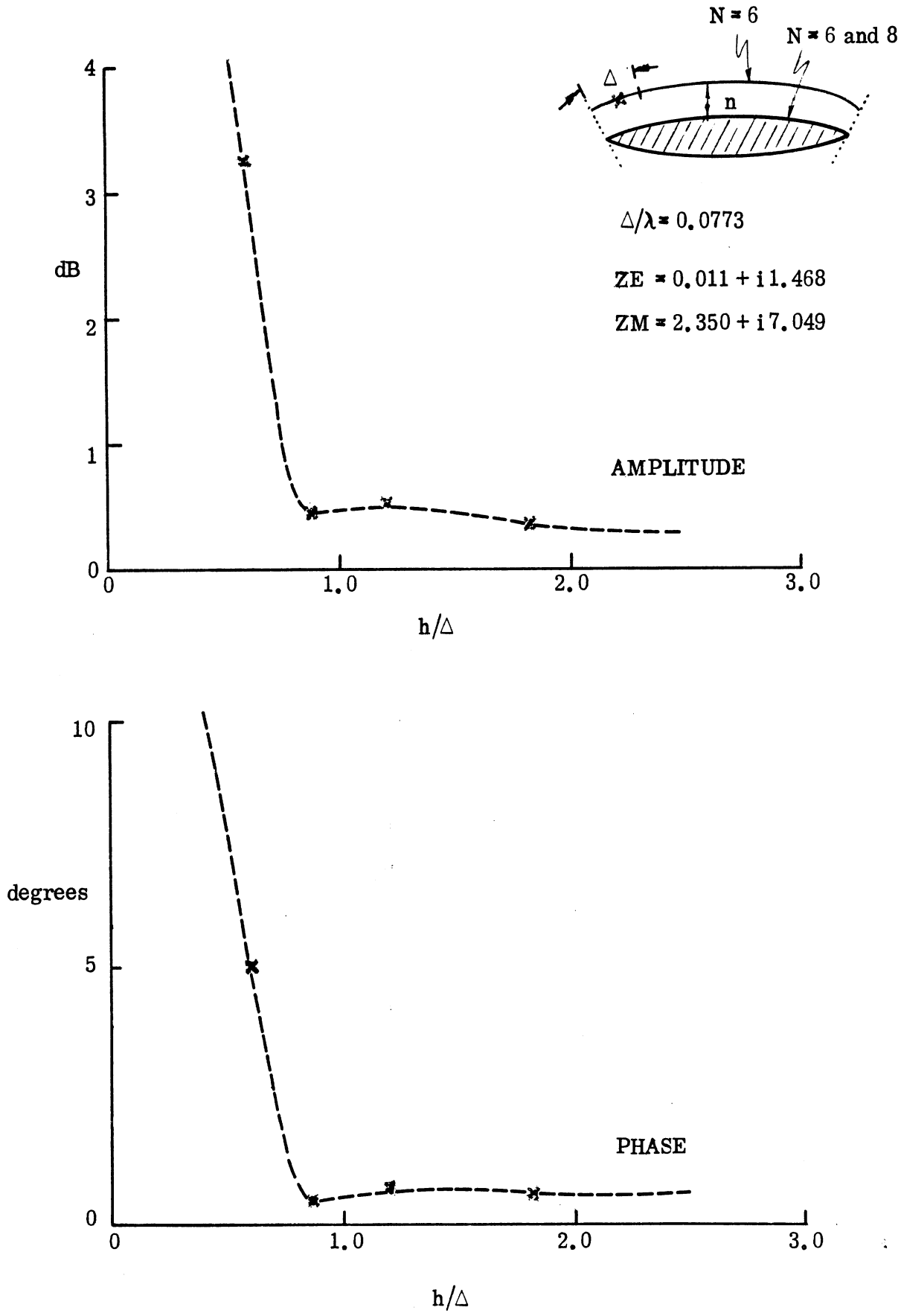

Figure A-1: "Failure" of RAMVS as the body-sheet spacing decreases.

of the ogive. The sheet parameters were chosen in an effort to simulate a layer of the OG-C-1 material 0.05 inches thick, but the results were substantially different from those measured by Emerson and Cuming. To some degree this was not surprising since it is known that to obtain an accurate simulation the sheet must be placed at the mid-point of the layer, but because the discrepancies were much greater than we had hoped, we now ran the program for a circular cylinder with a surrounding sheet and compared the results with data obtained from a Mie series computation for a cylinder with a uniform coating. The comparison left no doubt that the sheet must be located within the layer it is designed to simulate, and only if the sheet is about 0.025 inches from the body could we hope to reproduce the effect of a coating 0.050 inches thick. In view of our previous findings we were now faced with the need for a cell size (or sampling distance) not exceeding (about) 0.020 inches, a quite intolerable requirement for the size of body to be considered.

Various approaches were tried in an attempt to overcome this limitation, for example, by choosing sampling points not directly opposite each other on the two adjacent surfaces. By moving the points around, we sought the most effective arrangement, and though it did prove beneficial to have the points staggered or interlaced, the allowed reduction in the minimum sheet-body spacing was no more than 10 percent. This finally convinced us that there was no simple remedy to the problem. We did look at the possibility of reformulating the program to permit its use for the purposes of this Contract. As a minimum, the reformulation would require the special treatment of all pairs of adjacent cells on the two surfaces and because of the magnitude of this task, it was felt impossible to accomplish it with the time and funds available on the Contract. We therefore had to abandon RAMVS as a tool for use in our investigation.

A complete fortran listing of RAMVS is as follows:

```
CCCCCCCCCCCCCCCCCCCCCCCCCCCCCCCCCCCCCCCCCCCCCCCCCCCCCCCCCCCCCCCCCCCCCCCCCC
C                                                                      C
C                          *** RAMVS ***                               C
C                        (10-03-74 VERSION)                    VVL     C
C                        (MODIFIED 30-08-75)                   VVL     C
C                        (MODIFIED 24-11-75)                   VVL     C
C                        (MODIFIED 25-5-76)                    VVL     C
C                        (MODIFIED 1-10-76)                    A.L.    C
C   THIS PROGRAM COMPUTES NEAR-FIELD AND FAR-FIELD SCATTERING FROM     C
C   A GENERAL IMPEDANCE BODY IN PRESENCE OF ABSORBER SHEETS;           C
C   TWO-DIMENSIONAL GEOMETRY, EXP(-IWT) TIME CONVENTION.               C
C                                                                      C
C   RE: V.V.LIEPA,E.F.KNOTT,AND T.B.A.SENIOR,"COMPUTER PROGRAM FOR     C
C   SCATTERING FROM TWO-DIMENSIONAL BODIES WITH ABSORBER SHEETS",      C
C   THE UNIVERSITY OF MICHIGAN RADIATION LABORATORY REPORT             C
C   NO.011764-2-T (AFAL-TR-74   ),      1974.                          C
C                                                                      C
CCCCCCCCCCCCCCCCCCCCCCCCCCCCCCCCCCCCCCCCCCCCCCCCCCCCCCCCCCCCCCCCCCCCCCCCCC
C                                                                      C
C                      *** INPUT DATA FORMAT ***                       C
C----------------------------------------------------------------------C
C     A    FORMAT (18A4)          TITLE CARD; USE UP TO 72 COLUMNS     C
C----------------------------------------------------------------------C
C     B    FORMAT (I2,I3,4F10.5)   MORE,IPOL,WAVE,ZSFAC,ZEFAC,ZMFAC   C
C          MORE=0       THIS WILL BE THE LAST RUN FOR THIS DATA SET   C
C          MORE=1       THERE ARE MORE DATA TO BE READ AFTER THIS SET C
C          IPOL=1       E-POLARIZATION                                C
C          IPOL=2       H-POLARIZATION                                C
C          WAVE         WAVELENGTH                                    C
C          ZSFAC        MULTIPLYING FACTOR(REAL) FOR ALL ZS           C
C          ZEFAC        MULTIPLYING FACTOR(REAL) FOR ALL ZE           C
C          ZMFAC        MULTIPLYING FACTOR(REAL) FOR ALL ZM           C
C----------------------------------------------------------------------C
C     C    FORMAT (I2,3X,4F10.5)  KODE,FIRST,LAST,INK,CANG            C
C          KODE=0       COMPUTES BISTATIC SCATTERING PATTERN          C
C          KODE=1       COMPUTES BACKSCATTERING PATTERN               C
C          FIRST        INITIAL SCATTERING AND INCIDENCE ANGLE        C
C          LAST         FINAL ANGLE                                   C
C          INK          ANGULAR INCREMENT                             C
C          CANG         ANGLE FOR SURFACE FIELD COMPUTATIONS          C
C----------------------------------------------------------------------C
C              (DATA D, E, AND F REQUIRED FOR EACH ABSORBER SEGMENT;   C
C               AT LEAST ONE ABSORBER AND ONE IMPEDANCE SEGMENT IS     C
C               REQUIRED. ABSRORBER SEGMENTS MUST BE READ IN FIRST.)   C
C     D    FORMAT (I2,I3,5F10.5)  TYPE,N,XA,YA,XB,YB,ANG              C
C          TYPE=1 ABSORBER SHEET                                       C
C          TYPE=2 IMPEDANCE SURFACE                                    C
C          N            NUMBER OF SAMPLING POINTS ON THIS SEGMENT     C
C          XA,YA,XB,YB  SEGMENT ENDPOINTS                             C
C          ANG          ANGLE SUBTENDED BY THE SEGMENT                C
C----------------------------------------------------------------------C
C     E    FORMAT (I2,3X,5F10.5)  FORM,ZEA,ZEB,ZEX                    C
C          FORM=-1      ZE(I)=(ZEA-ZEB*S(I))**ZEX                     C
C          FORM= 0      ZE(I)=ZEA+ZEB*S(I)**ZEX                       C
C          FORM= 1      ZE(I)=ZEA+ZEB*EXP(-ZEX*S(I))                  C
C          ZEA,ZEB      COMPLEX IMPEDANCE CONSTANTS                   C
C          ZEX          REAL IMPEDANCE CONSTANT                       C
C----------------------------------------------------------------------C
C     F    FORMAT (I2,3X,5F10.5)  FORM,ZMA,ZMB,ZMX                    C
C          FORM=-1      ZM(I)=(ZMA-ZMB*S(I))**ZMX                     C
```

```
C           FORM= 0       ZM(I)=ZMA+ZMB*S(I)**ZMX                          C
C           FORM= 1       ZM(I)=ZMA+ZMB*EXP(-ZMX*S(I))                     C
C           ZMA,ZMB       COMPLEX IMPEDANCE CONSTANTS                      C
C           ZMX           REAL IMPEDANCE CONSTANT                          C
C-----------------------------------------------------------------------C
C               (DATA G AND H REQUIRED FOR EACH IMPEDANCE SEGMENT.)        C
C     G     FORMAT (I2,I3,5F10.5)  TYPE,N,XA,YA,XB,YB,ANG                  C
C           TYPE=1 ABSORBER SHEET                                          C
C           TYPE=2 IMPEDANCE SURFACE                                       C
C           N             NUMBER OF SAMPLING POINTS ON THIS SEGMENT        C
C           XA,YA,XB,YB   SEGMENT ENDPOINTS                                C
C           ANG           ANGLE SUBTENDED BY THE SEGMENT                   C
C-----------------------------------------------------------------------C
C     H     FORMAT (I2,3X,5F10.5)  FORM,ZSA,ZSB,ZSX                        C
C           FORM=-1       ZS(I)=(ZSA-ZSB*S(I))**ZSX                        C
C           FORM= 0       ZS(I)=ZSA+ZSB*S(I)**ZSX                          C
C           FORM= 1       ZS(I)=ZSA+ZSB*EXP(-ZSX*S(I))                     C
C           ZSA,ZSB       COMPLEX IMPEDANCE CONSTANTS                      C
C           ZSX           REAL IMPEDANCE CONSTANT                          C
C-----------------------------------------------------------------------C
C     I     FORMAT (I5)             INTEGER ZERO IN COLUMN 5 SHUTS OFF     C
C                                   READING OF SEGMENT PARAMETERS          C
C-----------------------------------------------------------------------C
C               (USE THIS CARD ONLY IF, IN B, MORE=1)                      C
C     J     FORMAT (I2,I3,4F10.5)   MORE,IPOL,WAVE,ZSFAC,ZEFAC,ZMFAC       C
C                                                                          C
CCCCCCCCCCCCCCCCCCCCCCCCCCCCCCCCCCCCCCCCCCCCCCCCCCCCCCCCCCCCCCCCCCCCCCCCCCC
C                                                                          C
C                    *** DIMENSIONING FORMAT ***                           C
C-----------------------------------------------------------------------C
C   VECTORS ARE DIMENSIONED ONLY IN THE MAIN PROGRAM.                      C
C   IF K=NO. POINTS(CELLS) ON THE IMPEDANCE SURFACE AND                    C
C   M=NO. OF POINTS(CELLS) ON THE ABSORBER SHEET, THEN                     C
C                  MK=M+K AND MMK=M+M+K                                    C
C                                                                          C
C.....MAIN PROGRAM-----A STARTER PROGRAM                                   C
C  *  COMPLEX A(MMK,MMK+1),PHI(MMK),PINK(MMK),LL(MMK),MM(MMK)              C
C  *  COMPLEX ZE(MK),ZM(MK)                                                C
C  *  DIMENSION X(MK),Y(MK),XN(MK),YN(MK),S(MK),DSQ(MK)                    C
C  *  DIMENSION LUMP(2,MK)                                                 C
C  *  DATA MI/MMK/                                                         C
C     CALL SMAIN(MI,A,PHI,PINK,ZE,ZM,X,Y,XN,YN,S,DSQ,LL,MM,LUMP)          C
C     END                                                                  C
C                      * CARDS TO BE CHANGED WHEN REDIMENSIONING           C
C                                                                          C
CCCCCCCCCCCCCCCCCCCCCCCCCCCCCCCCCCCCCCCCCCCCCCCCCCCCCCCCCCCCCCCCCCCCCCCCCCC
C
C.....MAIN PROGRAM-----A STARTER PROGRAM
C**** RAMVS VERSION
      COMPLEX A(150,151),PHI(150),PINK(150),LL(150),MM(150)
      COMPLEX ZE(100),ZM(100)
      DIMENSION X(100),Y(100),XN(100),YN(100),S(100),DSQ(100)
      DIMENSION LUMP(2,100)
      DATA MI/150/
      CALL SMAIN(MI,A,PHI,PINK,ZE,ZM,X,Y,XN,YN,S,DSQ,LL,MM,LUMP)
      END
```

```
      SUBROUTINE SMAIN(MI,A,PHI,PINK,ZE,ZM,X,Y,XN,YN,
     &S,DSQ,LL,MM,LUMP)
C**** RAMVS VERSION E-&H-POLARIZATIONS
      DIMENSION LUMP(2,1)
      COMPLEX A(MI,1)
      COMPLEX PHI(1),PINK(1),ZE(1),ZM(1)
      COMPLEX SUM,DEL,SUME,SUMM,SUMK
      DIMENSION X(1),Y(1),XN(1),YN(1),S(1),DSQ(1),LL(1),MM(1)
      DIMENSION ID(18),IPP(2)
      COMMON/PIES/PI,TPI,PIT,PIPI,YZ,RED,DIG
      REAL LAST,INK
      DATA IPP/4HEEEE,4HHHHH/
C.....READ INPUT DATA AND GENERATE BODY PROFILE
    5 READ(5,100,END=999) ID
      READ (5,200) MORE,IPOL,WAVE,ZSFAC,ZEFAC,ZMFAC
      IF(ZSFAC.EQ.0) ZSFAC=1.E-10
      IF(ZEFAC.EQ.0) ZEFAC=1.E-10
      IF(ZMFAC.EQ.0) ZMFAC=1.E-10
      READ (5,210) KODE,FIRST,LAST,INK,CANG
      WRITE (6,150) ID
      CALL GEOM(LUMP,X,Y,XN,YN,S,DSQ,ZE,ZM,K,M)
      IF (KODE.NE.0) GO TO 25
      NINC=1
      NBIT=1+IFIX((LAST-FIRST)/INK)
      GO TO 28
   25 NBIT=0
      NINC=1+IFIX((LAST-FIRST)/INK)
   28 CONTINUE
C.....CONSTRUCT MATRIX ELEMENTS
      M1=M+1
      MK=M+K
      MMK=MK+M
      MM1=M1+M
      DO 35 I=M1,MK
   35 ZE(I)=ZE(I)*ZSFAC
      FACE=ZEFAC*WAVE
      FACM=ZMFAC*WAVE
      XK=TPI/WAVE
      DO 37 I=1,M
      ZE(I)=ZE(I)*FACE
   37 ZM(I)=ZM(I)*FACM
      DO 39 I=1,MK
      S(I)=S(I)/WAVE
   39 DSQ(I)=DSQ(I)/WAVE
      GO TO 50
   40 FAC=ZSFAC/PZSFAC
      DO 45 I=M1,MK
   45 ZE(I)=ZE(I)*FAC
      FAC=WAVE/PWAVE
      FACE=ZEFAC/PZEFAC*FAC
      FACM=ZMFAC/PZMFAC*FAC
      DO 47 I=1,M
      ZE(I)=ZE(I)*FACE
   47 ZM(I)=ZM(I)*FACM
      FAC=PWAVE/WAVE
      XK=TPI/WAVE
      DO 49 I=1,MK
      S(I)=S(I)*FAC
   49 DSQ(I)=DSQ(I)*FAC
   50 CONTINUE
```

```
      IF (IPOL.EQ.1) CALL MTXEL1(MI,M,K,XK,X,Y,XN,YN,DSQ,ZE,ZM,A)
      IF (IPOL.EQ.2) CALL MTXEL2(MI,M,K,XK,X,Y,XN,YN,DSQ,ZE,ZM,A)
      I=LUMP(2,MK)
      WRITE(6,400) IPP(IPOL),ZSFAC,ZEFAC,ZMFAC,MK,I,NINC,NBIT,WAVE
C.....COMPUTE INCIDENT FIELD AND INVERT MATRIX
      TETA=RED*CANG
      CT=COS(TETA)
      ST=SIN(TETA)
      DO 60 I=1,M
      HOLD=-XK*(CT*X(I)+ST*Y(I))
      DEL=CMPLX(COS(HOLD),SIN(HOLD))
      PINK(I)=DEL
   60 PINK(I+M)=-DEL*(XN(I)*CT+YN(I)*ST)
      DO 63 I=M1,MK
      HOLD=-XK*(CT*X(I)+ST*Y(I))
   63 PINK(I+M)=CMPLX(COS(HOLD),SIN(HOLD))
      CALL FLIP(A,MMK,MI,LL,MM,PINK,PHI,1)
      WRITE (6,150) ID
C.....PRINT OUT STUFF FOR THE ABSORBER SURFACE (SPECIFIED ANGLE ONLY)
      WRITE (6,350)CANG
      WRITE (6,375)
      DO 67 I=1,M
      DEL=PHI(I)+(1.E-50,0.)
      AMPE=CABS(DEL)
      PHASEE=DIG*ATAN2(AIMAG(DEL),REAL(DEL))
      DEL=PHI(I+M)+(1.E-50,0.)
      AMPH=CABS(DEL)
      PHASEH=DIG*ATAN2(AIMAG(DEL),REAL(DEL))
      IF (IPOL.EQ.1) WRITE(6,395) (LUMP(J,I),J=1,2),X(I),Y(I),S(I),
     &DSQ(I),ZE(I),ZM(I),AMPE,PHASEE,AMPH,PHASEH
   67 IF (IPOL.EQ.2) WRITE(6,395) (LUMP(J,I),J=1,2),X(I),Y(I),S(I),
     &DSQ(I),ZE(I),ZM(I),AMPH,PHASEH,AMPE,PHASEE
C.....PRINT OUT STUFF FOR THE IMPEDANCE SURFACE (SPECIFIED ANGLE ONLY)
      WRITE (6,300)CANG
      WRITE (6,325)
      DO 65 I=M1,MK
      IM=I+M
      DEL=PHI(IM)+(1.E-50,0.)
      AMP=CABS(DEL)
      PHASE=DIG*ATAN2(AIMAG(DEL),REAL(DEL))
      DEL=ZE(I)
   65 WRITE (6,250) (LUMP(J,I),J=1,2),X(I),Y(I),S(I),DSQ(I),
     &DEL,AMP,PHASE
C.....DOPE OUT THE APPROPRIATE FIELD FACTORS
      WRITE (6,150) ID
      THE=FIRST-INK
      IF (KODE.EQ.1) GO TO 70
      WRITE (6,800) CANG,IPP(IPOL)
      GO TO 75
   70 WRITE (6,600) IPP(IPOL)
   75 THE=THE+INK
      IF (THE.GT.LAST) GO TO 105
      IF (THE.EQ.FIRST .AND. CANG.EQ.FIRST) GO TO 85
      TETA=RED*THE
      CT=COS(TETA)
      ST=SIN(TETA)
C.....IN THE FOLLOWING LOOP COMPUTE THE NEW INCIDENT FIELD
      DO 80 I=1,M
      HOLD=-XK*(CT*X(I)+ST*Y(I))
      DEL=CMPLX(COS(HOLD),SIN(HOLD))
```

```
      PINK(I)=DEL
   80 PINK(I+M)=-DEL*(XN(I)*CT+YN(I)*ST)
      DO 83 I=M1,MK
      HOLD=-XK*(CT*X(I)+ST*Y(I))
   83 PINK(I+M)=CMPLX(COS(HOLD),SIN(HOLD))
      IF (KODE.EQ.0) GO TO 85
      CALL FLIP(A,MMK,MI,LL,MM,PINK,PHI,2)
   85 CONTINUE
C.....ADD UP THE CURRENTS FOR FAR FIELD
      SUM=(1.E-25,0.)
      SUME=SUM
      SUMM=SUM
      SUMK=SUM
      DO 93 I=1,M
      IM=I+M
      DS=DSQ(I)
      SUME=SUME-PHI(I)*PINK(I)*DS
   93 SUMM=SUMM+PHI(IM)*PINK(IM)*DS
      SUMM=SUMM*YZ
      IF (IPOL.EQ.2) GO TO 90
      DO 95 I=M1,MK
      IM=I+M
   95 SUMK=SUMK+(-1.+ZE(I)*(XN(I)*CT+YN(I)*ST))*PINK(IM)*DSQ(I)*PHI(IM)
      GO TO 99
   90 DEL=SUME
      SUME=-SUMM/YZ
      SUMM=DEL*YZ
      DO 97 I=M1,MK
      IM=I+M
   97 SUMK=SUMK+(-ZE(I)+(XN(I)*CT+YN(I)*ST))*PINK(IM)*DSQ(I)*PHI(IM)
   99 DEL=SUME+SUMM
      SUM=DEL+SUMK
      AMPR=REAL(SUME)
      AMPI=AIMAG(SUME)
      PHASEE=DIG*ATAN2(AMPI,AMPR)
      AMPR=PIT*(AMPR*AMPR+AMPI*AMPI)
      SCATE=10.*ALOG10(AMPR)
      AMPR=REAL(SUMM)
      AMPI=AIMAG(SUMM)
      PHASEM=DIG*ATAN2(AMPI,AMPR)
      AMPR=PIT*(AMPR*AMPR+AMPI*AMPI)
      SCATM=10.*ALOG10(AMPR)
      AMPR=REAL(DEL)
      AMPI=AIMAG(DEL)
      PHASED=DIG*ATAN2(AMPI,AMPR)
      AMPR=PIT*(AMPR*AMPR+AMPI*AMPI)
      SCATD=10.*ALOG10(AMPR)
      AMPR=REAL(SUMK)
      AMPI=AIMAG(SUMK)
      PHASEK=DIG*ATAN2(AMPI,AMPR)
      AMPR=PIT*(AMPR*AMPR+AMPI*AMPI)
      SCATK=10.*ALOG10(AMPR)
      AMPR=REAL(SUM)
      AMPI=AIMAG(SUM)
      PHASET=DIG*ATAN2(AMPI,AMPR)
      AMPR=PIT*(AMPR*AMPR+AMPI*AMPI)
      SCATT=10.*ALOG10(AMPR)
      WRITE(6,900) THE,SCATE,PHASEE,SCATM,PHASEM,SCATD,PHASED,
     &SCATK,PHASEK,SCATT,PHASET
      GO TO 75
```

```
105   PZSFAC=ZSFAC
      PWAVE=WAVE
      PZEFAC=ZEFAC
      PZMFAC=ZMFAC
      IF (MORE.EQ.0) GO TO 5
      READ (5,200) MORE,IPOL,WAVE,ZSFAC,ZEFAC,ZMFAC
      IF(ZSFAC.EQ.0) ZSFAC=1.E-10
      IF(ZEFAC.EQ.0) ZEFAC=1.E-10
      IF(ZMFAC.EQ.0) ZMFAC=1.E-10
      WRITE (6,150) ID
      GO TO 40
100   FORMAT (18A4)
150   FORMAT (1H1,18A4)
200   FORMAT (I2,I3,4F10.5)
210   FORMAT (I2,3X,4F10.5)
250   FORMAT(1H ,2I3,4F8.4,1X,2F11.3,F9.4,F9.3)
300   FORMAT(////18HOIMPEDANCE SURFACE,';INCIDENT FIELD DIRECTION=',F7.2)
350   FORMAT(17HOABSORBER SURFACE,';INCIDENT FIELD DIRECTION=',F7.2)
325   FORMAT(8HO  I SEG,4X,1HX,7X,1HY,7X,1HS,6X,3HDSQ,
     &11X,10H--- ZS ---,5X,7HMOD(JS),2X,7HARG(JS)/)
375   FORMAT(8HO  I SEG,4X,1HX,7X,1HY,7X,1HS,6X,3HDSQ,
     &11X,10H--- ZE ---,13X,10H--- ZM ---,5X,7HMOD(JE),2X,7HARG(JE),2X,
     &7HMOD(JM),2X,7HARG(JM)/)
395   FORMAT(1H ,2I3,4F8.4,2(1X,2F11.3),2(F9.4,F9.3))
400   FORMAT (//25X,14HKEY PARAMETERS//
     &10X,21HINCIDENT POLARIZATION,18X,1A1/
     &10X,24HSURFACE IMPEDANCE FACTOR,F22.5/
     &10X,25HELECTRIC IMPEDANCE FACTOR,F21.5/
     &10X,25HMAGNETIC IMPEDANCE FACTOR,F21.5/
     &10X,34HTOTAL NUMBER OF POINTS ON THE BODY,I6/
     &10X,23HNUMBER OF SEGMENTS USED,I17/
     &10X,35HNUMBER OF INCIDENT FIELD DIRECTIONS,I5/
     &10X,29HNUMBER OF BISTATIC DIRECTIONS,I11/
     &10X,10HWAVELENGTH,F34.3)
600   FORMAT(///,33X,28HBACKSCATTERING CROSS SECTION,/,
     &37X,20H10*LOG(SIGMA/LAMBDA),/,
     &39X,1H(,1A1,14H-POLARIZATION),///,
     &16X,10H(ELECTRIC),7X,10H(MAGNETIC),7X,10H(ABSORBER),7X,
     &11H(IMPEDANCE),8X,7H(TOTAL),/,6X,5HTHETA,2X,
     &5(17H   DB     PHASE  )/)
800   FORMAT(///,31X,33HBISTATIC SCATTERING CROSS SECTION,/,
     &37X,20H10*LOG(SIGMA/LAMBDA),/,
     &30X,29HFOR INCIDENT FIELD DIRECTION=,F6.1,/,
     &39X,1H(,1A1,14H-POLARIZATION),///,
     &16X,10H(ELECTRIC),7X,10H(MAGNETIC),7X,10H(ABSORBER),7X,
     &11H(IMPEDANCE),8X,7H(TOTAL),/,6X,5HTHETA,2X,
     &5(17H   DB     PHASE  )/)
900   FORMAT(4X,F7.2,5(1X,2F8.2))
999   RETURN
      END
```

```
      SUBROUTINE GEOM(LUMP,X,Y,XN,YN,S,DSQ,ZE,ZM,K,H)
C**** RAMVS VERSION
      COMPLEX ZEA,ZEB,ZMA,ZMB,ZFUN,ZE(1),ZM(1)
      DIMENSION X(1),Y(1),XN(1),YN(1),DSQ(1),S(1)
      DIMENSION LUMP(2,1)
      COMMON/PIES/PI,TPI,PIT,PIPI,YZ,RED,DIG
      I=0
      K=0
      L=0
      M=0
      WRITE (6,500)
C.....READ INPUT PARAMETERS AND PREPARE TO GENERATE SAMPLING POINTS
C.....IF TYPE=1 ABSORBER SHEET, M CELLS TOTAL
C.....IF TYPE=2 IMPEDANCE SURFACE,  K CELLS TOTAL
C.....TYPE=1 SURFACE MUST BE READ IN FIRST
   10 READ (5,200) ITYPE,N,XA,YA,XB,YB,ANG
      IF (N.EQ.0) GO TO 120
      LIM=2*N-1
      READ (5,250) IZEFRM,ZEA,ZEB,ZEX
      IF (ITYPE.EQ.1) READ (5,250) IZMFRM,ZMA,ZMB,ZMX
      TX=XB-XA
      TY=YB-YA
      D=SQRT(TX*TX+TY*TY)
      IF (ANG.EQ.0.0) GO TO 20
      T=0.5*RED*ANG
      TRX=TX+TY/TAN(T)
      TRY=TY-TX/TAN(T)
      RAD=0.5*D/SIN(T)
      ARC=2.0*RAD*T
      ALF=T/N
      DID=2.0*RAD*ALF
      GO TO 30
   20 RAD=999.
      ARC=D
      DID=D/N
C.....START GENERATING
   30 LAST=2
      IF(YA.EQ.0.0.AND.YB.EQ.0.0.AND.ANG.EQ.0.0) LAST=1
      DO 110 JIM=1,LAST
      L=L+1
      DO 100 J=1,LIM,2
      I=I+1
      LUMP(2,I)=I
      LUMP(1,I)=I
      IF (I.EQ.1000) WRITE (6,400)
      IF (JIM.EQ.2) GO TO 90
      IF (ANG.EQ.0.0) GO TO 40
      SINQ=SIN(J*ALF)
      COSQ=COS(J*ALF)
      X(I)=XA+0.5*(TRX*(1.0-COSQ)-TRY*SINQ)
      Y(I)=YA+0.5*(TRX*SINQ+TRY*(1.0-COSQ))
      XN(I)=-0.5*(TRX*COSQ+TRY*SINQ)/RAD
      YN(I)= 0.5*(TRX*SINQ-TRY*COSQ)/RAD
      GO TO 50
   40 X(I)=XA+0.5*J*TX/N
      Y(I)=YA+0.5*J*TY/N
      XN(I)=-TY/D
      YN(I)= TX/D
   50 ST=0.5*J*DID
      S(I)=ST
```

```
C.....COMPUTE THE ELECTRIC PARAMETERS
      IF(ITYPE.EQ.1) GO TO 60
C.....ZS IS STORED IN THE ZE VECTOR
      ZE(I)=ZFUN(IZEFRM,ZEA,ZEB,ZEX,ST)
      GO TO 100
   60 ZM(I)=ZFUN(IZMFRM,ZMA,ZMB,ZMX,ST)
      ZE(I)=ZFUN(IZEFRM,ZEA,ZEB,ZEX,ST)
      GO TO 100
C.....FROM HERE TO 100 WE CREATE THE SEGMENT IMAGE
   90 K=I-N
      X(I)=X(K)
      Y(I)=-Y(K)
      XN(I)=XN(K)
      YN(I)=-YN(K)
      S(I)=S(K)
      ZE(I)=ZE(K)
      ZM(I)=ZM(K)
  100 DSQ(I)=DID
      IF (JIM.EQ.1) GO TO 102
      YA=-YA
      YB=-YB
  102 IF(ITYPE.EQ.1) GO TO 105
      WRITE(6,300) L,N,XA,YA,XB,YB,ANG,RAD,ARC,IZEFRM,ZEA,ZEB,ZEX
      K=I-M
      GO TO 110
  105 WRITE(6,350) L,N,XA,YA,XB,YB,ANG,RAD,ARC,IZEFRM,ZEA,ZEB,ZEX
      WRITE(6,351) IZMFRM,ZMA,ZMB,ZMX
      M=I
  110 CONTINUE
      GO TO 10
  200 FORMAT (I2,I3,5F10.5)
  250 FORMAT(I2,3X,5F10.5)
  300 FORMAT(1H ,I2,5H  IMP,I4,1X,4F9.4,1X,2F7.2,F7.3,I4,1X,2F9.3,2X,
     &2F9.3,F10.3)
  350 FORMAT(1H ,I2,5H  ABS,I4,1X,4F9.4,1X,2F7.2,F7.3,I4,1X,2F9.3,2X,
     &2F9.3,F10.3)
  351 FORMAT(71X,I4,2H (,F8.3,1X,F8.3,3H) (,F8.3,1X,F8.3,2H) (,
     &F8.3,1H))
  400 FORMAT(37H0WARNING: WE'VE GENERATED 1000 POINTS/)
  500 FORMAT (13H0SEG SEG  NUM,3X,6H   -- ,21HENDPOINTS OF SEGMENTS,6H -
     &--  ,5X,27H ------------------------- ,18HSEGMENT PARAMETERS,27H -
     &------------------------ /14H NUM TYP CELLS,4X,2HXA,7X,2HYA,7X,
     &2HXB,7X,2HYB,6X,24HANGLE RADIUS LENGTH FORM,6X,8HZEA(ZMA),12X,
     &8HZEB(ZMB),6X,8HZEX(ZMX)/)
  120 RETURN
      END

C**** RAMVS VERSION
      COMPLEX FUNCTION ZFUN(IFORM,ZA,ZB,ZEX,ST)
      COMPLEX ZA,ZB
      IF(IFORM) 10,15,20
   10 ZFUN=CEXP(ZEX*CLOG(ZA-ZB*ST))
      RETURN
   15 ZFUN=ZA+ZB*ST**ZEX
      RETURN
   20 ZFUN=ZA+ZB*EXP(-ZEX*ST)
      RETURN
      END
```

```
      SUBROUTINE MTXEL1(MI,M,K,XK,X,Y,XN,YN,DSQ,ZE,ZM,A)
C**** RAMVS VERSION  E-POLARIZATION
      DIMENSION X(1),Y(1),XN(1),YN(1),DSQ(1)
      COMPLEX ZE(1),ZM(1),A(MI,1)
      COMPLEX AA,HZ,HZA,HZB,H1,H1A,H1B
      REAL NPDR,NDR,NDNP
      COMMON/PIES/PI,TPI,PIT,PIPI,YZ,RED,DIG
      M1=M+1
      MK=M+K
      WAVE=TPI/XK
      DO 300 II=1,M
      I=II
      IM=II+M
      XI=X(I)
      YI=Y(I)
      XNI=XN(I)
      YNI=YN(I)
C.....GENERATE ELEMENTS IN 1,2,4, AND 5
      DO 100 JJ=1,M
      J=JJ
      JM=J+M
      DS=DSQ(J)
      PDS=1./PIPI/DS
      DDS=0.25*DS*DS
      TPIDS=TPI*DS
      TEST=TPIDS*2.5
      IDS=TPIDS/24.
      PITDS=PIT*DS
      IF (I.EQ.J) GO TO 120
      CALL DIST(XI,YI,X(J),Y(J),XNI,YNI,XN(J),YN(J),5,
     &R,NPDR,NDR,NDNP,SDR,SPDR)
      RK=R*XK
      IF(RK.LE.TEST) GO TO 110
      CALL HANKZ1(RK,2,HZ,H1)
      A(I,J)=HZ*PITDS
      AA=H1*PITDS
      A(I,JM)=YZ*CMPLX(0.,NPDR)*AA
      A(IM,J)=CMPLX(0.,NDR)*AA
      B=NPDR*NDR
      AA=B*HZ+(SPDR*SDR-B)*H1/RK
      A(IM,JM)= AA*PITDS*YZ
      GO TO 100
  110 CONTINUE
      RW=R/WAVE
      B=RW*RW+DDS
      C=DS*RW*SPDR
      RAK=TPI*SQRT(B+C)
      IF (RAK.NE.RBK) GO TO 103
      HZA=HZB
      H1A=H1B
      GO TO 105
  103 CALL HANKZ1(RAK,2,HZA,H1A)
  105 RBK=TPI*SQRT(B-C)
      RK=R*XK
      CALL HANKZ1(RK,0,HZ,H1)
      CALL HANKZ1(RBK,2,HZB,H1B)
      AA=IDS*(HZA+4.*HZ+HZB)
      A(I,J)=AA
      A(IM,JM)=(0.25*SDR*(H1B-H1A)+NDNP*AA)*YZ
      AA=CMPLX(0.,-0.25)*SPDR*(HZB-HZA)
```

```
      A(I,JM)=AA*NPDR*YZ
      A(IM,J)=AA*NDR
      GO TO 100
  120 AA=CMPLX(PIT,ALOG(DS)+0.02879837)
      A(I,J)=ZE(J)+AA*DS
      A(I,JM)=(0.,0.)
      A(IM,J)=(0.,0.)
      A(IM,JM)=(ZM(J)+CMPLX(0.,PDS)+(AA-CMPLX(0.,0.5))*DS/2.)*YZ
  100 CONTINUE
C.....GENERATE ELEMENTS IN 3 AND 6
      DO 300 JJ=M1,MK
      J=JJ
      JM=J+M
      PITDS=PIT*DSQ(J)
      CALL DIST(XI,YI,X(J),Y(J),XNI,YNI,XN(J),YN(J),4,
     &R,NPDR,NDR,NDNP,SDR,SPDR)
      RK=R*XK
      CALL HANKZ1(RK,2,HZ,H1)
C     ***REMEMBER ZS IS STORED IN ZE***
      HZA=ZE(J)
      AA=HZ-CMPLX(0.,NPDR)*H1*HZA
      A(I,JM)=AA*PITDS
      B=NPDR*NDR
      AA=B*HZ+(SPDR*SDR-B)*H1/RK
      AA=CMPLX(0.,NDR)*H1-AA*HZA
  300 A(IM,JM)=AA*PITDS
      DO 500 II=M1,MK
      I=II
      IM=I+M
      XI=X(I)
      YI=Y(I)
      XNI=XN(I)
      YNI=YN(I)
C.....GENERATE ELEMENTS IN 7 AND 8
      DO 400 JJ=1,M
      J=JJ
      PITDS=PIT*DSQ(J)
      CALL DIST(XI,YI,X(J),Y(J),XNI,YNI,XN(J),YN(J),0,
     &R,NPDR,NDR,NDNP,SDR,SPDR)
      RK=R*XK
      CALL HANKZ1(RK,2,HZ,H1)
      A(IM,J)=HZ*PITDS
  400 A(IM,J+M)=CMPLX(0.,NPDR)*H1*PITDS*YZ
C.....GENERATE ELEMENTS IN 9
      DO 500 JJ=M1,MK
      J=JJ
      IF (I.EQ.J) GO TO 510
      CALL DIST(XI,YI,X(J),Y(J),XNI,YNI,XN(J),YN(J),0,
     &R,NPDR,NDR,NDNP,SDR,SPDR)
      RK=R*XK
      CALL HANKZ1(RK,2,HZ,H1)
      AA=HZ-CMPLX(0.,NPDR)*H1*ZE(J)
      A(IM,J+M)=PIT*AA*DSQ(J)
      GO TO 500
  510 DS=DSQ(J)
      A(IM,J+M)=0.5*ZE(J)+DS*CMPLX(PIT,ALOG(DS)+0.02879837)
  500 CONTINUE
      RETURN
      END
```

```
      SUBROUTINE MTXEL2(MI,M,K,XK,X,Y,XN,YN,DSQ,ZE,ZH,A)
C**** RAMVS VERSION  H-POLARIZATION
C**** RAMVS VERSION
      DIMENSION X(1),Y(1),XN(1),YN(1),DSQ(1)
      COMPLEX ZE(1),ZH(1),A(MI,1)
      COMPLEX AA,HZ,HZA,HZB,H1,H1A,H1B
      REAL NPDR,NDR,NDNP
      COMMON/PIES/PI,TPI,PIT,PIPI,YZ,RED,DIG
      M1=M+1
      MK=M+K
      WAVE=TPI/XK
      DO 300 II=1,M
      I=II
      IM=II+M
      XI=X(I)
      YI=Y(I)
      XNI=XN(I)
      YNI=YN(I)
C.....GENERATE ELEMENTS IN 1,2,4, AND 5
      DO 100 JJ=1,M
      J=JJ
      JM=J+M
      DS=DSQ(J)
      PDS=1./PIPI/DS
      DDS=0.25*DS*DS
      TPIDS=TPI*DS
      TEST=TPIDS*2.5
      TDS=TPIDS/24.
      PITDS=PIT*DS
      IF (I.EQ.J) GO TO 120
      CALL DIST(XI,YI,X(J),Y(J),XNI,YNI,XN(J),YN(J),5,
     &R,NPDR,NDR,NDNP,SDR,SPDR)
      RK=R*XK
      IF(RK.LE.TEST) GO TO 110
      CALL HANKZ1(RK,2,HZ,H1)
      A(I,J)=HZ*PITDS*YZ
      AA=H1*PITDS
      A(I,JM)=CMPLX(0.,-NPDR)*AA
      A(IM,J)=CMPLX(0.,NDR)*AA*YZ
      B=NPDR*NDR
      AA=B*HZ+(SPDR*SDR-B)*H1/RK
      A(IM,JM)=-AA*PITDS
      GO TO 100
  110 CONTINUE
      RW=R/WAVE
      B=RW*RW+DDS
      C=DS*RW*SPDR
      RAK=TPI*SQRT(B+C)
      IF (RAK.NE.RBK) GO TO 103
      HZA=HZB
      H1A=H1B
      GO TO 105
  103 CALL HANKZ1(RAK,2,HZA,H1A)
  105 RBK=TPI*SQRT(B-C)
      RK=R*XK
      CALL HANKZ1(RK,0,HZ,H1)
      CALL HANKZ1(RBK,2,HZB,H1B)
      AA=TDS*(HZA+4.*HZ+HZB)
      A(I,J)=AA*YZ
      A(IM,JM)=-0.25*SDR*(H1B-H1A)-NDNP*AA
```

```
      AA=CMPLX(0.,0.25)*SPDR*(HZB-HZA)
      A(I,JM)=AA*NPDR
      A(IM,J)=-AA*NDR*YZ
      GO TO 100
  120 AA=CMPLX(PIT,ALOG(DS)+0.02879837)
      A(I,J)=(ZM(J)+AA*DS)*YZ
      A(I,JM)=(0.,0.)
      A(IM,J)=(0.,0.)
      A(IM,JM)=-ZE(J)-CMPLX(0.,PDS)-(AA-CMPLX(0.,0.5))*DS/2.
  100 CONTINUE
C.....GENERATE ELEMENTS IN 3 AND 6
      DO 300 JJ=M1,MK
      J=JJ
      JM=J+M
      PITDS=PIT*DSQ(J)
      CALL DIST(XI,YI,X(J),Y(J),XNI,YNI,XN(J),YN(J),4,
     &R,NPDR,NDR,NDNP,SDR,SPDR)
      RK=R*XK
      CALL HANKZ1(RK,2,HZ,H1)
C     ***REMEMBER ZS IS STORED IN ZE***
      HZA=ZE(J)
      AA=HZ*HZA-CMPLX(0.,NPDR)*H1
      A(I,JM)=AA*PITDS
      B=NPDR*NDR
      AA=B*HZ+(SPDR*SDR-B)*H1/RK
      AA=CMPLX(0.,NDR)*H1*HZA-AA
  300 A(IM,JM)=AA*PITDS
      DO 500 II=M1,MK
      I=II
      IM=I+M
      XI=X(I)
      YI=Y(I)
      XNI=XN(I)
      YNI=YN(I)
C.....GENERATE ELEMENTS IN 7 AND 8
      DO 400 JJ=1,M
      J=JJ
      PITDS=PIT*DSQ(J)
      CALL DIST(XI,YI,X(J),Y(J),XNI,YNI,XN(J),YN(J),0,
     &R,NPDR,NDR,NDNP,SDR,SPDR)
      RK=R*XK
      CALL HANKZ1(RK,2,HZ,H1)
      A(IM,J)=HZ*PITDS*YZ
  400 A(IM,J+M)=CMPLX(0.,NPDR)*H1*PITDS
C.....GENERATE ELEMENTS IN 9
      DO 500 JJ=M1,MK
      J=JJ
      IF (I.EQ.J) GO TO 510
      CALL DIST(XI,YI,X(J),Y(J),XNI,YNI,XN(J),YN(J),0,
     &R,NPDR,NDR,NDNP,SDR,SPDR)
      RK=R*XK
      CALL HANKZ1(RK,2,HZ,H1)
      AA=HZ*ZE(J)-CMPLX(0.,NPDR)*H1
      A(IM,J+M)=PIT*AA*DSQ(J)
      GO TO 500
  510 DS=DSQ(J)
      A(IM,J+M)=0.5+DS*CMPLX(PIT,ALOG(DS)+0.02879837)*ZE(J)
  500 CONTINUE
      RETURN
      END
```

```
      SUBROUTINE DIST(XI,YI,XJ,YJ,XNI,YNI,XNJ,YNJ,I,
     &R,NPDR,NDR,NDNP,SDR,SPDR)
C.....I=0 R,NPDR
C.....I=1 R,NPDR,NDR
C.....I=2 R,NPDR,NDR,NDNP
C.....I=3 R           NDNP,SDR,SPDR
C.....I=4 R,NPDR,NDR,      SDR,SPDR
C.....I=5 R,NPDR,NDR,NDNP,SDR,SPDR
      REAL NPDR,NDR,NDNP
      IF (I.LT.0.OR.I.GT.5) GO TO 50
      RX=XI-XJ
      RY=YI-YJ
      R=SQRT(RX*RX+RY*RY)
      IF (I.EQ.3) GO TO 10
      NPDR=(RX*XNJ+RY*YNJ)/R
      IF (I.EQ.0) RETURN
      NDR=(RX*XNI+RY*YNI)/R
      IF (I.EQ.1) RETURN
      IF(I.EQ.4) GO TO 15
   10 NDNP=XNI*XNJ+YNI*YNJ
   15 IF (I.EQ.2) RETURN
      SDR=(RX*YNI-RY*XNI)/R
      SPDR=(RX*YNJ-RY*XNJ)/R
      RETURN
   50 WRITE(6,90) I,R
   90 FORMAT(31HOSICK DATA IN DIST   *QUIT*  I=,I2,2X,2HR=,E11.3)
      CALL SYSTEM
      END

      SUBROUTINE HANKZ1(R,N,HZERO,HONE)
C.....HANKEL FUNCTIONS ARE OF FIRST KIND--J+IY
C.....   N=0 RETURNS HZERO
C.....   N=1 RETURNS HONE
C.....   N=2 RETURNS HZERO AND HONE
C.....SUBROUTINE REQUIRES R>0
C.....SUBROUTINE ADAM MUST BE SUPPLIED BY USER
      DIMENSION A(7),B(7),C(7),D(7),E(7),F(7),G(7),H(7)
      COMPLEX HZERO,HONE
      DATA A,B,C,D,E,F,G,H/1.0,-2.2499997,1.2656208,-0.3163866,
     &0.0444479,-0.0039444,0.00021,0.36746691,0.60559366,-0.74350384,
     &0.25300117,-0.04261214,0.00427916,-0.00024846,0.5,-0.56249985,
     &0.21093573,-0.03954289,0.00443319,-0.00031761,0.00001109,
     &-0.6366198,0.2212091,2.1682709,-1.3164827,0.3123951,-0.0400976,
     &0.0027873,0.79788456,-0.00000077,-0.0055274,-0.00009512,
     &0.00137237,-0.00072805,0.00014476,-0.78539816,-0.04166397,
     &-0.00003954,0.00262573,-0.00054125,-0.00029333,0.00013558,
     &0.79788456,0.00000156,0.01659667,0.00017105,-0.00249511,
     &0.00113653,-0.00020033,-2.35619449,0.12499612,0.0000565,
     &-0.00637879,0.00074348,0.00079824,-0.00029166/
      IF (R.LE.0.0) GO TO 50
      IF (N.LT.0.OR.N.GT.2) GO TO 50
      IF (R.GT.3.0) GO TO 20
      X=R*R/9.0
      IF (N.EQ.1) GO TO 10
      CALL ADAM(A,X,BJ)
      CALL ADAM(B,X,Y)
      BY=0.6366198*ALOG(0.5*R)*BJ+Y
      HZERO=CMPLX(BJ,BY)
      IF (N.EQ.0) RETURN
```

```
10   CALL ADAM(C,X,Y)
     BJ=R*Y
     CALL ADAM(D,X,Y)
     BY=0.6366198*ALOG(0.5*R)*BJ+Y/R
     HONE=CMPLX(BJ,BY)
     RETURN
20   X=3.0/R
     IF (N.EQ.1) GO TO 30
     CALL ADAM(E,X,Y)
     FOOL=Y/SQRT(R)
     CALL ADAM(F,X,Y)
     T=R+Y
     BJ=FOOL*COS(T)
     BY=FOOL*SIN(T)
     HZERO=CMPLX(BJ,BY)
     IF (N.EQ.0) RETURN
30   CALL ADAM(G,X,Y)
     FOOL=Y/SQRT(R)
     CALL ADAM(H,X,Y)
     T=R+Y
     BJ=FOOL*COS(T)
     BY=FOOL*SIN(T)
     HONE=CMPLX(BJ,BY)
     RETURN
50   WRITE(6,90) N,R
90   FORMAT(32HOSICK DATA IN HANKZ1  *QUIT*  N=,I2,2X,2HR=,E11.3)
     CALL SYSTEM
     END

     SUBROUTINE ADAM(C,X,Y)
     DIMENSION C(7)
     Y=X*C(7)
     DO 10 I=1,5
10   Y=X*(C(7-I)+Y)
     Y=Y+C(1)
     RETURN
     END

     SUBROUTINE FLIP(A,N,MI,L,M,X,Y,IAT)
     COMPLEX A(MI,1),X(1),Y(1),D,BIGA,HOLD
     DIMENSION L(1),M(1)
     IF (IAT.GT.1) GO TO 150
     D=CMPLX(1.0,0.0)
     DO 80 K=1,N
     L(K)=K
     M(K)=K
     BIGA=A(K,K)
     DO 20 J=K,N
     DO 20 I=K,N
10   IF (CABS(BIGA).GE.CABS(A(I,J))) GO TO 20
     BIGA=A(I,J)
     L(K)=I
     M(K)=J
20   CONTINUE
     J=L(K)
     IF (J.LE.K) GO TO 35
     DO 30 I=1,N
     HOLD=-A(K,I)
     A(K,I)=A(J,I)
30   A(J,I)=HOLD
35   I=M(K)
     IF (I.LE.K) GO TO 45
     DO 40 J=1,N
     HOLD=-A(J,K)
     A(J,K)=A(J,I)
```

```
 40   A(J,I)=HOLD
 45   IF (CABS(BIGA).NE.0.0) GO TO 50
      D=CMPLX(0.0,0.0)
      RETURN
 50   DO 55 I=1,N
      IF (I.EQ.K) GO TO 55
      A(I,K)=-A(I,K)/BIGA
 55   CONTINUE
      DO 65 I=1,N
      DO 65 J=1,N
      IF (I.EQ.K.OR.J.EQ.K) GO TO 65
      A(I,J)=A(I,K)*A(K,J)+A(I,J)
 65   CONTINUE
      DO 75 J=1,N
      IF (J.EQ.K) GO TO 75
      A(K,J)=A(K,J)/BIGA
 75   CONTINUE
      D=D*BIGA
 80   A(K,K)=1.0/BIGA
      K=N
100   K=K-1
      IF (K.LE.0) GO TO 150
      I=L(K)
      IF (I.LE.K) GO TO 120
      DO 110 J=1,N
      HOLD=A(J,K)
      A(J,K)=-A(J,I)
110   A(J,I)=HOLD
120   J=M(K)
      IF (J.LE.K) GO TO 100
      DO 130 I=1,N
      HOLD=A(K,I)
      A(K,I)=-A(J,I)
130   A(J,I)=HOLD
      GO TO 100
150   DO 200 I=1,N
      Y(I)=CMPLX(0.0,0.0)
      DO 200 J=1,N
200   Y(I)=A(I,J)*X(J)+Y(I)
      RETURN
      END

      BLOCK DATA
      COMMON/PIES/PI,TPI,PIT,PIPI,YZ,RED,DIG
      DATA PI,TPI,PIT,PIPI,YZ,RED,DIG/3.1415927,6.2831853,
     &1.5707963,9.8696044,0.0026525824,0.01745329,57.29578/
      END
```

APPENDIX B

COMPUTER PROGRAM RAMD (as of January 1977)

Program RAMD solves the integral equations for the currents induced on a two dimensional body subject to an impedance boundary condition when illuminated by a plane E or H polarized electromagnetic wave, and then computes the scattered field. The equations on which the program is based are (Knott and Senior, 1974)

$$H_z^i(s) = K(s) + \lim_{\rho \to C} \frac{1}{4} \int_C \left\{ \eta(s') H_o^{(1)}(kr) - i(\hat{n}' \cdot \hat{r}) H_1^{(1)}(kr) \right\} K_s(s') d(ks') \quad \text{(B.1)}$$

for H polarization and

$$Y_o E_z^i = \eta(s) K_z(s) + \lim_{\rho \to C} \frac{1}{4} \int_C \left\{ H_o^{(1)}(kr) - i\eta(s')(\hat{n}' \cdot \hat{r}) H_1^{(1)}(kr) \right\} K_z(s') d(ks') \quad \text{(B.2)}$$

for E polarization. When the limit and integral operations are interchanged, the integrands become singular when the field and integration points coincide, and although the singularities are integrable, for a numerical solution it is still necessary to evaluate the self cell contributions analytically. The forms used in the digital solution are actually as follows:

$$H_z^i(s) = \left[0.5 + \frac{\alpha}{4\pi} + \frac{\Delta}{\lambda} \left\{ \frac{\pi}{2} + i\,(0.0287985 + \ell n \frac{\Delta}{\lambda}) \right\} \eta(s) \right] K_s(s)$$

$$+ \frac{k}{4} \int_{C-\Delta} \eta(s') K_s(s') H_o^{(1)}(kr)\, ds' - \frac{ik}{4} \int_{C-\Delta} K_s(s')(\hat{n}' \cdot \hat{r}) H_1^{(1)}(kr)\, ds' \quad \text{(B.3)}$$

and

$$Y_o E_z^i(s) = \left[(0.5 + \frac{\alpha}{4\pi}) \eta(s) + \frac{\Delta}{\lambda} \left\{ \frac{\pi}{2} + i(0.0287985 + \ell n \frac{\Delta}{\lambda}) \right\} \right] K_z(s)$$

$$+ \frac{k}{4} \int_{C-\Delta} K_z(s') H_o^{(1)}(kr)\, ds' - \frac{ik}{4} \int_{C-\Delta} \eta(s') K_z(s')(\hat{n}' \cdot \hat{r}) H_1^{(1)}(kr)\, ds' \quad \text{(B.4)}$$

for H and E polarizations respectively.

In each equation the first term on the right hand side is the contribution from the self cell of size Δ, and the integrals then represent the contribution from the rest of the body. The only difference from the equations used in the original program RAMD is in the self cell terms, and instead of writing a new program we have chosen to modify the old one. The changes made are

(i) inclusion of a curvature effect contribution

(ii) addition of a number of impedance generation subroutines designated ZFUN

and (iii) some cleaning up to make the program simple and more versatile.

The added term representing the effect of the curvature of the self cell is $\frac{\alpha}{4\pi}$ where α is the angle in radians subtended at the center of curvature. Although its expression is simple the need for such a term became apparent only when the results obtained with RAMD for a perfectly conducting circular cylinder were compared with those computed from the Mie series expression. An analytical derivation of this term is given by Senior (1976), and its inclusion in the program markedly improved the accuracy achieved for a given number of sampling points. Since the magnitude of the correction increases with increasing curvature, the improvement is most dramatic for bodies of small radius, for example, a cylinder having $ka = 1$. It is relatively unimportant for a body such as the ogival cylinder of interest in this investigation, and the results previously obtained for this geometry are in fact still valid.

The second modification to the program was the addition of numerous ZFUN subroutines to generate the surface impedance at each point when either a specific surface impedance variation, or the thickness and material properties of a homogeneous coating is given. In the main program there are options to generate an impedance having either a power law variation with distance s or an exponential form, and subroutine ZFUN is used only when a more complicated variation is

required. As many as 8 ZFUN's were used in the course of our study. Some compute specific impedance variations and others are directed at the case of a coating in the form of a layer. Three ZFUN's are included in the program listing to compute the impedance for

(i) a 'cylindrical tip' impedance

(ii) a 'cylindrical tip' layer thickness

and (iii) a two layer coating.

Of these three, only the first complements RAMD and derives all the input information from the input data. When the impedance is computed from the given thickness and material properties of a layer, more input parameters are needed than can be assigned in the input data list. Instead of changing RAMD to accept all input information, we chose to input part of the data via the original data input and the rest through the source statements in the subroutines. Thus, in the second ZFUN for a cylindrical tip layer thickness, μ (MU), ϵ (EPS) and frequency (FREQ) are inputted as data, but the tip thickness (TTIP), the taper length S_1 and the maximum layer thickness go in as source statements. Although a change in the data then requires recompiling the subroutine, the procedure is not difficult when running the program from a terminal.

The other change made in the original RAMD was to remove the option for reading in the geometry and surface impedance on a point by point basis. This seemed a worthwhile option when RAMD was developed but there has proved to be little need for it. All the geometries and impedances for which RAMD has been used so far have been generated internally and in the subroutines ZFUN.

A complete Fortran listing of RAMD is as follows:

```
C*************************************************************************C
C  INPUT FORMAT FOR PROGRAM RAMD-B----VERSION OF AUG 5,1976                C
C  MODIFIED NOV 18,1976                                                    C
C  PROGRAM NOW COMPUTES SURFACE FIELD FOR SPECIFIED ANGLE CANG             C
C*************************************************************************C
C  CARD 1  FORMAT (18A4)          TITLE CARD; USE UP TO 72 COLUMNS         C
C*************************************************************************C
C  CARD 2  FORMAT (I2,I3,2F10.5)   MORE,KODE,ZFAC,WAVE                     C
C          MORE=0       THIS WILL BE THE LAST RUN FOR THIS DATA SET        C
C          MORE=1       THERE ARE MORE DATA TO BE READ FOR THIS SET        C
C          KODE=0       COMPUTES BISTATIC SCATTERING PATTERN               C
C          KODE=1       COMPUTES BACKSCATTERING PATTERN                    C
C          ZFAC         A FACTOR MULTIPLYING ALL ELEMENT IMPEDANCES        C
C          WAVE         WAVELENGTH                                         C
C*************************************************************************C
C  CARD 3  FORMAT (I2,I3,4F10.5)  IPP,IOPT,FIRST,LAST,INK,CANG             C
C          IPP=1        E-POLARIZATION                                     C
C          IPP=2        H-POLARIZATION                                     C
C          IOPT=0       SURFACE PARAMETERS NOT PRINTED                     C
C          IOPT=1       SURFACE PARAMETERS PRINTED                         C
C          FIRST        INITIAL SCATTERING AND INCIDENCE ANGLE             C
C          LAST         FINAL ANGLE                                        C
C          INK          ANGULAR INCREMENT                                  C
C          CANG         ANGLE FOR SURFACE FIELD COMPUTATIONS               C
C*************************************************************************C
C  CARD 4  FORMAT (I2,I3,5F10.5)  N,IMP,XA,YA,XB,YB,ANGLE                  C
C          N            NUMBER OF SAMPLING POINTS ON THIS SEGMENT          C
C          IMP=-1       IMPEDANCE GIVEN BY USER-SUPPLIED SUBROUTINE        C
C          IMP=0        ZS(I)=ZA+ZB*S(I)**ZEX                              C
C          IMP=1        ZS(I)=ZA+ZB*EXP(-ZEX*S(I))                         C
C          XA,YA,XB,YB  SEGMENT ENDPOINTS                                  C
C          ANGLE        ANGLE SUBTENDED BY THE SEGMENT                     C
C*************************************************************************C
C  CARD 5  FORMAT (5X,5F10.5)      ZA,ZB,ZEX                               C
C          ZA,ZB        COMPLEX IMPEDANCE CONSTANTS                        C
C          ZEX          REAL IMPEDANCE CONSTANT                            C
C*************************************************************************C
C  CARD 6  FORMAT (I2)             INTEGER ZERO IN COLUMN 2;  SHUTS        C
C                                  OFF READING OF SEGMENT PARAMETERS       C
C*************************************************************************C
C   CARD 7  FORMAT (I2,I3,2F10.5)  MORE,KODE,ZFAC,WAVE                      C
C                          THIS CARD IS USED ONLY IF, ON CARD 2, MORE=1     C
C*************************************************************************C
      COMPLEX A(100,101),PHI(100),PINK(100),SUM,DEL,B1,B2,ZS(100)
      COMPLEX ZSFAC(100)
      REAL LAST,INK
      DIMENSION X(100),Y(100),XN(100),YN(100),S(100),DSQ(100),ANG(100)
      DIMENSION ID(18),LUMP(100,2),IPOL(2)
      DATA RED,DIG,PIF,IPOL/0.01745329,57.29578,0.07957747151,4HEEEE,4HHHHH/
C.....READ INPUT DATA AND GENERATE BODY PROFILE
    5 READ (5,100) ID
      READ (5,200) MORE,KODE,ZFAC,WAVE
      READ (5,200) IPP,IOPT,FIRST,LAST,INK,CANG
      WRITE (6,150) ID
      WRITE (6,300)
      CALL GEOM(LUMP,X,Y,XN,YN,S,DSQ,ANG,ZS,M,LL)
   20 IF (KODE.NE.0) GO TO 25
      NINC=1
      NBIT=1+IFIX((LAST-FIRST)/INK)
      GO TO 30
```

```
 61    25  NBIT=0
 62        NINC=1+IFIX((LAST-FIRST)/INK)
 63    30  WRITE (6,400) IPOL(IPP),ZFAC,LL,M,NINC,NBIT,WAVE
 64        XK=6.283185/WAVE
 65        DO 35 I=1,M
 66        ZSFAC(I)=ZS(I)*ZFAC
 67    35  DSQ(I)=DSQ(I)/WAVE
 68 C.....CONSTRUCT MATRIX ELEMENTS
 69    38  DO 55 I=1,M
 70        DO 55 J=1,M
 71        IF (I.EQ.J) GO TO 40
 72        TX=X(I)-X(J)
 73        TY=Y(I)-Y(J)
 74        P=SQRT(TX*TX+TY*TY)
 75        RPQ=P*XK
 76 C.....CNR=(N-PRIME DOT R)
 77        CNR=-(TX*XN(J)+TY*YN(J))/P
 78        CALL HANK(RPQ,1,BJ,BY)
 79        B1=1.570796*DSQ(J)*CNR*CMPLX(-BY,BJ)
 80        CALL HANK(RPQ,0,BJ,BY)
 81        B2=1.570796*DSQ(J)*CMPLX(BJ,BY)
 82        GO TO 45
 83    40  B1=CMPLX(0.5,0.0)+ANG(J)*PIF
 84        B2=DSQ(J)*CMPLX(1.570796,0.0287985+ALOG(DSQ(J)))
 85    45  IF (IPP.EQ.1) GO TO 50
 86        A(I,J)=B1+B2*ZSFAC(J)
 87        GO TO 55
 88    50  A(I,J)=B2+B1*ZSFAC(J)
 89    55  CONTINUE
 90 C.....COMPUTE INCIDENT FIELD AND INVERT MATRIX
 91        TETA=RED*CANG
 92        CT=COS(TETA)
 93        ST=SIN(TETA)
 94        DO 60 I=1,M
 95        HOLD=-XK*(CT*X(I)+ST*Y(I))
 96    60  PINK(I)=CMPLX(COS(HOLD),SIN(HOLD))
 97        CALL FLIP(A,M,PINK,PHI,1)
 98 C.....PRINT OUT CURRENTS AND ELEMENT PROPERTIES FOR FIRST ANGLE
 99        IF (IOPT.EQ.0) GO TO 63
100        WRITE (6,151) ID
101        WRITE(6,350) CANG
102        WRITE (6,500)
103    63  DO 65 I=1,M
104        AMP=CABS(PHI(I))
105        PHASE=DIG*ATAN2(AIMAG(PHI(I)),REAL(PHI(I)))
106        IF (IOPT.EQ.0) GO TO 65
107        WRITE(6,250) (LUMP(I,J),J=1,2),X(I),Y(I),S(I),DSQ(I),AMP,PHASE,
108       &ZSFAC(I)
109    65  CONTINUE
110 C.....DOPE OUT THE APPROPRIATE FIELD FACTORS
111        THE=FIRST-INK
112        IF (KODE.EQ.1) GO TO 70
113        WRITE (6,800) CANG
114        GO TO 75
115    70  WRITE (6,600)
116    75  THE=THE+INK
117        IF (THE.GT.LAST) GO TO 105
118        IF (THE.EQ.FIRST .AND. FIRST.EQ.CANG) GO TO 85
119        TETA=RED*THE
120        CT=COS(TETA)
```

```
      ST=SIN(TETA)
C.....IN THE FOLLOWING LOOP, PINK IS NOT NECESSARILY THE INCIDENT FIELD
      DO 80 J=1,M
      HOLD=-XK*(CT*X(J)+ST*Y(J))
   80 PINK(J)=CMPLX(COS(HOLD),SIN(HOLD))
      IF (KODE.EQ.0) GO TO 85
      CALL FLIP(A,M,PINK,PHI,2)
   85 SUM=CMPLX(0.0,0.0)
C.....ADD UP THE CURRENTS
      DO 95 J=1,M
      DEL=DSQ(J)*PHI(J)*PINK(J)
      IF (IPP.EQ.1) GO TO 90
      SUM=SUM+DEL*( ZSFAC(J)-CT*XN(J)-ST*YN(J))
      GO TO 95
   90 SUM=SUM+DEL*(1.0- ZSFAC(J)*(CT*XN(J)+ST*YN(J)))
   95 CONTINUE
      SCAT=20.0*ALOG10(CABS(SUM))+1.9612
      FASE=180.0+DIG*ATAN2(AIMAG(SUM),REAL(SUM))
      WRITE (6,900) THE,SCAT,FASE
      GO TO 75
  105 IF (MORE.EQ.0) GO TO 5
      DO 108 I=1,M
  108 DSQ(I)=DSQ(I)*WAVE
      READ (5,200) MORE,KODE,ZFAC,WAVE
      WRITE(6,150) ID
      GO TO 30
  100 FORMAT (18A4)
  150 FORMAT (1H1,18A4)
  151 FORMAT(1H0,18A4)
  200 FORMAT (I2,I3,5F10.5)
  250 FORMAT (2I5,5F10.5,F10.3,2F10.5)
  300 FORMAT (10H0SEG   NUM,11X,24HENDPOINTS OF THE SEGMENT,11X,
     &' ---------------------- SEGMENT PARAMETERS ----------------------
     &-----'/11H NUM  CELLS,6X,2HXA,8X,2HYA,8X,2HXB,8X,
     &2HYB,6X,21HANGLE  RADIUS  LENGTH,2X,'FORM',10X,'ZA',16X,
     &'ZB',14X,'ZX')
  350 FORMAT(1H0,'SURFACE IMPEDANCE;   INCIDENT FIELD DIRECTION=',F7.2)
  400 FORMAT (//25X,14HKEY PARAMETERS//
     &10X,21HINCIDENT POLARIZATION,22X,1A1/
     &10X,'SURFACE IMPEDANCE FACTOR',F20.5/
     &10X,23HNUMBER OF SEGMENTS USED,I21/
     &10X,34HTOTAL NUMBER OF POINTS ON THE BODY,I10/
     &10X,35HNUMBER OF INCIDENT FIELD DIRECTIONS,I9/
     &10X,29HNUMBER OF BISTATIC DIRECTIONS,I15/
     &10X,10HWAVELENGTH,F34.5)
  500 FORMAT (11HC   I   SEG,4X,4HX(I),6X,4HY(I),6X,4HS(I),5X,6HDSQ(I),
     &4X,6HMOD(J),4X,6HARG(J),4X,5HRS(I),5X,5HXS(I)/)
  600 FORMAT (///,20X,28HBACKSCATTERING CROSS SECTION/17X,
     &36HTHETA   10*LOG(SIGMA/LAMBDA)   PHASE/)
  800 FORMAT (///,19X,33HBISTATIC SCATTERING CROSS SECTION/18X,
     &29HFOR INCIDENT FIELD DIRECTION=,F7.2/24X,
     &28HTHETA   10*LOG(SIGMA/LAMBDA)/)
  900 FORMAT (9X,F13.2,F15.2,F16.1)
      END
```

```
175         SUBROUTINE GEOM(LUMP,X,Y,XN,YN,S,DSQ,ANG,ZS,M,LL)
176         COMPLEX ZS(100),ZA,ZB
177         DIMENSION X(100),Y(100),XN(100),YN(100),DSQ(100),S(100),ANG(100)
178         DIMENSION LUMP(100,2)
179         DATA RED/0.01745329/
180         I=0
181         L=0
182 C.....READ INPUT PARAMETERS AND PREPARE TO GENERATE SAMPLING POINTS
183    10   READ (5,200) N,IMP,XA,YA,XB,YB,ANGLE
184         IF (N.EQ.0) GO TO 120
185         LIM=2*N-1
186         READ (5,250) ZA,ZB,ZEX
187         TX=XB-XA
188         TY=YB-YA
189         D=SQRT(TX*TX+TY*TY)
190         IF (ANGLE.EQ.0.0) GO TO 20
191         T=0.5*RED*ANGLE
192         TRX=TX+TY/TAN(T)
193         TRY=TY-TX/TAN(T)
194         RAD=0.5*D/SIN(T)
195         ARC=2.0*RAD*T
196         ALF=T/N
197         DID=2.0*RAD*ALF
198         GO TO 30
199    20   RAD=999.999
200         ARC=D
201         DID=D/N
202 C.....START GENERATING
203    30   DO 110 JIM=1,2
204         L=L+1
205         DO 100 J=1,LIM,2
206         I=I+1
207         LUMP(I,1)=I
208         LUMP(I,2)=L
209         IF (JIM.EQ.2) GO TO 90
210         IF (ANGLE.EQ.0.0) GO TO 40
211         SINQ=SIN(J*ALF)
212         COSQ=COS(J*ALF)
213         X(I)=XA+0.5*(TRX*(1.0-COSQ)-TRY*SINQ)
214         Y(I)=YA+0.5*(TRX*SINQ+TRY*(1.0-COSQ))
215         XN(I)=-0.5*(TRX*COSQ+TRY*SINQ)/RAD
216         YN(I)= 0.5*(TRX*SINQ-TRY*COSQ)/RAD
217         ANG(I)=(ANGLE/N)*RED
218         GO TO 50
219    40   X(I)=XA+0.5*J*TX/N
220         Y(I)=YA+0.5*J*TY/N
221         XN(I)=-TY/D
222         YN(I)= TX/D
223         ANG(I)=(ANGLE/N)*RED
224    50   S(I)=0.5*J*DID
225 C.....COMPUTE THE IMPEDANCES
226         IF (IMP) 60,70,80
227    60   CALL ZFUN(ZA,ZB,ZEX,S(I),ZS(I))
228         GO TO 100
229    70   ZS(I)=ZA+ZB*S(I)**ZEX
230         GO TO 100
231    80   ZS(I)=ZA+ZB*EXP(-ZEX*S(I))
232         GO TO 100
233 C.....FROM HERE TO 100 WE CREATE THE SEGMENT IMAGE
234    90   K=I-N
```

```
      X(I)=X(K)
      Y(I)=-Y(K)
      XN(I)=XN(K)
      YN(I)=-YN(K)
      ANG(I)=ANG(K)
      S(I)=S(K)
      ZS(I)=ZS(K)
100   DSQ(I)=DID
      IF (JIM.EQ.1) GO TO 110
      YA=-YA
      YB=-YB
110   WRITE (6,300) L,N,XA,YA,XB,YB,ANGLE,RAD,ARC,
     &IMP,ZA,ZB,ZEX
      GO TO 10
120   M=I
      LL=L
200   FORMAT (I2,I3,5F10.5)
250   FORMAT (5X,5F10.5)
300   FORMAT (I3,I6,3X,4F10.5,F8.2,F8.3,F8.4,I5,2X,
     &2(F8.3,F9.3,2X),F9.3)
      RETURN
      END

      SUBROUTINE FLIP(A,N,X,Y,IAT)
      COMPLEX A(100,101),X(100),Y(100),D,BIGA,HOLD
      DIMENSION L(100),M(100)
      IF (IAT.GT.1) GO TO 150
      D=CMPLX(1.0,0.0)
      DO 80 K=1,N
      L(K)=K
      M(K)=K
      BIGA=A(K,K)
      DO 20 J=K,N
      DO 20 I=K,N
10    IF (CABS(BIGA).GE.CABS(A(I,J))) GO TO 20
      BIGA=A(I,J)
      L(K)=I
      M(K)=J
20    CONTINUE
      J=L(K)
      IF (J.LE.K) GO TO 35
      DO 30 I=1,N
      HOLD=-A(K,I)
      A(K,I)=A(J,I)
30    A(J,I)=HOLD
35    I=M(K)
      IF (I.LE.K) GO TO 45
      DO 40 J=1,N
      HOLD=-A(J,K)
      A(J,K)=A(J,I)
40    A(J,I)=HOLD
45    IF (CABS(BIGA).NE.0.0) GO TO 50
      D=CMPLX(0.0,0.0)
      RETURN
```

```
288    50  DO 55 I=1,N
289        IF (I.EQ.K) GO TO 55
290        A(I,K)=-A(I,K)/BIGA
291    55  CONTINUE
292        DO 65 I=1,N
293        DO 65 J=1,N
294        IF (I.EQ.K.OR.J.EQ.K) GO TO 65
295        A(I,J)=A(I,K)*A(K,J)+A(I,J)
296    65  CONTINUE
297        DO 75 J=1,N
298        IF (J.EQ.K) GO TO 75
299        A(K,J)=A(K,J)/BIGA
300    75  CONTINUE
301        D=D*BIGA
302    80  A(K,K)=1.0/BIGA
303        K=N
304   100  K=K-1
305        IF (K.LE.0) GO TO 150
306        I=L(K)
307        IF (I.LE.K) GO TO 120
308        DO 110 J=1,N
309        HOLD=A(J,K)
310        A(J,K)=-A(J,I)
311   110  A(J,I)=HOLD
312   120  J=M(K)
313        IF (J.LE.K) GO TO 100
314        DO 130 I=1,N
315        HOLD=A(K,I)
316        A(K,I)=-A(J,I)
317   130  A(J,I)=HOLD
318        GO TO 100
319   150  DO 200 I=1,N
320        Y(I)=CMPLX(0.0,0.0)
321        DO 200 J=1,N
322   200  Y(I)=A(I,J)*X(J)+Y(I)
323        RETURN
324        END

325        SUBROUTINE HANK(R,N,BJ,BY)
326  C.....SUBROUTINE REQUIRES R>0 AND N EITHER 0 OR 1
327        DIMENSION A(7),B(7),C(7),D(7),E(7),F(7),G(7),H(7)
328        DATA A,B,C,D,E,F,G,H/1.0,-2.2499997,1.2656208,-0.3163866,
329       &0.0444479,-0.0039444,0.00021,0.36746691,0.60559366,-0.74350384,
330       &0.25300117,-0.04261214,0.00427916,-0.00024846,0.5,-0.56249985,
331       &0.21093573,-0.03954289,0.00443319,-0.00031761,0.00001109,
332       &-0.6366198,0.2212091,2.1682709,-1.3164827,0.3123951,-0.0400976,
333       &0.0027873,0.79788456,-0.00000077,-0.0055274,-0.00009512,
334       &0.00137237,-0.00072805,0.00014476,-0.78539816,-0.04166397,
335       &-0.00003954,0.00262573,-0.00054125,-0.00029333,0.00013558,
336       &0.79788456,0.00000156,0.01659667,0.00017105,-0.00249511,
337       &0.00113653,-0.00020033,-2.35619449,0.12499612,0.0000565,
338       &-0.00637879,0.00074348,0.00079824,-0.00029166/
339        IF (R.LE.0.0) GO TO 50
340        IF (R.GT.3.0) GO TO 20
341        X=R*R/9.0
342        IF (N.NE.0) GO TO 10
343        CALL ADAM(A,X,BJ)
344        CALL ADAM(B,X,Y)
345        BY=0.6366198*ALOG(0.5*R)*BJ+Y
346        RETURN
```

```
347    10  IF (N.NE.1) GO TO 50
348        CALL ADAM(C,X,Y)
349        BJ=R*Y
350        CALL ADAM(D,X,Y)
351        BY=0.6366198*ALOG(0.5*R)*BJ+Y/R
352        RETURN
353    20  X=3.0/R
354        IF (N.NE.0) GO TO 30
355        CALL ADAM(E,X,Y)
356        FOOL=Y/SQRT(R)
357        CALL ADAM(F,X,Y)
358        GO TO 40
359    30  IF (N.NE.1) GO TO 50
360        CALL ADAM(G,X,Y)
361        FOOL=Y/SQRT(R)
362        CALL ADAM(H,X,Y)
363    40  T=R+Y
364        BJ=FOOL*COS(T)
365        BY=FOOL*SIN(T)
366        RETURN
367    50  N=100
368        RETURN
369        END

370        SUBROUTINE ADAM(C,X,Y)
371        DIMENSION C(7)
372        Y=X*C(7)
373        DO 10 I=1,5
374    10  Y=X*(C(7-I)+Y)
375        Y=Y+C(1)
376        RETURN
377        END

378        SUBROUTINE ZFUN(ZA,ZB,ZEX,SS,ZZ)
379 C        IMPEDANCE FOR CYLINDRICAL TIP CONTOUR
380 C           ZA  - TIP VALUE (COMPLEX)
381 C           ZB  - MAXIMUM VALUE (COMPLEX)
382 C           ZEX - JOIN POINT (REAL)
383        COMPLEX ZA,ZB,ZZ
384        DATA PIT/1.5707963/
385        ZZ=ZB
386        IF (SS.LE.ZEX) ZZ=ZA+(ZB-ZA)*SIN((PIT*SS)/ZEX)
387        RETURN
388        END

389        SUBROUTINE ZFUN(MU,EPS,F,S,ZZ)
390 C        IMPEDANCE FOR A CYLINDRICAL TIP
391 C        MATERIAL THICKNESS VARIATION
392 C        TAPER 1 INCH LONG, MAX THICKNESS 0.050 INCH.
393 C        DATA INPUT INFO:
394 C          ZA = MU
395 C          ZB = EPS
396 C          ZEX= F, FREQ IN GHZ.
397        COMPLEX MU,EPS,ZZ,XPLUS,XMINUS,ETA
398        DATA TOLD/-1./, PIT/1.5707963/,ANG/90./,TPI/6.283185/
399        DATA RAD/.0174533/
400 C        COMPUTE LAYER THICKNESS T
```

```
      S1=1.0
      TTIP=0.0
      T=0.050
      IF (S.LE.S1) T=TTIP+(0.05-TTIP)*SIN(PIT*S/S1)
      ZZ=ETA
      IF (TOLD.EQ.T) RETURN
C       COMPUTE IMPEDANCE FOR GIVEN T
      ARG=ANG*RAD
      SINSQ=SIN(ARG)
      SINSQ=SINSQ*SINSQ
      ETA=TPI*T*F*(0.084667)*CSQRT(MU*EPS-SINSQ)*(0.,-1.)
      XPLUS=CEXP(ETA)
      XMINUS=(1.,0.)/XPLUS
      ETA=CSQRT(MU/EPS)*(XPLUS-XMINUS)/(XPLUS+XMINUS)
      ETA=ETA*CSQRT(1.-SINSQ/(MU*EPS))
      ZZ=ETA
      TOLD=T
      RETURN
      END

      SUBROUTINE ZFUN(MU,EPS,F,S,ZZ)
C        IMPEDANCE FOR S**1 MATERIAL THICKNESS VARIATION,
C       MAX THICKNESS 0.100 INCH.
C       DATA INPUT INFO:
C         ZA = MU
C         ZB = EPS
C         ZEX= F, FREQ IN GHZ.
      COMPLEX MU,EPS,ZZ,XPLUS,XMINUS,ETA
      DATA TOLD/-1./, PIT/1.5707963/,ANG/90./,TPI/6.283185/
      DATA RAD/.0174533/
C       COMPUTE THICKNESS
      T=0.1*S/4.9912
      ARG=ANG*RAD
C       COMPUTE IMPEDANCE
      SINSQ=SIN(ARG)
      SINSQ=SINSQ*SINSQ
      ETA=TPI*T*F*(0.084667)*CSQRT(MU*EPS-SINSQ)*(0.,-1.)
      XPLUS=CEXP(ETA)
      XMINUS=(1.,0.)/XPLUS
      ETA=CSQRT(MU/EPS)*(XPLUS-XMINUS)/(XPLUS+XMINUS)
      ETA=ETA*CSQRT(1.-SINSQ/(MU*EPS))
      ZZ=ETA
      TOLD=T
      RETURN
      END
```